



DUDLEY KNOX LIBRARY  
NAVAL POSTGRADUATE SCHOOL  
MONTEREY CA 93943-5101







# NAVAL POSTGRADUATE SCHOOL MONTEREY, CALIFORNIA



## THESIS

### APPLICATION OF PRESSURE-SENSITIVE PAINT IN SHOCK-BOUNDARY LAYER INTERACTION EXPERIMENTS

by

Douglas L. Seivwright

March, 1996

Thesis Advisor:

Raymond P. Shreeve

Approved for public release; distribution is unlimited.



# REPORT DOCUMENTATION PAGE

Form Approved OMB No. 0704-0188

Public reporting burden for this collection of information is estimated to average 1 hour per response, including the time for reviewing instruction, searching existing data sources, gathering and maintaining the data needed, and completing and reviewing the collection of information. Send comments regarding this burden estimate or any other aspect of this collection of information, including suggestions for reducing this burden, to Washington Headquarters Services, Directorate for Information Operations and Reports, 1215 Jefferson Davis Highway, Suite 1204, Arlington, VA 22202-4302, and to the Office of Management and Budget, Paperwork Reduction Project (0704-0188) Washington DC 20503.

1. AGENCY USE ONLY (Leave blank)	2. REPORT DATE March 1996	3. REPORT TYPE AND DATES COVERED Master's Thesis	
4. TITLE AND SUBTITLE APPLICATION OF PRESSURE-SENSITIVE PAINT IN SHOCK-BOUNDARY LAYER INTERACTION EXPERIMENTS		5. FUNDING NUMBERS	
6. AUTHOR(S) Seivwright, Douglas L.			
7. PERFORMING ORGANIZATION NAME(S) AND ADDRESS(ES) Naval Postgraduate School Monterey CA 93943-5000		8. PERFORMING ORGANIZATION REPORT NUMBER	
9. SPONSORING/MONITORING AGENCY NAME(S) AND ADDRESS(ES)		10. SPONSORING/MONITORING AGENCY REPORT NUMBER	
11. SUPPLEMENTARY NOTES The views expressed in this thesis are those of the author and do not reflect the official policy or position of the Department of Defense or the U.S. Government.			
12a. DISTRIBUTION/AVAILABILITY STATEMENT Approved for public release; distribution is unlimited.		12b. DISTRIBUTION CODE	
13. ABSTRACT (maximum 200 words) A new type of pressure transducer, pressure-sensitive paint, was used to obtain pressure distributions associated with shock-boundary layer interaction. Based on the principle of photoluminescence and the process of oxygen quenching, pressure-sensitive paint provides a continous mapping of a pressure field over a surface of interest. The data measurement and acquisition system developed for use with the photoluminescence sensor was evaluated first using an underexpanded jet blowing over a flat plate. Once satisfactory results were obtained, the system was used to examine shock-boundary layer interaction in a blow-down supersonic wind tunnel at Mach numbers of 1.4 and 1.7. Details of the measurement technique, and discussion of the flow fields which were examined, are reported.			
14. SUBJECT TERMS APPLICATION OF PRESSURE SENSITIVE PAINT IN SHOCK-BOUNDARY LAYER INTERACTION EXPERIMENTS		15. NUMBER OF PAGES 203	
		16. PRICE CODE	
17. SECURITY CLASSIFICATION OF REPORT Unclassified	18. SECURITY CLASSIFICATION OF THIS PAGE Unclassified	19. SECURITY CLASSIFICATION OF ABSTRACT Unclassified	20. LIMITATION OF ABSTRACT UL

NSN 7540-01-280-5500

Standard Form 298 (Rev. 2-89)  
Prescribed by ANSI Std. Z39-18 298-102



**Approved for public release; distribution is unlimited.**

**APPLICATION OF PRESSURE-SENSITIVE PAINT  
IN SHOCK-BOUNDARY LAYER INTERACTION EXPERIMENTS**

Douglas L. Seivwright  
Lieutenant, United States Navy  
B.S., Embry-Riddle Aeronautical University, 1985

Submitted in partial fulfillment  
of the requirements for the degree of

**MASTER OF SCIENCE IN AERONAUTICAL ENGINEERING**

from the

**NAVAL POSTGRADUATE SCHOOL  
March 1996**



## ABSTRACT

A new type of pressure transducer, pressure-sensitive paint, was used to obtain pressure distributions associated with shock-boundary layer interaction. Based on the principle of photoluminescence and the process of oxygen quenching, pressure-sensitive paint provides a continuous mapping of a pressure field over a surface of interest. The data measurement and acquisition system developed for use with the photoluminescence sensor was evaluated first using an underexpanded jet blowing over a flat plate. Once satisfactory results were obtained, the system was used to examine shock-boundary layer interaction in a blow-down supersonic wind tunnel at Mach numbers of 1.4 and 1.7. Details of the measurement technique, and discussion of the flow fields which were examined, are reported.





## TABLE OF CONTENTS

I. INTRODUCTION .....	1
A. DESCRIPTION OF THE CONCEPT .....	2
B. APPROACH TO THE PROBLEM .....	3
II. THEORY OF MEASUREMENT .....	5
A. BACKGROUND .....	5
B. LUMINESCENCE .....	5
C. ABSORPTION AND EMISSION MECHANICS .....	6
1. Perturbation Theory .....	7
2. Spontaneous Emission .....	10
3. Triplet and Singlet States .....	10
4. Intramolecular Processes Involving Excited States .....	12
D. OXYGEN QUENCHING .....	16
E. MATHEMATICAL MODEL DEVELOPMENT .....	17
1. Temperature Effects .....	20
2. Aerodynamic Application .....	21
III. EARLY DEVELOPMENT USING A FREE-JET APPARATUS .....	23
A. APPARATUS AND FLAT PLATE ASSEMBLY .....	23
1. Freestream Flow Field of the Underexpanded Sonic Jet .....	27
a. Further Flow Field Studies .....	33

B. OPTICAL MEASUREMENT SYSTEM .....	41
1. Luminescence Coating .....	41
a. Reflective Backing .....	43
2. Illumination Source .....	43
a. Filters .....	45
3. Detection System .....	46
C. EXPERIMENTAL PROGRAM .....	48
1. Flat Plate Preparation .....	48
2. Experimental Procedure .....	49
3. Image Data Reduction .....	51
a. Image Processing .....	51
(1) Averaging .....	52
(2) Dark Current .....	54
(3) Registration .....	54
(4) Ratioing .....	63
b. Calibration .....	70
c. Field Pressure Map .....	77
IV APPLICATION TO SHOCK-BOUNDARY LAYER INTERACTION IN A SUPERSONIC WIND TUNNEL .....	83
A. DESCRIPTION OF FACILITY .....	83
1. Nozzle Blocks .....	86
a. Performance Evaluation of the Mach 1.7 Nozzle Blocks .....	86

B. INSTRUMENTATION .....	90
C. EXPERIMENTAL PROCEDURE .....	90
D. DISCUSSION AND RESULTS .....	94
V. CONCLUSIONS AND RECOMMENDATIONS .....	103
APPENDIX A. RUSSELL-SANDERS COUPLING .....	107
APPENDIX B. LUMINESCENCE COATING CHARACTERISTICS .....	109
A. TEMPERATURE SENSITIVITY .....	109
B. PHOTODEGRADATION .....	110
C. TIME RESPONSE .....	112
D. COATING THICKNESS / INDUCTION PERIOD .....	112
APPENDIX C. EPIX SOFTWARE SUMMARY .....	115
A. IMAGE DATA ACQUISITION .....	115
B. IMAGE PROCESSING .....	120
1. Averaging .....	120
2. Subtraction .....	121
3. Registration .....	123
4. Ratioing .....	126
5. Thresholding .....	127
6. Pseudo-coloring .....	128
APPENDIX D. DARK CURRENT .....	131

APPENDIX E. SUPERSONIC NOZZLE DESIGN PROGRAM .....135

    A. INVISCID CONTOUR SOFTWARE (Program char6) .....136

        1. Category 1: Characteristic Lengths and Nozzle Types .....137

        2. Category 2: Nozzle Flow and Geometry Specifications .....140

        3. "outpt1" Example and Description .....143

    B. MODIFICATION FOR VISCOUS EFFECTS (Program nbl6) ...146

        1. Category 1: Functional Modes .....148

        2. Category 2: Flow Conditions and Nozzle Dimensions .....151

        3. File "outpt3" Format Description .....155

    C. PROGRAM LISTINGS .....159

REFERENCES .....179

INITIAL DISTRIBUTION LIST .....183

## LIST OF FIGURES

<b>Figure 1</b>	Schematic Representation of the Pressure-Sensitive Luminescent Coating Concept .....	3
<b>Figure 2</b>	Energy Level Diagram for the Representation of Fluorescence and Phosphorescence .....	8
<b>Figure 3</b>	Energy Levels of Molecular Excited States and Transitions Between Them .....	13
<b>Figure 4</b>	Summary of Transition Types and Associated Rates .....	18
<b>Figure 5</b>	Schematic of the Underexpanded, Sonic Jet Nozzle and Supporting Facility .....	23
<b>Figure 6</b>	Underexpanded Jet Nozzle Apparatus .....	24
<b>Figure 7</b>	Schematic of the Pressure Port Arrangement on the Plate Surface .....	25
<b>Figure 8</b>	Bracket and Model Assembly .....	26
<b>Figure 9</b>	Bracket and Model Assembly Mounted to the Face of the Sonic Jet .....	26
<b>Figure 10</b>	Sketch of Jet Structure Behind a Highly Underexpanded Nozzle .....	27
<b>Figure 11</b>	Underexpanded Free Jet at 65 psig Plenum Pressure .....	28
<b>Figure 12</b>	Flow Visualization and Pressure Distribution Across Flat Plate at 65 psig ...	29
<b>Figure 13</b>	Flow Visualization and Pressure Distribution Across Flat Plate at 80 psig ...	30
<b>Figure 14</b>	Flow Visualization and Pressure Distribution Across Flat Plate at 90 psig ...	31
<b>Figure 15</b>	Flow Field Comparison Without (Top) and With (Bottom) the Flat Plate .....	32
<b>Figure 16</b>	Flow Visualization at 30 psig .....	34



<b>Figure 17</b> Flow Visualization at 38 psig .....	35
<b>Figure 18</b> Flow Visualization at 65 psig .....	36
<b>Figure 19</b> Details of Separation Bubble .....	37
<b>Figure 20</b> Flow Visualization at 25 psig .....	39
<b>Figure 21</b> Flow Visualization at 40 psig .....	39
<b>Figure 22</b> Flow Visualization at 68 psig .....	40
<b>Figure 23</b> Flow Visualization at 75 psig .....	40
<b>Figure 24</b> Schematic of Pressure Measurement System .....	41
<b>Figure 25</b> Excitation and Emission of Platinum Octaethylporphyrin .....	42
<b>Figure 26</b> Modification of Focusing Assembly of the Light Source .....	44
<b>Figure 27</b> Spectral Response Curve for the COHU Camera Model 4910 .....	47
<b>Figure 28a</b> Single Image of the Underexpanded Jet Across the Flat Plate at 65 psig ....	55
<b>Figure 28b</b> Graphical Representation of a Single Line of Pixels of a Single Image .....	56
<b>Figure 29a</b> Ten Averaged Images of the Underexpanded Jet Across the Flat Plate .....	57
<b>Figure 29b</b> Graphical Representation of a Single Line of Pixels of Ten Averaged Images .....	58
<b>Figure 30a</b> One Hundred Averaged Images of the Underexpanded Jet/Flat Plate .....	59
<b>Figure 30b</b> Graphical Representation of a Single Line of Pixels of One Hundred Images .....	60
<b>Figure 31</b> Wind-On Image of the Underexpanded Jet at 65 psig Across a Flat Plate ....	64
<b>Figure 32</b> Wind-Off Image for the 80 psig Condition .....	65
<b>Figure 33</b> Three Dimensional Intensity Plot of the Surface of the Plate .....	66



<b>Figure 34</b>	Ratioed Image of the Wind-On and Wind-Off Images for the Flat Plate/Jet Interaction .....	68
<b>Figure 35</b>	Result of a Ratioed Image Following Improper Registration Technique .....	69
<b>Figure 36</b>	Calibration Line of Pixels for the 65 psig Case Prior to Spatial Averaging ...	72
<b>Figure 37</b>	Calibration Line of Pixels for the 65 psig Case After Spatial Averaging .....	73
<b>Figure 38</b>	Calibration Curve for the Underexpanded Jet/Flat Plate at 65 psig .....	74
<b>Figure 39</b>	Calibration Curve for the Underexpanded Jet/Flat Plate at 80 psig .....	75
<b>Figure 40</b>	Calibration Curve for the Underexpanded Jet/Flat plate at 90 psig .....	76
<b>Figure 41</b>	Graphical Representation of the Red, Green, and Blue Lookup Tables .....	78
<b>Figure 42</b>	Pressure Map of the Underexpanded Jet at 65 psig Across a Flat Plate .....	79
<b>Figure 43</b>	Pressure Map of the Underexpanded Jet at 80 psig Across a Flat Plate .....	80
<b>Figure 44</b>	Pressure Map of the Underexpanded Jet at 90 psig Across a Flat Plate .....	81
<b>Figure 45</b>	Schematic of the Supersonic Wind Tunnel and Supporting Facility .....	84
<b>Figure 46</b>	Supersonic Wind Tunnel Apparatus .....	84
<b>Figure 47</b>	Nozzle Blocks and Test Section Exploded View .....	85
<b>Figure 48</b>	Tunnel Pressure Distributions as a Result of Varying Rod Diameters .....	88
<b>Figure 49</b>	Cross-Sectional View of the Mass Bleed-Off System .....	89
<b>Figure 50</b>	Mass Bleed-Off Tube Mounted in the Tunnel .....	89
<b>Figure 51</b>	Spectrometer Results for the Optical Window .....	91
<b>Figure 52</b>	Instrumentation Setup for the Supersonic Wind Tunnel Shock-Boundary Layer Experiment .....	92
<b>Figure 53</b>	Schematic of the Normal Shock-Boundary Layer Interaction .....	95

<b>Figure 54</b>	Mach 1.4 Pressure Map of the Shock-Boundary Layer Interaction .....	96
<b>Figure 55</b>	Graphical Representation of the Pressure Distribution of the Shock-Boundary Layer Interaction at Mach 1.4 .....	97
<b>Figure 56</b>	Mach 1.7 Pressure Map of the Shock-Boundary Layer Interaction .....	98
<b>Figure 57</b>	Graphical Representation of the Pressure Distribution of the Shock-Boundary Layer Interaction at Mach 1.7 .....	99
<b>Figure 58</b>	Calibration Curve for the Mach 1.4 Interaction .....	100
<b>Figure 59</b>	Calibration Curve for the Mach 1.7 Interaction .....	101
<b>Figure B1</b>	Luminescence Intensity as a Function of Temperature .....	110
<b>Figure B2</b>	Effect of Temperature on Coating Calibration Curve .....	111
<b>Figure B3</b>	Illustrative Example of the Effect of Photodegradation on Response Time .....	111
<b>Figure B4</b>	Induction Period of the Luminescent Coating with Thicknesses in Excess of 17 Micrometers .....	113
<b>Figure C1</b>	"Main Menu" for EPIX Interactive Image Analysis Software .....	116
<b>Figure C2</b>	"Video Resolution" Sub-Menu .....	116
<b>Figure C3</b>	"Video Digitize/Display" Menu .....	117
<b>Figure C4</b>	"Motion Sequence Capture/Display" Sub-Menu .....	118
<b>Figure C5</b>	"Image Processing" Sub-Menu .....	122
<b>Figure C6</b>	"Two Image Arithmetic" Sub-Menu .....	123
<b>Figure C7</b>	"Pixel Peek, Poke and Plot" Sub-Menu .....	124
<b>Figure C8</b>	"Image, Copy, Resize, Rotate" Sub-Menu .....	125
<b>Figure C9</b>	"Contrast & Lookup Table" Sub-Menu .....	128

<b>Figure C10</b>	<b>"Define Lookup Table" Sub-Menu</b>	129
<b>Figure D1</b>	<b>Representation of the Effect of Dark Current on the Creation of Charge</b>	132
<b>Figure E1</b>	<b>Illustrative Example of the Introductory Remarks for Program "char6"</b>	136
<b>Figure E2</b>	<b>Schematic of Supersonic Nozzle Design by Method of Characteristics</b>	138
<b>Figure E3</b>	<b>Example Showing the Format of File "outpt1"</b>	144
<b>Figure E4</b>	<b>Nozzle Wall Correction for Boundary Layer</b>	147
<b>Figure E5</b>	<b>Example Showing the Format of File "outpt3"</b>	156



## ACKNOWLEDGMENTS

I would like to take this opportunity to express my deep appreciation to those people who have contributed to this seemingly endless endeavor. To Professor Raymond Shreeve for his invaluable guidance and knowledge, and for instilling in me the qualities that are necessary to successfully investigate the scientific unknown. To Rick Still for his incredible technical expertise, creativity, and steadying influence. I thank Thad Best for his support and sound judgment. Finally, I would like to thank my wife, Angelica, whose patience, support, and encouragement has shown me that there is no obstacle that cannot be overcome to attain your dreams and desires.





## I. INTRODUCTION

One of the major thrusts of military aircraft engine design is towards achieving higher pressure ratios per compressor stage in order to reduce the number of stages and thereby reduce engine weight. This requires higher aerodynamic loading on the blades, and/or higher relative flow velocities over the blading. Where the relative Mach number is supersonic, shock waves will occur in front of and within the blade passages. The interaction of strong shocks with blade surface boundary layers can lead to high losses and reduced turning. Thus shock-boundary layer interaction, and methods to alleviate its attendant negative effects on compressor blade performance, warrant careful investigation. It was the need to make surface pressure measurements in a model simulation of shock-boundary layer interaction in a fan blade passage, which motivated the present study.

Currently, aerodynamic (surface) pressure measurements are made by installing a prearranged distribution of pressure ports in a wind-tunnel model or prototype aircraft. Since the installation of taps is an expensive process, the location and number of taps is normally predicated on a pre-selected area of interest. Obviously, this arrangement offers little flexibility if the area of aerodynamic interest is broad and fine spatial resolution is needed. Even with a substantially instrumented region, the information obtained is spatially discrete. It is often difficult to decide where to position the taps before the model is tested.



Within the last six years, the Central Aero-Hydrodynamic Institute in Moscow, the University of Washington (with support from Boeing and NASA) and McDonnell Douglas Aerospace have independently developed a new technique to measure surface pressures which is based on photoluminescent coatings [Ref. 1 through Ref. 9]. The pressure-sensitive coatings contain photoluminescent probe molecules. With the proper excitation of light, the molecules luminesce with an intensity which is inversely proportional to the local surface pressure. As a result, pressure-sensitive paints offer almost limitless spatial resolution, in addition to being applicable to surface locations which may not be accessible for pressure ports.

## **A. DESCRIPTION OF THE CONCEPT**

Figure 1 illustrates the general concept of the method. A luminescent molecule dissolved in an oxygen-permeable plastic resin is applied to a surface of interest. When illuminated by ultraviolet radiation the coating luminesces with an intensity that depends on the oxygen partial pressure seen by the active molecule. Thus the oxygen partial pressure can be determined from the emitted light intensity and since the mole fraction of oxygen in air is a known constant, the air pressure may then be readily calculated. The result of this oxygen dependence is that the airflow-induced surface-pressure field (and the corresponding oxygen partial-pressure field), gives rise to a luminescence intensity distribution. The intensity field can be imaged using a video camera, the image digitized, processed and stored on a computer. The end result is a map of the surface pressure field.

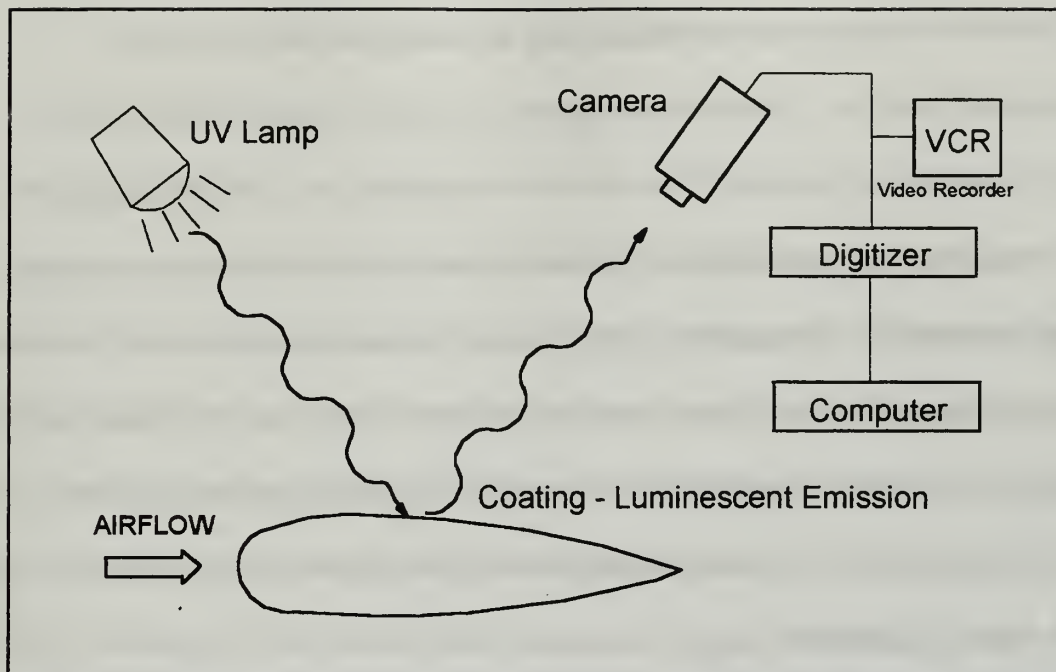


**Figure 1.** Schematic Representation of the Pressure-Sensitive Luminescent Coating Concept<sup>1</sup>

The processing of the surface pressure image relies on a calibration curve for the coating material, which is based on the Stern-Volmer relation.[Ref. 1: p. 34]

## **B. APPROACH TO THE PROBLEM**

The present work was focused on the development of a working pressure-measurement system, utilizing pressure-sensitive paints, for use in the Gas Dynamics and Turbopropulsion Laboratories at the Naval Postgraduate School. Although the system's initial application was tailored for use in the study of shock-boundary layer interaction in a pilot transonic cascade wind tunnel, and subsequently in a larger supersonic wind-tunnel, its use for other compressible flow studies was anticipated.

---

<sup>1</sup> See Ref. 1, page 34, Figure 1

The initial development was carried out using an existing flat-plate model in an underexpanded sonic jet. This was an arrangement that would produce effects similar to those to be measured in the tunnel, (i.e. shock waves impinging on a surface, creating a near-discontinuity in a pressure distribution) but be visually unrestricted since no walls and windows were present. Subsequently, measurements were made of the interaction of the starting shock wave with the side-wall boundary layer in the test section of a blow down wind tunnel. Results were obtained at  $M=1.4$  and  $M=1.7$  using different fixed nozzle blocks. The blocks for  $M=1.7$  were designed and built for the present study, and the design is detailed in Appendix E.

In reporting the work, Section II first provides some preliminary background work done in photoluminescent barometry in addition to the theory of photoluminescent coatings. Section III describes the development program using the sonic free-jet. Section IV provides results of applying the system in the supersonic wind tunnel, and Section V gives conclusions and recommendations. Since the system represents a powerful new tool for two laboratories, the attempt has been made to include all information and details necessary to both use and extend the present system.

## **II. THEORY OF MEASUREMENT**

### **A. BACKGROUND**

Photoluminescence and the process of quenching by oxygen is a photo-chemical interaction that is well documented and reasonably well-understood. In 1980, Peterson and Fitzgerald first recognized its potential as a means to make qualitative assessments in flow visualization studies [Ref. 3]. They reported on a technique in which fluorescent dye, when applied to a surface and excited by a blue light, illuminated in varying degrees of intensity, depending on the introduction of nitrogen or oxygen. When nitrogen was injected through a wall static-pressure tap, a bright streak of luminescence, moving in the direction of the surface flow, was observed. The nitrogen, in close proximity to the fluorescent dye, reduced the effect of the quenching (by displacing the oxygen) and allowed the intensity of the luminescence to increase. The introduction of oxygen, on the other hand, enhanced the quenching process and decreased the luminescence, producing a dark streak. This demonstrated that the concept of quenching could be used to acquire surface pressure measurements.

### **B. LUMINESCENCE**

According to the laws of thermodynamics, a system in an excited energy state due to the absorption of radiation, must be such that the reverse process of emission of radiation can occur. If no other process is available to allow the system to return to its initial state,



then emission must take place. Light emission excited by light absorption is called photoluminescence.

Luminescence is a broad term which encompasses both fluorescence and phosphorescence. The basic, underlying difference between these two processes is the time of emission with respect to the end of excitation; fluorescence has a relatively short lifetime, approximately  $10^{-9}$ - $10^{-7}$  seconds, whereas phosphorescence's lifetime persists for  $10^{-4}$ - $10^{-2}$  seconds. It is the phosphorescent emission that was used in the present work to quantitatively measure the static pressure on a surface of interest.

### **C. ABSORPTION AND EMISSION MECHANICS**

Quantum mechanics provides the necessary theoretical tools to describe the absorption and emission processes of light that were previously unexplainable by wave theory [Ref. 10: p. 457]. Instead of considering light as a wave train of infinite length, the radiation is instead composed of discrete photons (or quanta) whose energies are equal to  $h\nu$ , where  $h$  is the universal Planck constant,  $6.63 \times 10^{-27}$  erg sec. The concepts of light being considered as a wave train and that of discrete photons are linked in that the energy of the quantum is proportional to the light excitation frequency,  $\nu$ . This led to the hypothesis that radiation of frequency  $\nu$  could not be emitted or absorbed in arbitrary amounts, but only in quanta of energy  $\epsilon = h\nu$ . During an emission process following light absorption, less energy release by emission could occur, but would radiate at a lower frequency.

An absorbing molecule can exist in discrete, sharply defined levels in which transitions between states occur in certain definite steps. The lowest of these states is the ground state. States of higher energy are called excited states. There is a large number of possible excited states, but usually only several of those of the lowest energy are produced with visible or ultraviolet light. A simplistic description of the nature of these excited states is that a single electron has been promoted from an orbital occupied in the ground state to an orbital that is vacant while in the ground state.

Figure 2 illustrates several energy levels of an arbitrary molecule which are represented by the horizontal lines. The vertical distance between two of these lines is proportional to the corresponding difference in energy,  $h\nu$ ; the level N represents the ground state. By absorption of light frequency  $\nu_{NF}$  the molecule is raised to the state F and if no other energy levels exist between N and F, the molecule can return to N only by re-emission of a photon of light of the same frequency. Theoretically this is the simplest case of photoluminescence; it is called "resonance radiation". However, if, as indicated in Figure 2, several other levels C, D, ... are located between N and F, other transitions to C, D, ... can occur, resulting in the emission of spectral lines of frequency  $\nu_{FC}$ ,  $\nu_{FD}$ , ... These frequencies must be smaller than  $\nu_{FN}$  and therefore photoluminescence can have no greater frequency or shorter wave-length than the exciting light.[Ref. 11: p. 2]

## **1. Perturbation Theory**

For a molecule that absorbs or emits quanta of radiation under the influence of an electric field, perturbation theory of quantum mechanics provides the theoretical model

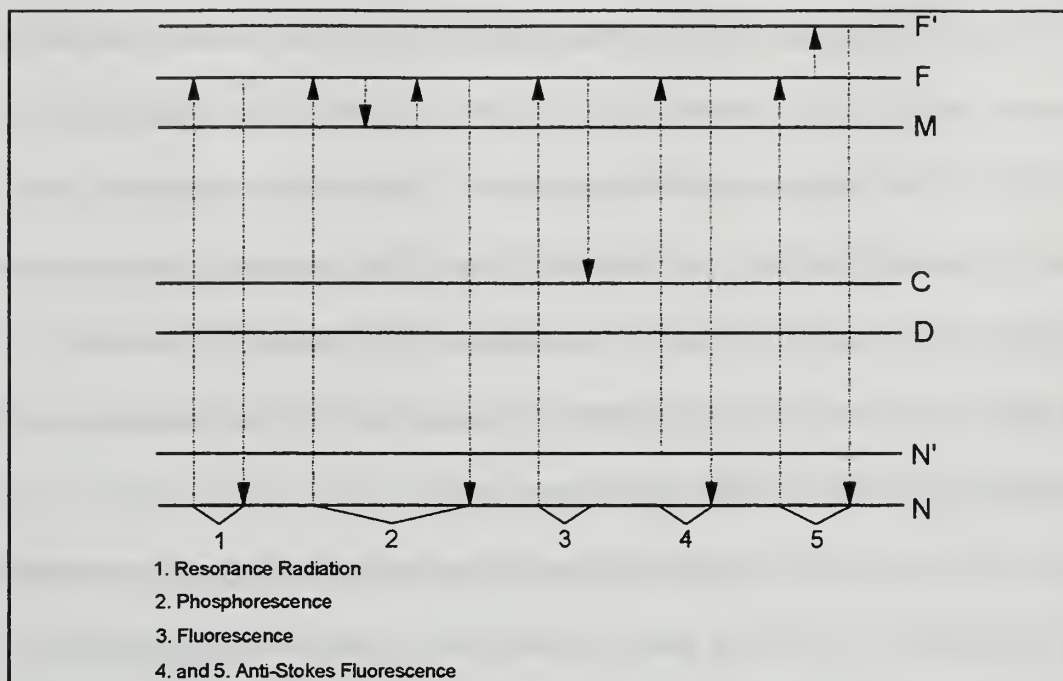


**Figure 2.** Energy Level Diagram for the Representation of Fluorescence and Phosphorescence<sup>2</sup>

that defines the physical interaction. The general solution of the wave equation for a molecule in the presence of a perturbing field results in certain derived relations that govern the changes of the molecule. One such outcome mandates that for radiation to be absorbed and transition from a stable ground state of energy to an electronically excited state of energy to occur, the frequency of the quantum must be proportional to the difference in energy between the states, a situation previously discussed. Once this condition is met, the probability of the transition is governed by the value of the transition moment integral, a second corollary from the solution of the perturbed wave equation:

<sup>2</sup>Figure 2 is found in Ref. 11, page 4, as Figure 2



$$m = \int \Psi_u \mathbf{M} \Psi_l d\tau$$

Here,  $\Psi_u$  and  $\Psi_l$  are the total wave functions for the upper and lower states respectively ( the wave functions result from the unperturbed solution of the Schrödinger wave equation ) and  $\mathbf{M}$  is defined as the dipole moment operator [Ref. 10: p. 583]. Evaluation of this integral determines the probability of an optical transition between two states. Detailed analysis has shown that transitions are probable only between states characterized by wave functions of a certain class. The results have been summarized in the form of selection rules which are formulated in terms of the quantum numbers that describe the electronic states involved [Ref.12: p. 51].

Perhaps the most important is the rule governing spin multiplicity. This states that the spin of an electron must not change during an electronic transition. As will be seen later, although from a theoretical standpoint transitions between states of different "multiplicity" do not intercombine, in practice they are observed, but the probability is usually much lower than an allowed transition. Thus, selection rules are good empirical guides, but they are not inviolable.[Ref. 13: p. 36]

Although the selection rules considered have been based on the absorption and emission of light by a molecule under the influence of a perturbing field, a second set of selection rules similar to the first but derived under a different set of circumstances govern radiationless processes. These processes, in addition to the spontaneous emission of light, compete with the excited state of a molecule in depleting its acquired energy and allowing it to return to its ground state.

## 2. Spontaneous Emission

An excited state may undergo a third radiation-related transition to a lower state by means of spontaneous emission, i.e., fluorescence and phosphorescence. In this process, an excited species loses energy in a spontaneous manner in the absence of an electric field. It is a random process: the rate-of-loss of excited species following a kinetic first-order reaction. If a process follows first-order kinetics described by a rate constant "k", the mean radiative lifetime, (the time  $\tau$  taken for the intensity to fall to 1/e of its initial value), is given by

$$\tau = 1/k$$

When a radiative transition occurs between states of similar multiplicity, it corresponds, according to the selection rules, to an allowed transition. Such transitions are characteristic of fluorescence emission having lifetimes equal to  $\tau = 10^{-8}$  seconds.

However, there are transitions in which  $\tau$  is much higher,  $10^{-3}$  seconds. When selection rules suggest a low probability for a transition to occur, such as between states of different multiplicity, the transition, though theoretically forbidden, can occur, but the process is relatively slow. This is representative of phosphorescent emission. [Ref. 10: p. 585]

## 3. Triplet and Singlet States

In the absence of a magnetic field, the energy of a single unpaired electron characterized by its given values of "n" (the principle quantum number) and "l" (the azimuthal quantum number) must be further refined to explain the observed fine structure of atomic spectra. The additional amount of energy that the spectroscopic evidence

indicates is attributed to the interaction that occurs between the angular momenta from the intrinsic spin and orbital motion of the electron. When several electrons within an atom (or molecule) are present, the resultant orbit and resultant spin angular momenta components can combine in several ways resulting in several energy levels for a single configuration of an atom (or molecule). This interaction is known as Russell-Sanders coupling, the result of which is the "multiplicity" of energy levels that a given electron configuration of an atom may possess. Thus, a single energy level for a given electron configuration for an atom (or molecule) is referred to as singlet state, two energy levels as a doublet, three energy levels a triplet, etc. [Ref. 14: p. 79] A more thorough discussion is given in Appendix A.

Nearly all molecules have a ground-state electronic configuration in which the spin of each electron is opposed to, or paired up with, the spin of another electron which otherwise has the same spatial quantum numbers, a consequence of the Pauli exclusion principle. In this instance the total angular momentum of each electron within the pair, composed of the spin and orbital momenta, tend to cancel with each other. When all the pairs of electrons within the molecule are considered, the net result is zero total angular momentum (vector), producing a single energy level for the given electron configuration. Molecules will have, in addition to a ground state that is usually a singlet state, a number of excited states that also have all the electrons paired and that are, therefore, also singlet states. [Ref. 15: p. 16]

Whether or not the ground state is a singlet state for molecules with an even number of electrons, there will be excited states in which a pair of electrons have their spins in the same direction, giving the molecule a net total angular momentum (vector). In this case, the coupling interaction results in three energy levels for the configuration, and thus the designation triplet state.

Therefore, promotion of an electron to an upper state can in principle give rise to two types of energy states, the triplet and singlet, while still maintaining the same electron configuration. Therefore, for every singlet state there is a corresponding triplet state, with the triplet state displaying a lower energy level. Figure 3 illustrates the two types of electronically excited states, where the spin orientations for each state are depicted as arrows next to the appropriate state. The additional lines within each electronic state refer to the various vibrational and rotational energy levels the molecule may acquire with the absorption of energy.

#### **4. Intramolecular Processes Involving Excited States**

With the absorption of a quantum, a molecule is raised from a singlet ground to a singlet excited state. The selection rules stipulate that the absorption of electromagnetic radiation does not "unpair" the electrons of a molecule (transitions occur between states of like multiplicity) thus preventing direct absorption of light from a singlet to a triplet state. The molecule, having been raised to an upper vibrational level within the excited state, begins to lose the excess vibrational energy by collisions with surrounding molecules. The



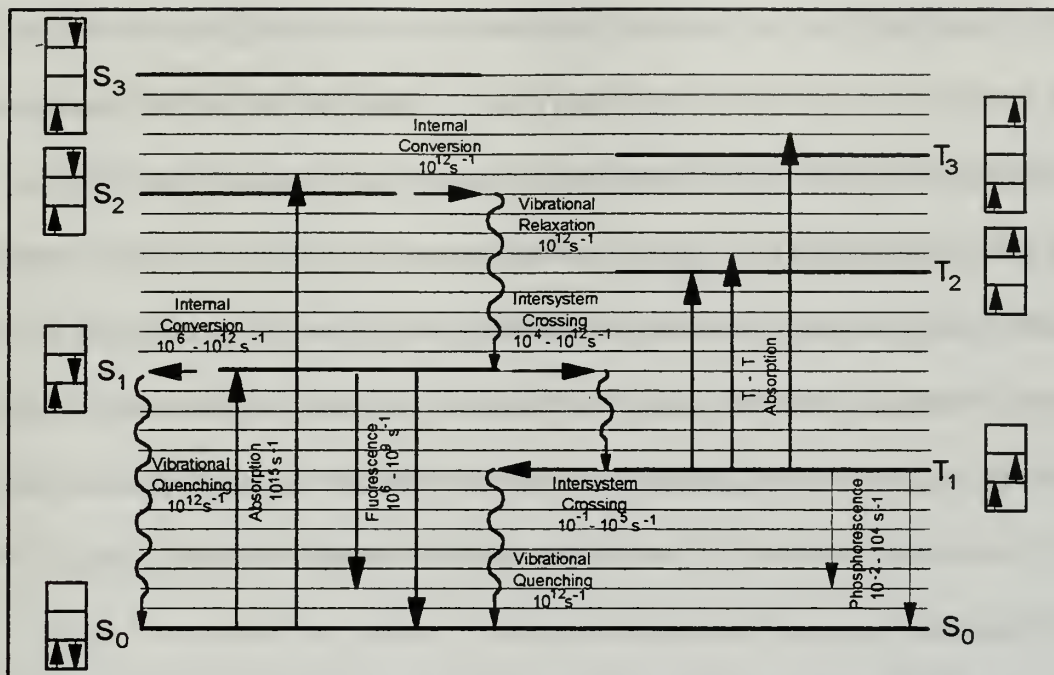
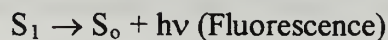


**Figure 3.** Energy Levels of Molecular Excited States and Transitions Between Them<sup>3</sup>

radiationless process of internal conservation then occurs whereby the molecule passes from a low vibrational level of the upper state to a high vibrational level of a lower state having the same total energy. Once internal conversion is complete, this cycle of events repeats itself leading to the net result of the molecule falling to the lowest vibrational level of the first excited singlet state as illustrated in Figure 3. [Ref. 15: p. 9]

At this point, the molecule may return to the ground state by one of three paths:



<sup>3</sup> Figure 3 is found in Ref. 16, page 71, as Figure 5-1.

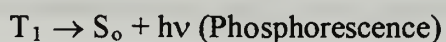
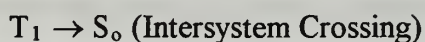
The internal-conversion process, involved with the intramolecular energy transfer between the first excited singlet and ground state, takes place at a much slower rate ( $10^{-9}$  seconds) as compared with the same process occurring between the upper excited singlet states to the first excited singlet state ( $10^{-12}$  seconds). The increase in inefficiency in energy transfer is explained by the relatively large energy separation between  $S_1$  and  $S_0$  as compared to the energy differences between the upper excited states. This allows fluorescence ( $10^{-9}$  to  $10^{-7}$  seconds) and, with the combined effect of the spin-forbidden nature of the states, the process of intersystem crossing ( $10^{-9}$  seconds) to effectively compete with the internal conversion process.

When a molecule returns to the ground state via the first excited triplet state, it undergoes a conversion process known as intersystem crossing. Intersystem crossing is a non-radiative process between states of different multiplicity. It is theoretically forbidden with regard to the formal selection rules, but in practice, these transitions do take place (although with extremely low probability). This is made possible through the "breakdown" of the spin-orbit coupling model discussed in Appendix A. In the absence of magnetic or electric fields the total angular momentum of the molecule remains constant, and the ability to discern between specific states such as singlet and triplet is possible. However, when an electromagnetic field is present, though the total angular momentum vector remains constant, the spin and orbital degrees of freedom become time dependent, and it becomes meaningless to speak of specific states [Ref. 16: p. 12]. This ultimately leads to the mixing of states. The interaction is enhanced by heavier elements

due to an increase of the magnetic field developed by the nucleus, as in the case of platinum octaethylporphyrin (PtOEP).

The lowest vibrational level of the lowest triplet state is generally situated at an energy level below that of the lowest excited singlet state, but its upper vibrational levels reach to the bottom of the singlet level, and intersystem crossing occurs with the molecule crossing over to one of these upper vibrational levels of the lowest triplet state. From here the molecule rapidly loses its excess vibrational energy and falls to near the lowest vibrational level of the triplet state.

Again, the molecule may return to the ground state from this point by one of the following paths:



As before, it might be expected that the analogous process of intersystem crossing from the lowest vibrational level of the triplet state to the ground state would take place with equal facility as the transition from  $S_1 \rightarrow T_1$ . In fact it is usually some  $10^6 - 10^9$  times slower. If radiationless  $T_1 \rightarrow S_0$  transitions occurred with rate constants of  $10^8$  seconds, the molecule would have no time to emit  $T_1 \rightarrow S_0$  phosphorescence by the spin-forbidden radiative process. On the other hand, if the  $S_1 \rightarrow T_1$  intersystem crossing process were as slow as that of the  $T_1 \rightarrow S_0$  radiationless process, then it could not compete effectively with fluorescence. Phosphorescence would then be a rare phenomenon and the photochemical behavior would be very different. The difference between the rates of the



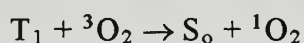
$S_1 \rightarrow T_1$  and  $T_1 \rightarrow S_0$  radiationless processes is, as was the case with internal conversion, a function of the energy differences between  $S_1$  and  $T_1$ , and,  $T_1$  and  $S_0$ . [Ref. 15: p. 41]

#### D. OXYGEN QUENCHING

The exceptionally long radiative lifetimes of molecules in the lowest triplet state make them vulnerable to a variety of radiationless processes that deactivate the molecule, allowing it to return to the ground state. As an example, they are very susceptible to collisions with molecules, and in such cases may encounter molecules of a specific nature which are particularly effective in removing excitation energy.

Previous reference was made to the fact that most molecules with an even number of electrons have a ground state in which their electrons occupy orbitals in pairs. These molecules were said to have singlet states. There are however some molecules containing an even number of electrons for which the states of lowest energy have two unpaired electrons occupying different orbitals. The most important of these is molecular oxygen, of which the ground state is a triplet. Molecular oxygen is very effective in removing triplet excitation energy, and can act at exceedingly low concentrations. [Ref. 15: p. 36]

The energy transfer that takes place when an excited triplet PtOEP molecule collides with a triplet oxygen results in a ground-state singlet PtOEP molecule and a singlet excited oxygen molecule. The reaction is expressed as follows:



The reaction occurs very rapidly but is consistent with the formal selection rules. It is this bimolecular reaction that results in the quenching of the phosphorescence. The University

of Washington found that when PtOEP was embedded in an oxygen-permeable silicon resin and subject to atmospheric pressure, the quenching reaction had a rate comparable to that of phosphorescence. Variations in atmospheric pressure from 0 to 1 atmospheres demonstrated a suitable drop in phosphorescence yield of PtOEP that would allow it to be useful as a measurement tool in the study of static pressure changes in aerodynamic wind tunnel testing. [Ref. 9: p. 18]

## E. MATHEMATICAL MODEL DEVELOPMENT

Oxygen quenching of luminescence by collisional deactivation of the emission process is the basis for developing a prediction model. It is important to note that the end result of this development, the Stern-Volmer relation, is strictly valid only for free molecules in solution. However, it has been found that it describes accurately the quenching process that occurs in the present situation. The basis for the present development is the work of Parker [Ref. 15], which may be consulted for further details.

The development first begins with the definition of the triplet formation efficiency,  $\phi_t$ , being the number of triplet molecules formed per quantum of exciting light absorbed. Assuming now that a system, illuminated with a beam of exciting light of constant intensity, is in a photochemically steady state. The rate of population of the lowest excited singlet state,  $S_1$ , is found to equal the rate of light absorption,  $I_0$ , and the rate of formation of triplet molecules by crossing from  $S_1$  is equal to  $I_0\phi_t$ .

Figure 4 illustrates the rates of the various processes by which the triplet is produced and consumed; these are represented in equation form as follows:

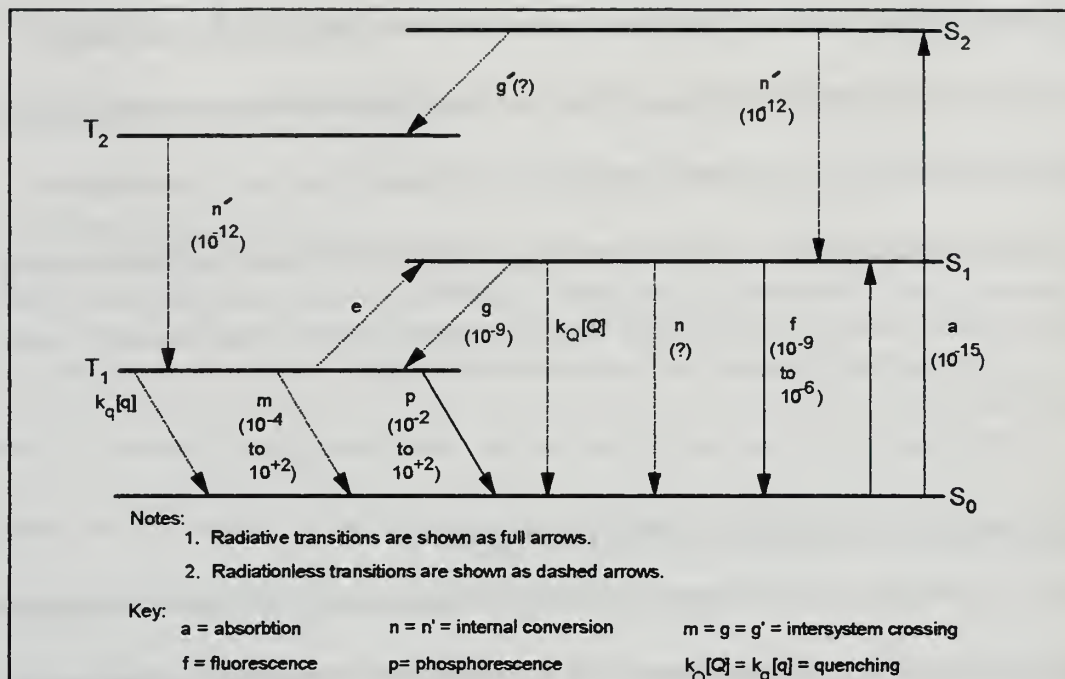
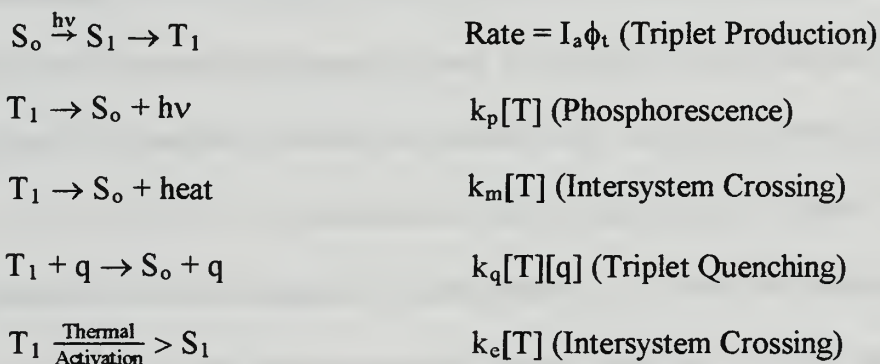


**Figure 4.** Summary of Transition Types and Associated Rates<sup>4</sup>



The square bracketed  $[q]$  and  $[T]$  represent concentrations.  $[q]$  represents the concentration of all quenching impurities in the system,  $k_q[q]$  a composite pseudo first-order rate constant for impurity quenching, and  $k_e[T]$  represents the rate of thermal activation of triplet molecules back to the excited singlet level [Ref. 15: p. 87].

<sup>4</sup>Figure 4 is found in Ref. 15, page 69, as Figure 23

[T] represents the concentration of excited triplet molecules when the steady state has been achieved. All processes so far considered in Figure 4, with the exception of light absorption, are first-order reactions having rate constants equal to the reciprocals of the lifetimes quoted.

Now consider, in addition to the previous statements and definitions made with respect to the steady state of the system, that the rate of production of excited triplet molecules (in state  $T_1$ ) is just balanced by their rate of disappearance via the various processes discussed above. This can be expressed as

$$I_a \phi_t = (k_p + k_m + k_q[q] + k_e)[T] \quad (1)$$

Since the rate of emission of phosphorescence is  $k_p[T]$ , the phosphorescence efficiency  $\phi_p$  is given by

$$\phi_p = k_p[T] / I_a \quad (2)$$

Equation (1) may be solved for  $I_a$  and substituted into equation (2) to arrive at

$$\phi_p = k_p \phi_t / (k_p + k_m + k_q[q] + k_e) \quad (3)$$

In the absence of quenching agents affecting the removal of triplet excitation energy, equation (3) gives, for the phosphorescence efficiency,

$$\phi_p^0 = k_p \phi_t / (k_p + k_m + k_e) \quad (4)$$

Taking the ratio of equations (3) and (4):

$$\phi_p^0 / \phi_p = 1 + k_q[q] / (k_p + k_m + k_e) \quad (5)$$

or,

$$\phi_p^0/\phi_p = 1 + K[q] \quad (6)$$

where

$$K = \tau_0 k_q \text{ and } 1/\tau_0 = (k_p + k_m + k_e) \quad (7)$$

Equation (6) is known as the Stern-Volmer equation for quenching, and the constant  $K$  as defined in equation (7) is referred to as the Stern-Volmer quenching constant.

For this particular application, the quenching impurity,  $[q]$ , may be defined as

$$[q] = S P_{O_2} \quad (8)$$

where  $S$  is the solubility of oxygen in the system and  $P_{O_2}$  is the partial pressure of oxygen in equilibrium with it. This leads to the relation

$$\phi_p^0/\phi_p = 1 + K' P_{O_2} \quad (9)$$

Finally, by definition, the luminescence,  $I$ , is linearly proportional to the quantum yield ( $\phi$  = photons emitted/photons absorbed) for a given quenching condition, (i.e.,  $I = I_{abs}\phi$ ), where  $I_{abs}$  is the excitation light intensity by the luminescent species. Thus

$$I_{max}/I = 1 + K' P_{O_2} \quad (10)$$

where  $I_{max}$  is the maximum possible value that occurs in the absence of a quencher.

## 1. Temperature Effects

The effect that temperature has on the efficiency of phosphorescence may lead to a decrease in the intensity by several orders of magnitude over the range of 77° K to room temperature. The effect results in the long lifetime of triplet states and the correspondingly greater susceptibility to impurity quenching and intersystem crossing [Ref. 15: p. 89].



The rate constants for each of the intramolecular processes depend on temperature, following the Arrhenius equation,

$$k = A e^{-E_a / R T},$$

where  $k$  is the rate constant,  $A$  is the pre-exponential factor,  $E_a$  is the activation energy,  $R$  is the gas constant, and  $T$  is the temperature in degrees Kelvin [Ref. 9: p. 20]. Hence, in equation (10),  $I$ ,  $I_{\max}$ , and  $K$  are all functions of temperature.

## 2. Aerodynamic Application

In order to apply the form of the Stern-Volmer relation presented in equation (10), it would be necessary to purge the vicinity of the surface of interest of all oxygen in order to determine  $I_{\max}$ . In most cases of experimental work, this is impractical. A more convenient approach is to manipulate the governing equation so that determination of  $I_{\max}$  becomes unnecessary.

Equation (10) is first modified by noting that the oxygen partial pressure,  $P_{O_2}$ , is related to the air pressure,  $P$ , by  $P_{O_2} = X P$ , where  $X$  is equal to the mole fraction of oxygen. Equation (10) then becomes:

$$I_{\max}/I = 1 + K' X P \quad (11)$$

In the method used in the present work, two images are taken. In the "flow-on" case, the pressures are unknown. In the "flow-off" case, the pressure distribution is constant on the surface and equal to atmospheric pressure. These conditions are represented, respectively, as follows:



$$I_{\max}/I = 1 + K' \times P \quad (12)$$

and 
$$I_{\max}/I_o = 1 + K' \times P_o \quad (13)$$

where the subscript "o" denotes the value for the flow-off conditions. Dividing equation (13) by equation (12),

$$I_o/I = (1 + K' \times P)/(1 + K' \times P_o) \quad (14)$$

Rearranging,

$$I_o/I = 1/(1 + K' \times P_o) + [(K' \times P_o)/(1 + K' \times P_o)](P/P_o) \quad (15)$$

which gives

$$I_o/I = A + B (P/P_o) \quad (16)$$

where,

$$A = 1/(1 + K' \times P_o) \text{ and } B = (K' \times P_o)/(1 + K' \times P_o) \quad (17)$$

A and B represent the coating sensitivity coefficients and are, in general, functions of temperature for both wind-on and wind-off conditions. In the absence of a temperature variation across the surface, A and B have the same value over the whole image. Notice that  $A + B = 1$ . This condition occurs only when the images of I and  $I_o$  are taken at the same temperature. If any temperature variation is present between the two images, a value other than one will result. [Ref. 1: p. 34] Techniques discussed in Section 3 will outline the procedures used for determining these coefficients.

### III. EARLY DEVELOPMENT USING A FREE JET APPARATUS

#### A. APPARATUS AND FLAT PLATE ASSEMBLY

A sonic-jet nozzle system located in the Gas Dynamics Laboratory (Bldg. 216) at the Naval Postgraduate School was used in the initial experiments. A schematic of the facility is illustrated in Figure 5. A photograph of the jet nozzle is shown in Figure 6.

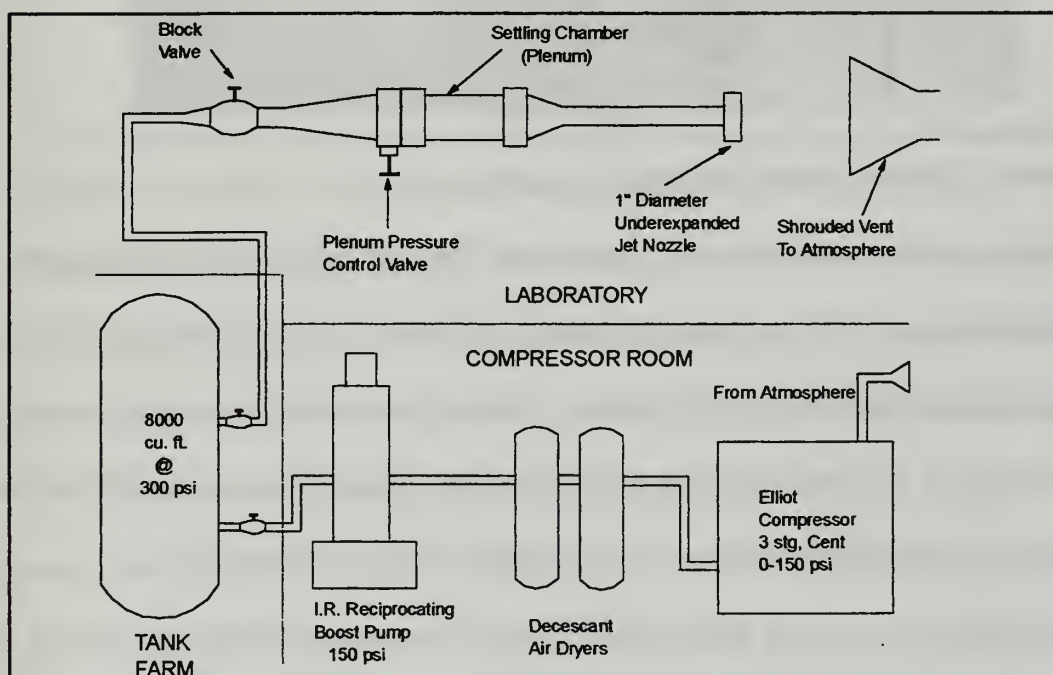


**Figure 5.** Schematic of the Underexpanded, Sonic Jet Nozzle and Supporting Facility

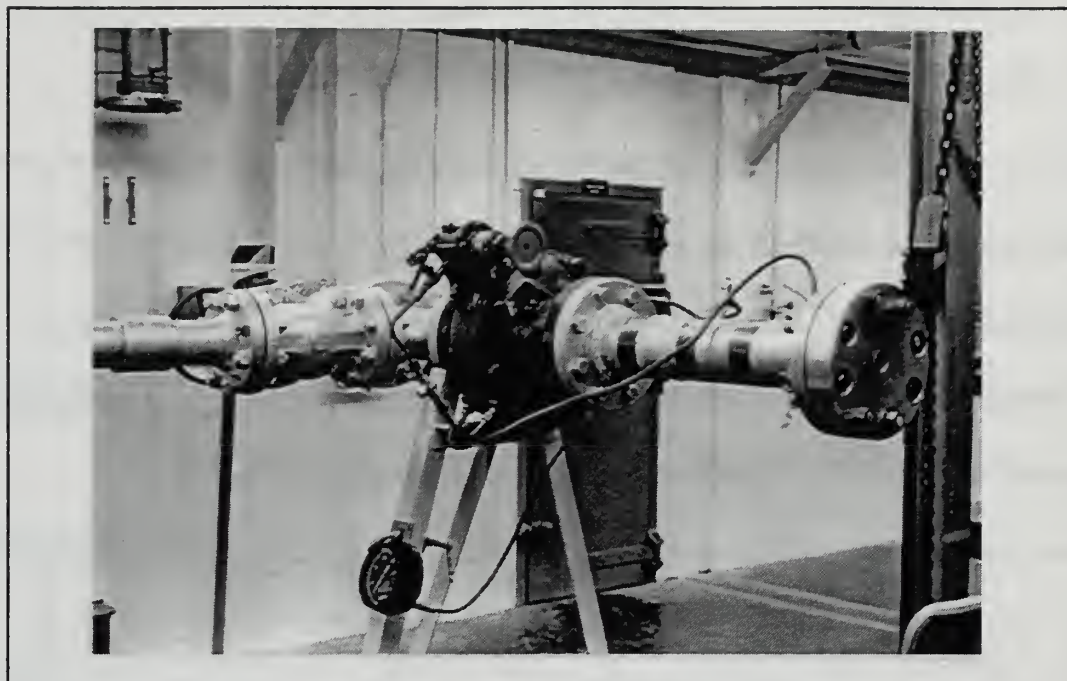


**Figure 6.** Underexpanded Jet Nozzle Apparatus

The flat plate used in the present work was a model designed and previously used for jet interaction studies in the supersonic wind tunnel. The plate was made of stainless steel with a leading edge diameter of 0.008 inches. Twelve of the existing pressure taps were chosen as close to the centerline of the plate as possible. Figure 7 shows a schematic of the surface of the plate showing the twelve taps relative to the centerline. The pre-arrangement of the taps, in addition to discovering two plugged ports, required that three offset taps be used to maintain near uniform spacing in the streamwise direction.

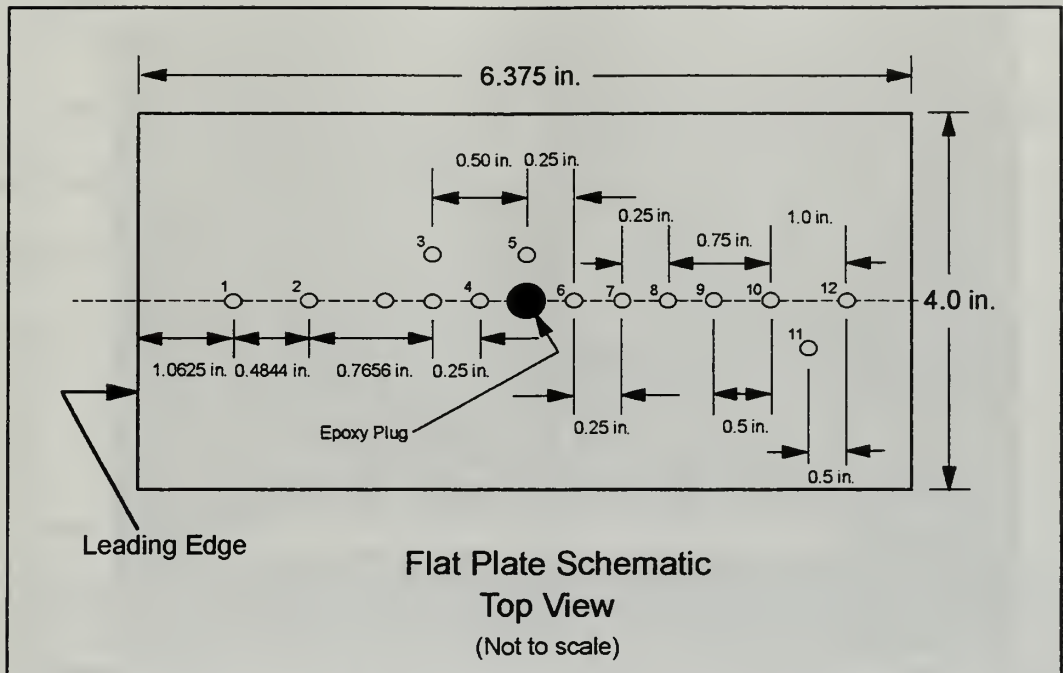


**Figure 7.** Schematic of the Pressure Port Arrangement on the Plate Surface

A simple bracket was made to mount the model so that the surface of the flat plate become a radial plane, effectively dividing the axi-symmetric jet in half. The bracket and model are shown in Figure 8 while Figure 9 illustrates this assembly mounted to the face of the jet. Plate washers were placed on the mounting bolts to create a 1/4 inch gap between the leading edge of the plate and nozzle face. This was necessary as it was found that the jet would not properly form if the plate were installed with its leading edge at the plane of the nozzle opening. Pneumatic pressure measurements were made using the Scanivalve ZOC system developed by Wendland [Ref. 17].



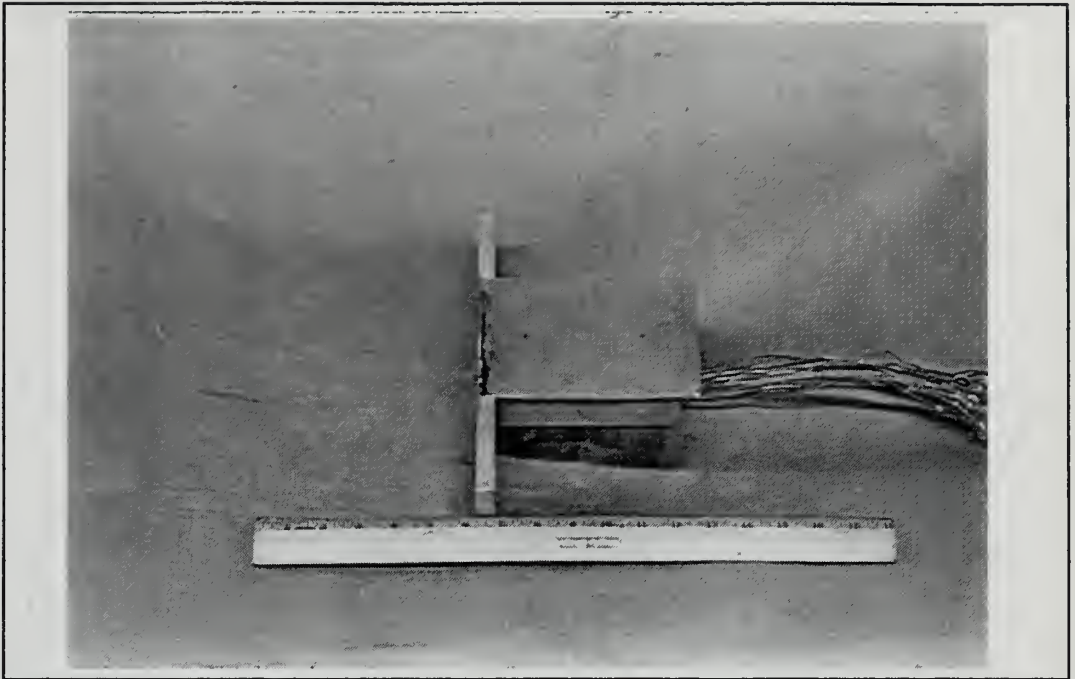


**Figure 8.** Bracket and Model Assembly

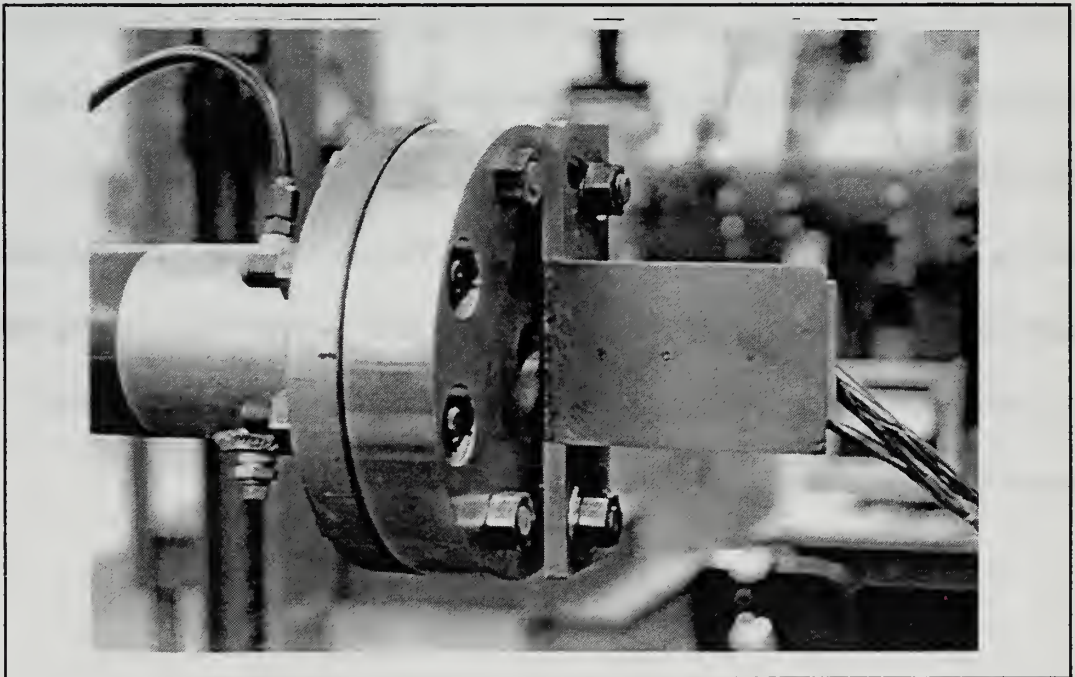


**Figure 9.** Bracket and Model Assembly Mounted to the Face of the Sonic Jet



## 1. Freestream Flow Field of the Underexpanded Sonic Jet

The mechanics of formation and structure of an underexpanded jet from a sonic nozzle have been studied in detail by Adamson and Nicholls [Ref. 18: p. 265]. A schematic of the structure is illustrated in Figure 10.

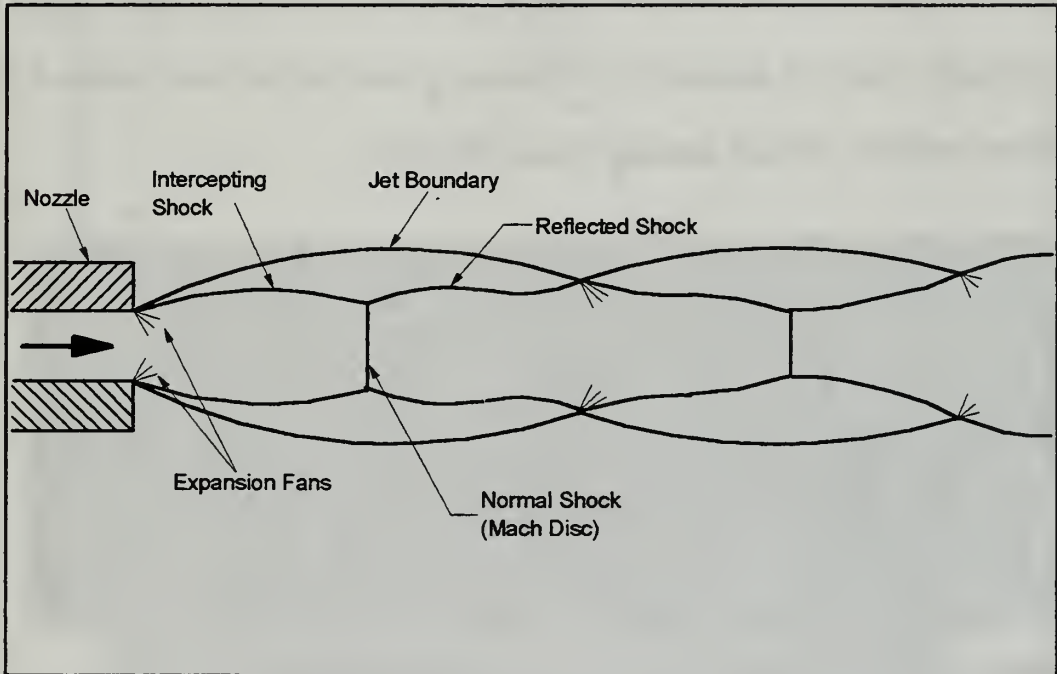


**Figure 10.** Sketch of Jet Structure Behind a Highly Underexpanded Nozzle<sup>5</sup>

The "Mach disc" within the free-jet offered an event that would produce a pressure discontinuity similar to that of the starting-shock structure in the supersonic wind tunnel, but without the visual restrictions imposed by thick test-section windows.

Using the schlieren technique, visualization studies of the flow field across the flat plate were recorded. The data acquired using the pressure-sensitive paint on the flat plate

---

<sup>5</sup>Figure 10 is found in Ref. 18, page 265, as Figure 1

could then be interpreted with reference to the flow structure. These studies began by observing the underexpanded jet without the flat plate mounted to the jet nozzle. This was done to provide a reference for changes in the flowfield as a result of the interaction with the plate. Since the jet structure was axi-symmetric, it was anticipated that, with the plate surface aligned along the centerline of the jet, the plate would simply isolate half of the jet structure. Figure 11 illustrates the jet structure without the flat plate installed at 65 psig plenum pressure. The flow proceeds from right to left.

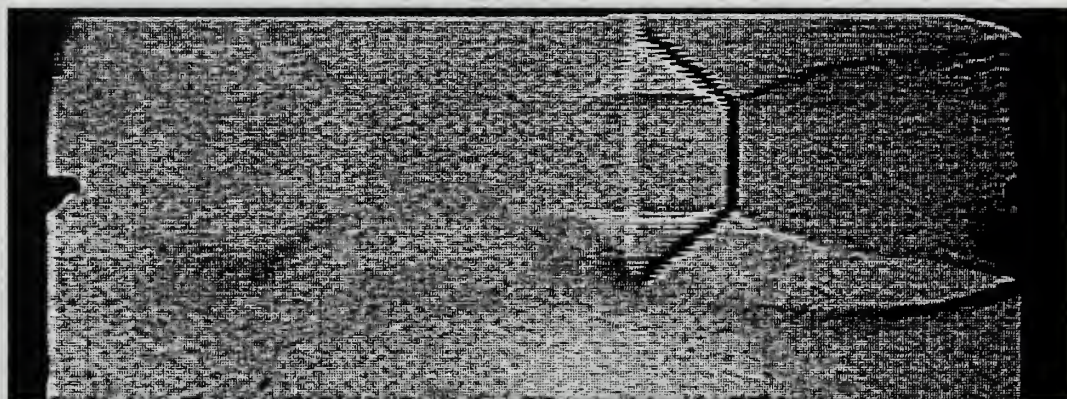


**Figure 11.** Underexpanded Free Jet at 65 psig Plenum Pressure

The flat plate was then bolted to the nozzle face and several runs were made at varying plenum pressures to record the shock structure. Three specific plenum pressures, 65, 80, and 90 psig were chosen as test points at which to compare pressure measurements with data using the luminescent paint, and the schlieren images of the flow field. The schlieren images of the three events and the corresponding pressure measurements from the orifices along the flat plate are illustrated in Figures 12, 13, and 14.

# PRESSURE DISTRIBUTION ACROSS FLAT PLATE

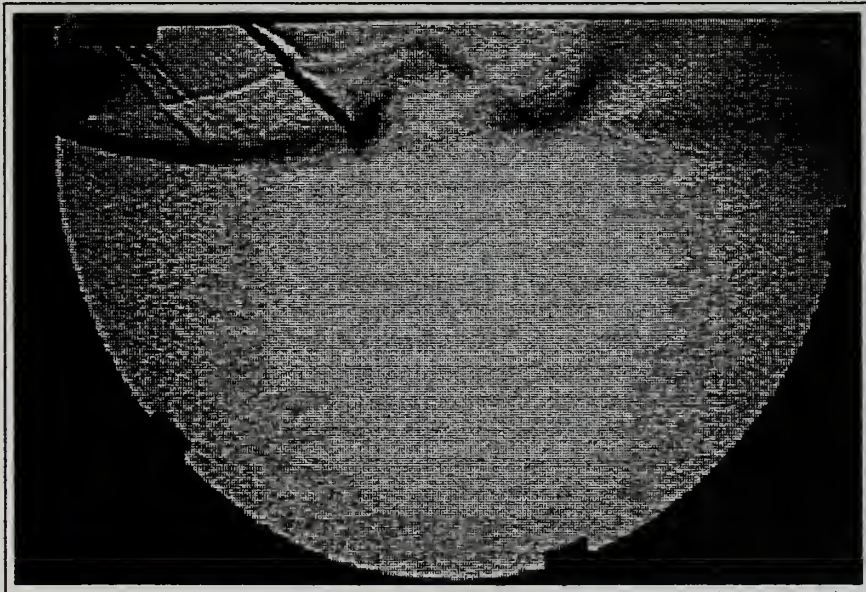
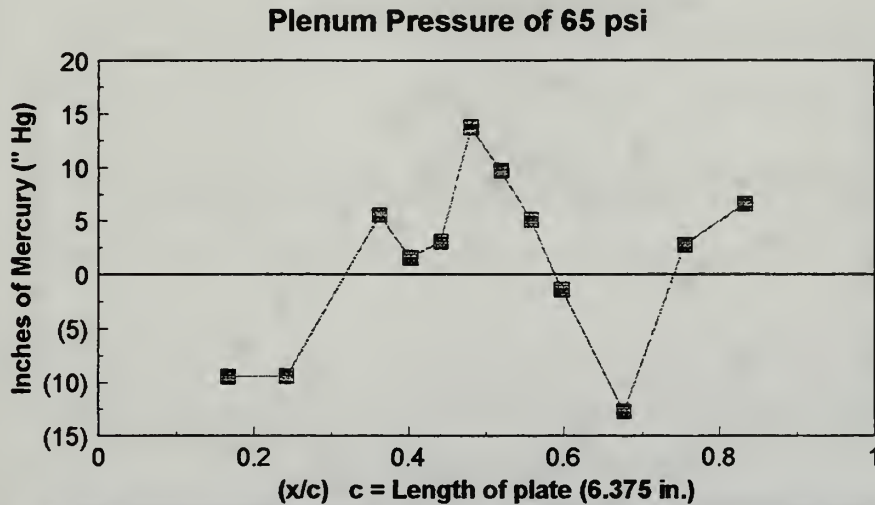


**Figure 12.** Flow Visualization and Pressure Distribution Across Flat Plate at 65 psig  
(Flow is from left to right)



# PRESSURE DISTRIBUTION ACROSS FLAT PLATE

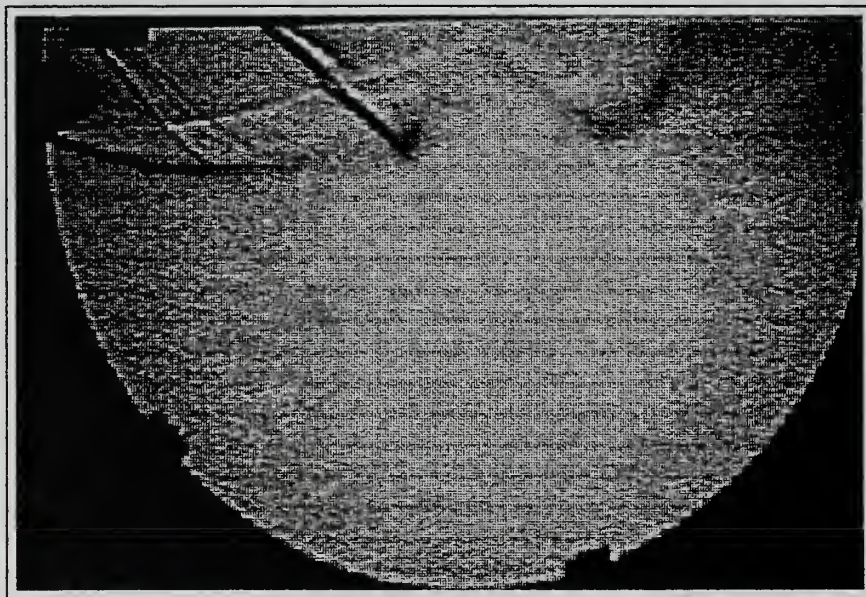
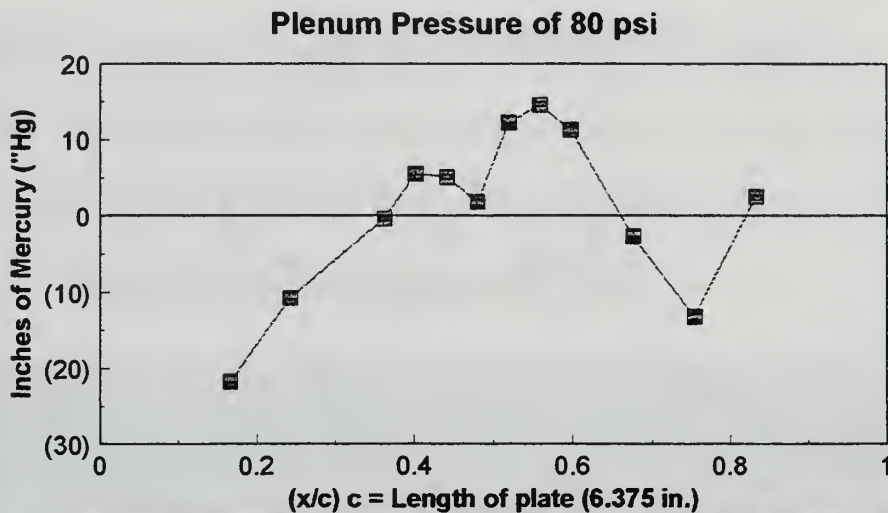


**Figure 13.** Flow Visualization and Pressure Distribution Across Flat Plate at 80 psig  
(Flow is from left to right)

# PRESSURE DISTRIBUTION ACROSS FLAT PLATE

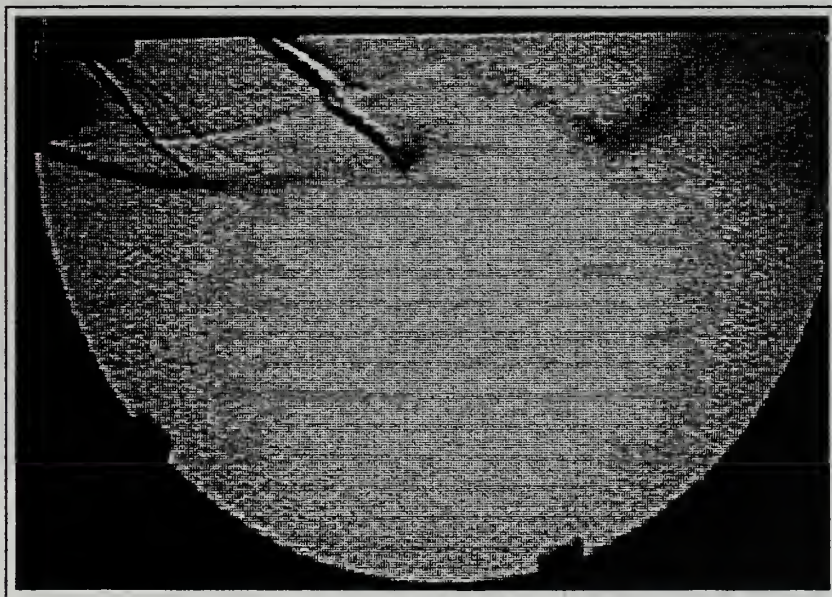
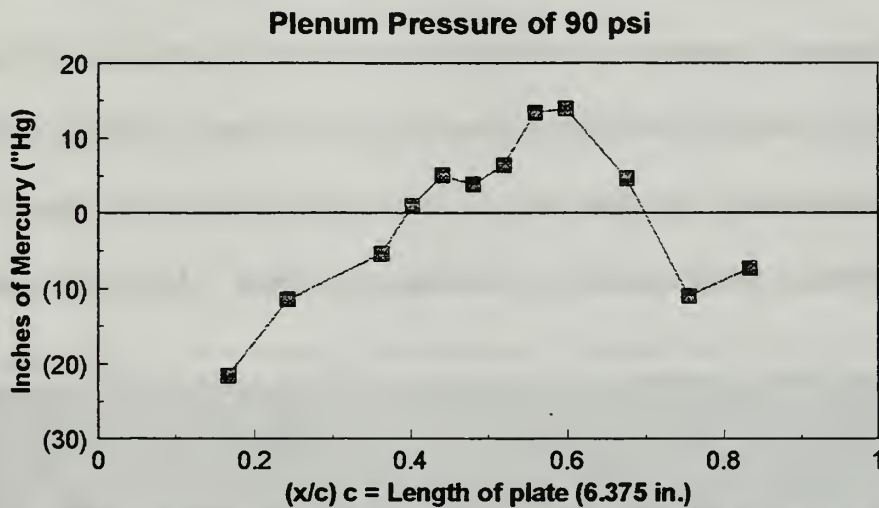


**Figure 14.** Flow Visualization and Pressure Distribution Across Flat Plate at 90 psig  
(Flow is from left to right)



The images and the pressure measurement graphs have been aligned so that the pressure changes seen on the graphs correspond to the events occurring on the plate surface.

As can be discerned from the schlieren images in Figures 12, 13, and 14, two oblique shocks appear, a consequence of the plate being placed in the flow field. Figure 15 shows a comparison of the flow fields with and without the plate. The oblique shock emanating from the leading edge of the plate can be explained as being due to the underexpanded process the flow undergoes as it leaves the nozzle. The flow, as it exits

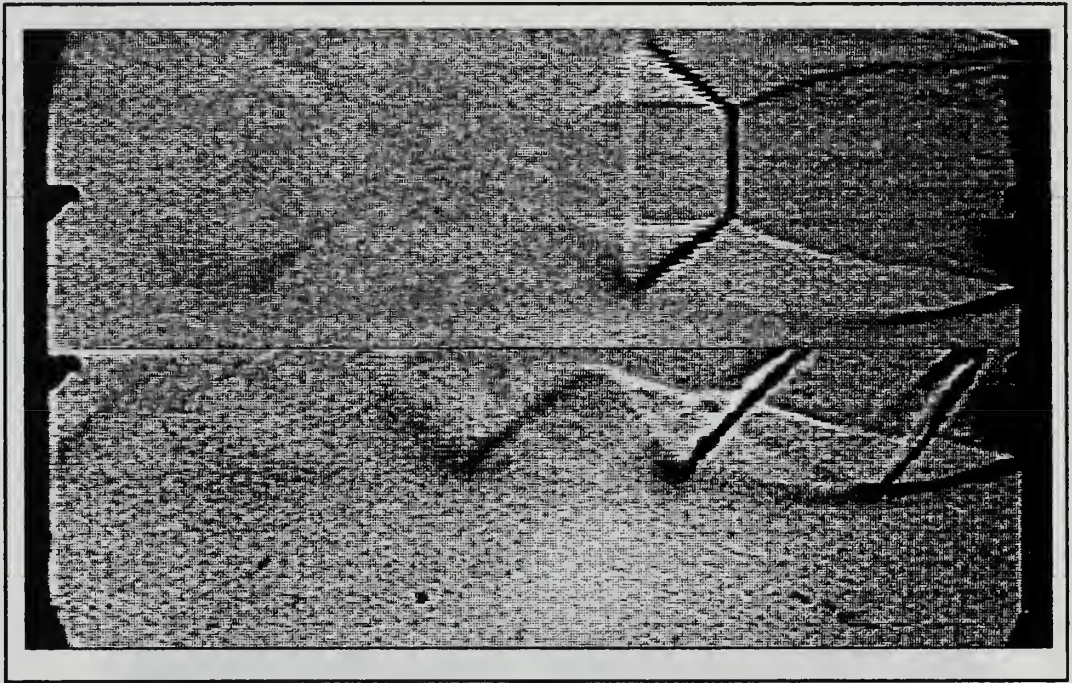


**Figure 15.** Flow Field Comparison Without (Top) and With (Bottom) the Flat Plate the nozzle, is off-axis with respect to the centerline of the plate thus encountering the plate at an incidence angle other than zero degrees. The flow in these images is from right to left.

The second oblique shock's structure gives the perception that it extends from the surface of the plate to the jet boundary; however, closer examination of the two images in Figure 15 shows that the oblique shock actually merges with the reflected shock (see Figure 10) giving the erroneous illusion of a single entity. Of greater interest is the extent of the oblique shock to the point of total suppression of the normal shock. The sensitivity of the flow to the plate was much greater than first thought, and it was unclear what events were taking place to justify the magnitude of the oblique shock. Additional study seemed warranted.

#### ***a. Further Flow Field Studies***

To visualize the flow, methanol was injected through the second pressure port in the plate surface. Several light fixtures were placed around the plate to better illuminate the injection area and to provide contrast between the background and flow field. A video recorder was used to record the events.

Figures 16 through 18 show the sequence of events from selected frames of the video at two different vantage points. In each set of images, the flow proceeds from left to right.

In Figure 16, the plenum pressure was steady at 30 psig -- the boundary layer up to this point remained attached. At 38 psig, Figure 17 shows initial indications of reversed flow at the center of the plate. In addition, 1/2 inch to the left of this point, a pooling of methanol formed. This behavior indicated the presence of a bubble in which a



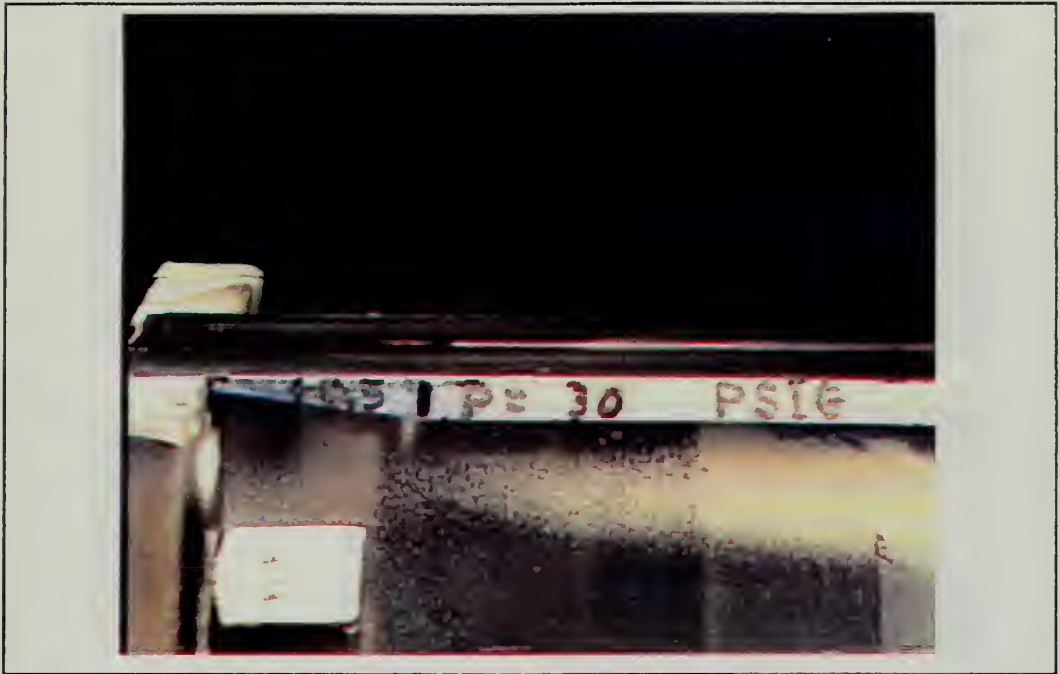


**Figure 16a.** Flow Visualization at 30psig -- Cross Flow View

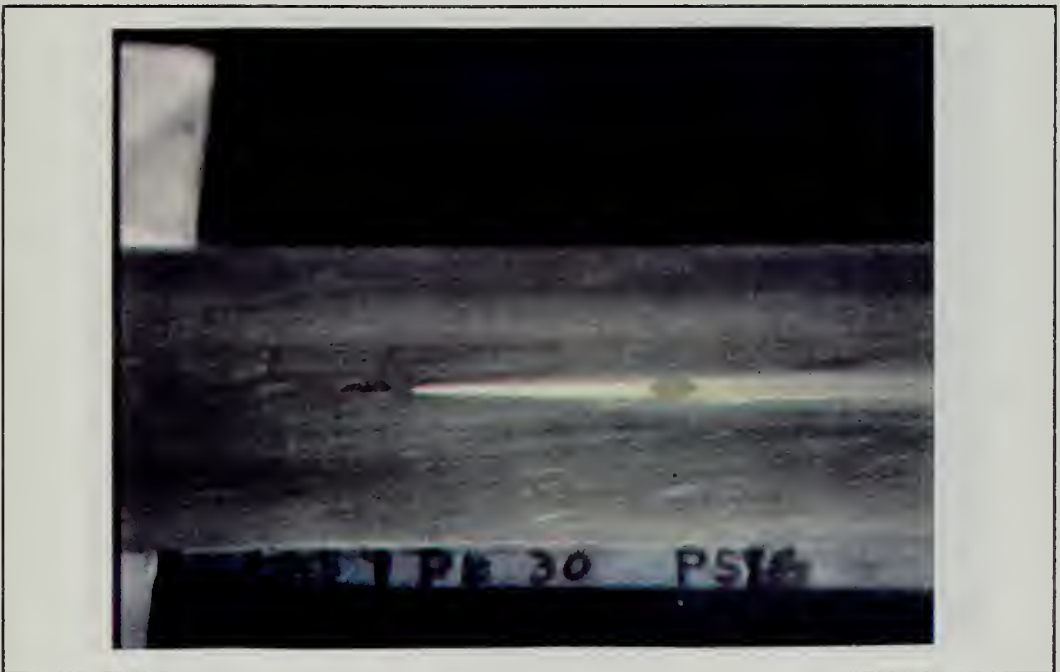


**Figure 16b.** Flow Visualization at 30 psig -- Acute View







**Figure 17a.** Flow Visualization at 38 psig -- Cross Flow View



**Figure 17b.** Flow Visualization at 38 psig -- Acute View





**Figure 18a.** Flow Visualization at 65 psig -- Cross Flow View

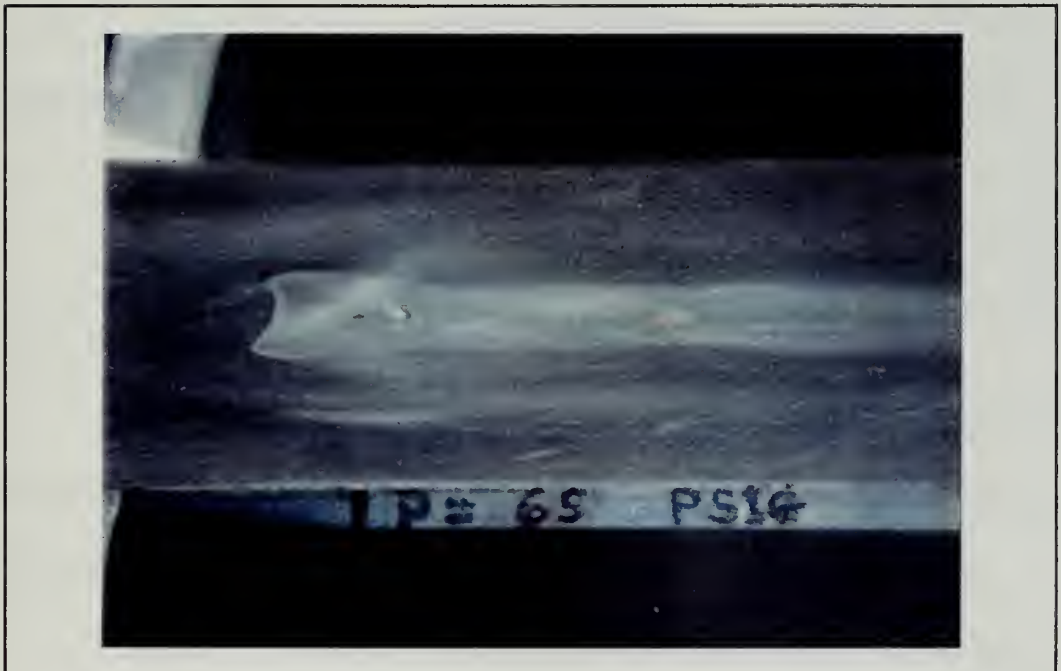


**Figure 18b.** Flow Visualization at 65 psig -- Acute View



portion of the injected mass would be expected to stagnate near the separation point, as the flow re-circulated within the bubble's boundaries. This is more clearly shown in the schematic of Figure 19. With increasing plenum pressure, the separation and recirculation region of the flow field gradually moved downstream, eventually encompassing the injection port, and allowing the alcohol to more clearly define the boundary of what was indicated to be a separation bubble.

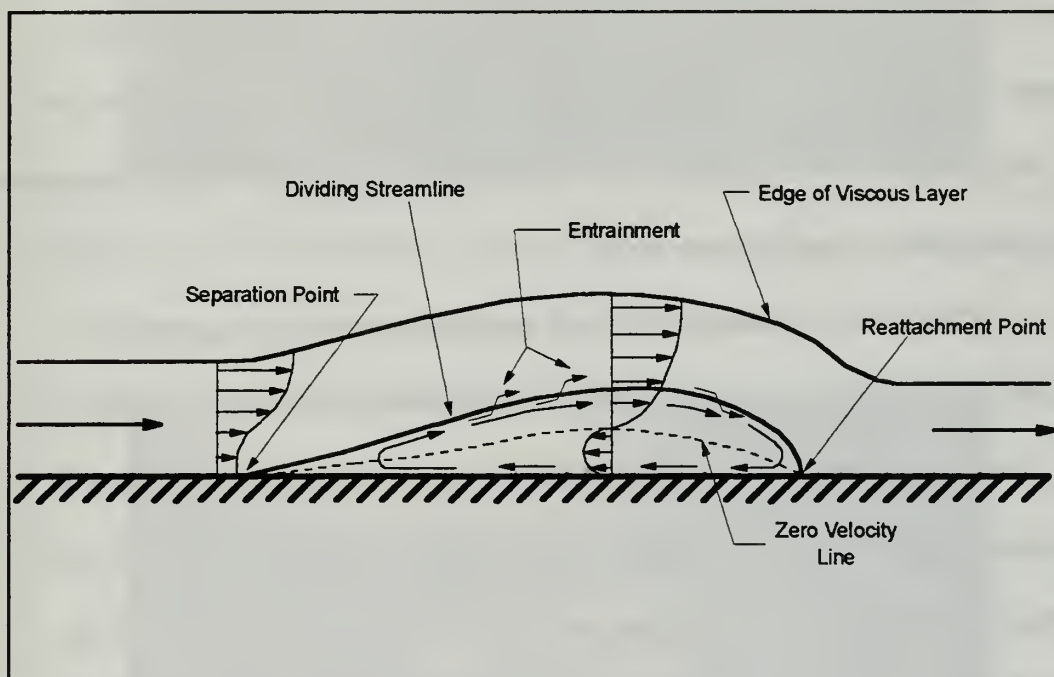


**Figure 19.** Details of Separation Bubble

To verify whether flow reattachment was in fact occurring downstream, a second injection port, port number 5, was rigged to concurrently admit methanol into the flow. Figures 20 through 23 show the sequence of images recorded in one such test.

Figure 20 shows that at 25 psig, attached flow was prevalent. At 40 psig, in Figure 21, the injectant at the first port (port number 2) indicated the presence of reversed



flow, while the injectant at the second port (port number 5) continued to indicate attached flow. The vortex patterns are an indication of the pressure gradients that exist within the bubble. In Figure 22, with the plenum pressure at 68 psig, the first sign of reversed flow is evident at the second injection port, while Figure 23 shows the port fully immersed in reversed flow at 75 psig.

The orientation of the plate relative to the centerline of the nozzle exit, and thus the centerline of the flow, was found to be 89.7 degrees. Since alignment could significantly influence the flow characteristics, the plate's inclination was changed to 90.3 degrees and the test runs were repeated. No dissimilarities between the results obtained at corresponding plenum pressures were noted.

The evidence of reversed flow and reattachment strongly suggested the presence of a closed separation bubble within the underexpanded jet when the plate was present. The apparent extent of the bubble, reaching 3/8 to 1/2 inch above the plate, is very surprising. However, it is consistent with the oblique shock in place of the normal shock. Further data are needed, such as impact probe measurements, in order to fully define the flow structure. For the present purpose, which was the investigation of pressure sensitive paint, this was not needed.



**Figure 20.** Flow Visualization at 25 psig



**Figure 21.** Flow Visualization at 40 psig





**Figure 22.** Flow Visualization at 68 psig



**Figure 23.** Flow Visualization at 75 psig





## B. OPTICAL MEASUREMENT SYSTEM

The measurement system was composed of three main components: (1) the luminescence coating, (2) the illumination source, and (3) the luminescence detector and associated data processing hardware and software. Each component is discussed individually below. A schematic of the system used in conjunction with the free jet apparatus is illustrated in Figure 24.

### 1. Luminescence Coating

The luminescence coating used in the present work was developed by the Chemistry Department at the University of Washington and was provided, as a sample, by the NASA-Ames Research Center.

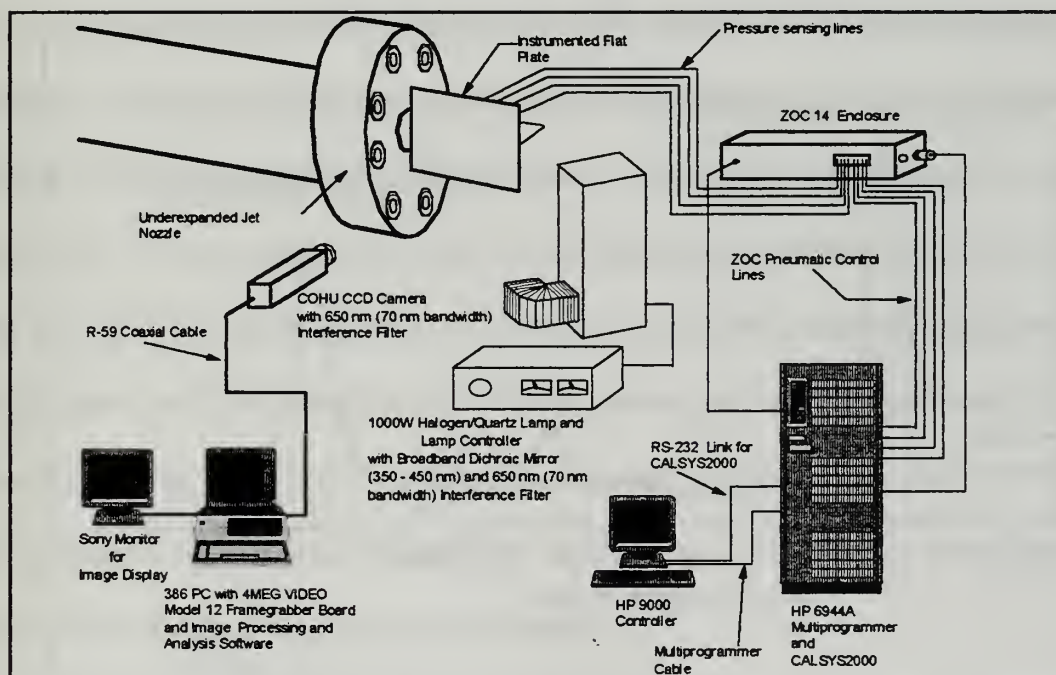


**Figure 24.** Schematic of Pressure Measurement System

The coating contained platinum octaethylporphyrin (PtOEP) as its active molecule. PtOEP has characteristics of high luminescent quantum yield (~90%), short triplet life (~100 micro seconds), and a high sensitivity to oxygen quenching [Ref. 1: p.35]. Figure 25 shows the excitation and emission spectra for the molecule. Excitation (absorption) peaks at 380 or 530 nm, whereas luminescence peaks at 650 nm.

The coating mixture consisted of the active molecule dispersed in a Genessee GP-197 polymer-resin solution. The concentration was 0.1 gm of PtOEP per liter of polymer resin [Ref. 19]. When the mixture was applied to the surface, the solvent evaporated leaving a hard, thin film of PtOEP dissolved in an oxygen-permeable polymer [Ref. 9: p. 35]. Several undesirable characteristics associated with this coating are described in Appendix B.

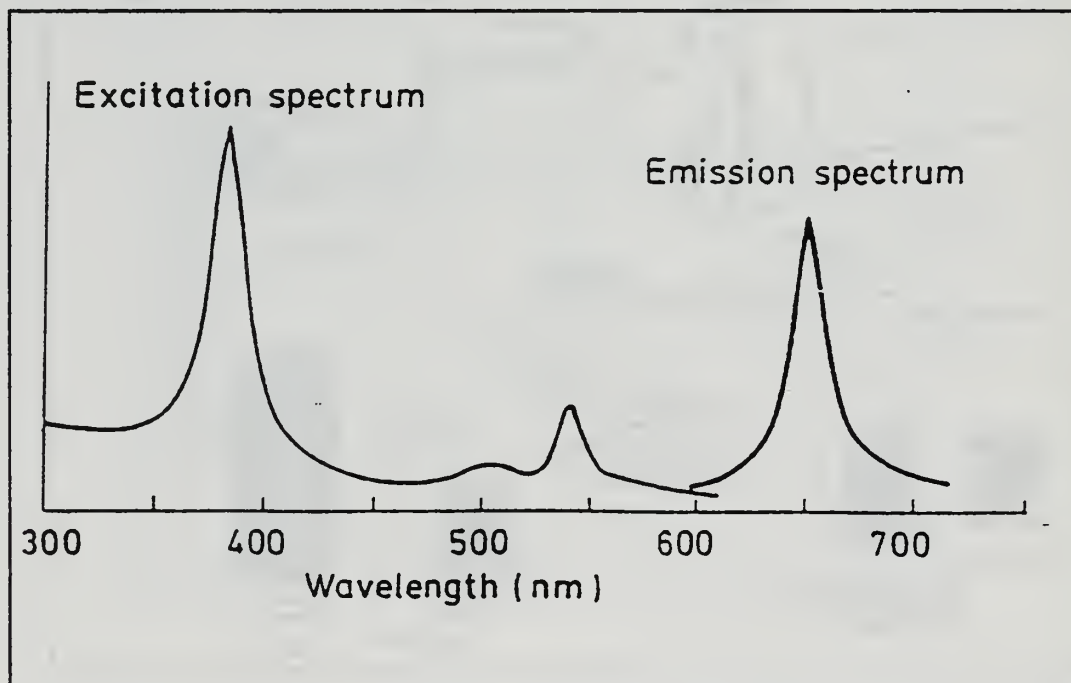


**Figure 25.** Excitation and Emission of Platinum Octaethylporphyrin

### *a. Reflective Backing*

Before applying the luminescent coating to the surface, a white backing was first applied. A significant improvement in luminescence performance was thereby gained [Ref. 9: p. 32], allowing the camera to see a larger signal and an enhanced signal to noise ratio.

The particular type of white paint used for this backing was an important consideration. Kavandi [Ref. 9: p. 33] found that some paints tend to darken after long exposure to air and ultraviolet light. Krylon glossy-white spray paint (#1501) reportedly offered the greatest resistance to this effect and was therefore used in the current work.

## **2. Illumination Source**

McDonnell-Douglas [Ref. 6: p. 3] considered several types of illumination sources to provide an adequate number of photons within the appropriate excitation wavelength of the paint. The results showed that tungsten-halogen incandescent sources were the most suitable in terms of compatibility and performance. Although the data in Figure 25 would suggest that arc lamps emit more energy in the excitation range of the coating, they also emit an EMF pulse that is damaging to CCD arrays. In addition, tungsten-halogen lamps are extremely stable, with minimum intensity fluctuations, and any such variations will directly effect the accuracy of the results. Consequently, an Oriel Corporation 1000 W quartz tungsten-halogen lamp, Model 66200, and the associated controller, Model 6405, were selected for the present measurement system.

Spatially-uniform illumination was also essential to reduce measurement errors. (According to McDonnell-Douglas [Ref. 6: p. 4], this is especially true when the surfaces are highly curved). Non-uniformity was found when the published procedures [Ref. 20: p.13] were followed to produce a collimated beam from the light source. The procedure resulted in generating a focused image of the filament in the lamp. However, by reversing the orientation of the barrel containing the lenses, a greater range of adjustment was achieved. Figure 26 illustrates this modification, which made it possible to produce a more uniform beam, although a slight degradation in spectral intensity was noted.

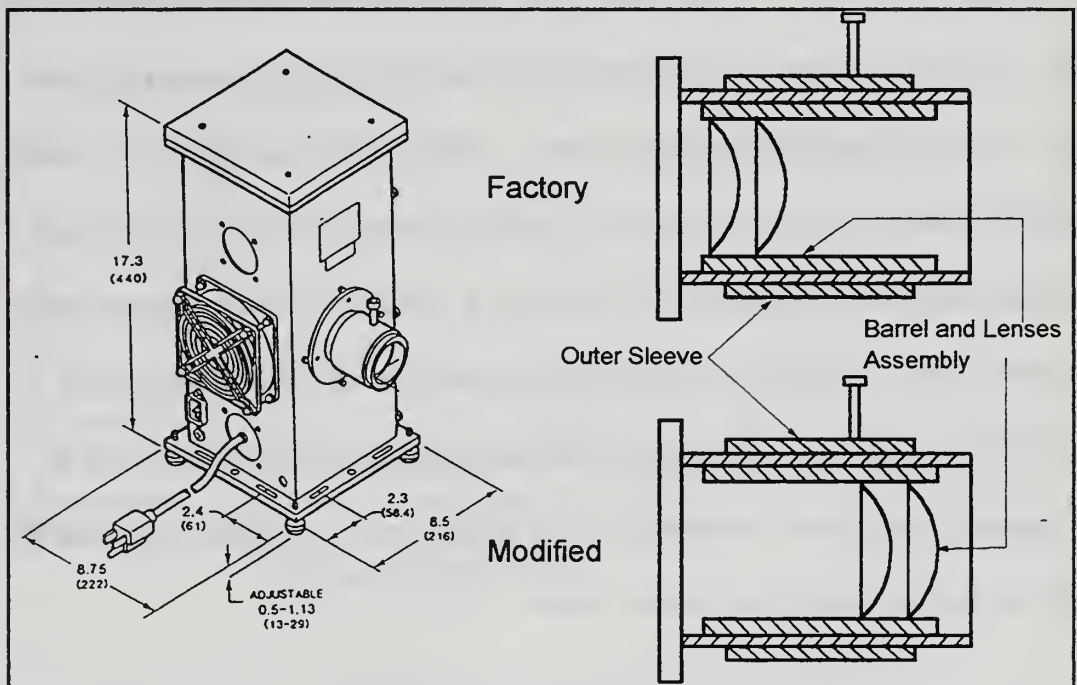


**Figure 26.** Modification of Focusing Assembly of the Light Source



### *a. Filters*

The use of a broad-band light source mandated the use of filters to ensure that the appropriate wavelength for excitation of the luminescence was allowed to pass while blocking unwanted light. Unwanted light was that which would pass through the narrow-band filter that was installed on the camera.

As Figure 25 shows, there are two wavelengths at which excitation of the luminescent paint is optimum. Although either wavelength could have been used, the 380 nm wavelength was chosen because of its greater separation from the emission wavelength of 650 nm. This also had the advantage, as discussed in [Ref. 6: p. 5], of allowing a filter with a more gradual cutoff to be used which would allow more light energy to be utilized to excite the paint.

A combination of filters was used in the illumination system to isolate the 380 nm wavelength. The source beam first passed through a dichoric or cold mirror, Oriel Model 66228, which had a spectral range of 350 - 450 nm and a cut-off frequency of 550 nm [Cold mirrors are oriented at 45 degrees relative to the incoming beam from a source. The infrared wavelengths are transmitted undeviated, while the ultraviolet wavelengths are reflected through 90 degrees. This prevents the infrared from being reflected back to the source and overheating the system.]

The source light was then directed through an Oriel interference filter, Model 57521, having a bandwidth of 70 nm centered at 400 nm. The filters were installed in a 90



degree beam turner and mirror holder, Oriel Model 66246, which was fitted to the lamp housing.

Finally, the camera used to record the emitted luminescent energy from the paint had a 650 nm interference filter with a 70 nm bandwidth, Oriel Model 57610, mounted over its lens to block out all other frequencies.

### **3. Detection System**

Luminescent data were acquired using a COHU Model 4910 high performance, monochrome, low-intensity CCD camera and transferred to a framegrabber board in a 80386 PC using an R-59 coaxial cable. The camera was fitted with a Cosmocar 16 mm, f/1.4 lens. To ensure the output signal would be linearly proportional to light intensity received, the camera was configured with the gamma set equal to one and the automatic gain control (AGC) disabled [Ref. 2: p. 3342]. The camera's spectral response, as shown in Figure 27, shows that its relative response at 650 nm is approximately 65%.

The camera produced a frame every 1/30 of a second and thus was limited to recording pressure fluctuations at rates less than 30 Hz. [A simple test to determine if the illumination system was bleeding over into the detection system was to illuminate an unpainted surface (i.e., no luminescent paint) and then direct the camera towards this surface to see if any spurious light was being detected. None should be present].

The analog output signal from the camera was initially digitized using an IDEC Supervision 16 framegrabber board residing in a 80386-based PC. The raw data were then reduced and analyzed using "Image Pro Plus" analysis and processing software.

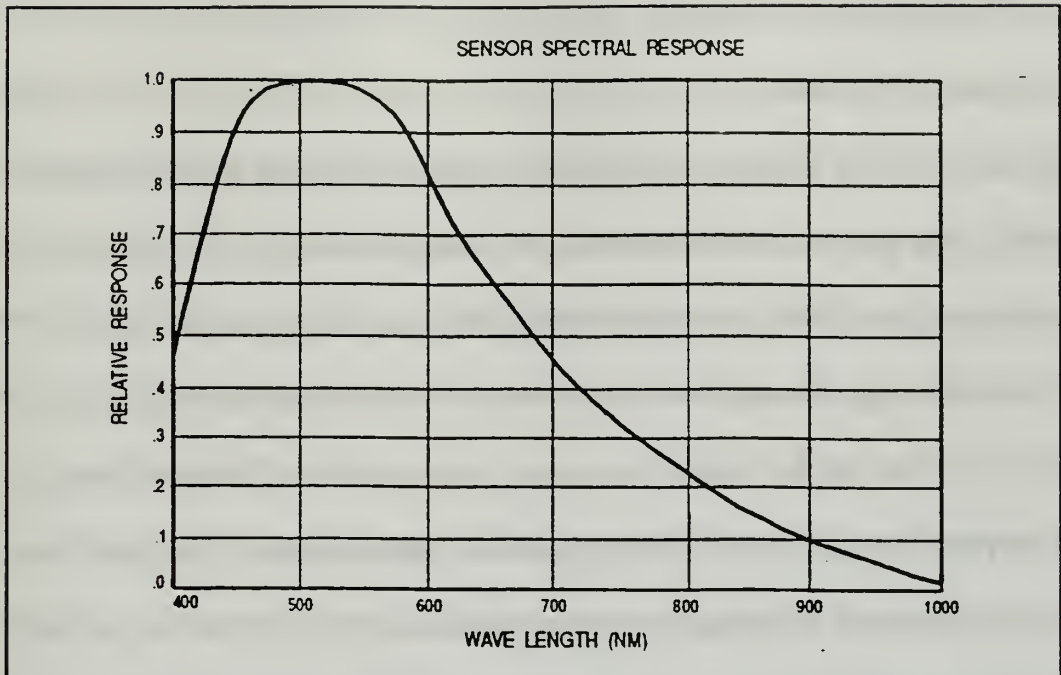


**Figure 27.** Spectral Response Curve for the COHU Camera Model 4910

However, this hardware/software combination was extremely limited in application resulting in long data acquisition periods and time-consuming data reduction. Because of the characteristic degradation of the luminescent coating, the accuracy of the data was questionable.

The initial hardware/software combination was replaced with a much more versatile Epix 4MEG Video Model 12 framegrabber board and software which included image analysis and processing programs. The spatial resolution of the framegrabber was operator adjustable, thus a balance between sampling resolution and the board's memory storage could be tailored to a given application. For the underexpanded-jet and flat-plate work, the spatial resolution was set to 752 x 480, the highest resolution setting. The gray-level resolution of the board was 8-bits.

## C. EXPERIMENTAL PROGRAM

### 1. Flat Plate Preparation

The surface of the flat plate was cleaned with acetone, ensuring the removal of all oils and dirt. Fine wire was then inserted into each of the pressure ports to prevent paint from entering the holes. The white Krylon undercoating was then applied in a series of three to four thin coats, allowing four to five minutes between coats. Ten minutes after applying the last coat, the fine wires were removed from the ports. This was necessary to prevent the paint from drying on the wire. [Significant portions of the undercoating could be removed from around the pressure port when extracting a wire to which the paint had hardened]. At this point, the white undercoating was allowed to dry for one hour.

Prior to the application of the pressure-sensitive paint, the fine wires were re-inserted into the ports. The luminescent coating was then applied to the surface using a standard hobby airbrush. The nitrogen supply in the Gas Dynamics Laboratory was used as the pressure source for the airbrush (instead of shop air) as it offered a contaminant-free pressure source. With a properly adjusted airbrush and a good painting technique, continuous application of the luminescent coating to the surface could be achieved until the surface was "suitably" covered. Although Kavandi *et al* [Ref. 2:p. 3343] refers to normal coating thickness as being in the range of 5 to 15 micrometers, it was both impractical and unnecessary to measure the coatings to determine if the paint fell within these prescribed limits. The approach used in the present work was simply to observe when the pigment of the pressure-sensitive paint seemed insensitive to further application,

and that the texture of the surface appeared smooth. Several attempts were necessary to develop the technique and the judgement in applying the luminescent coating. Three to four minutes after the completion of the coating, the fine wire were removed. Once the model was installed for testing, sufficient time had elapsed for the coating to have properly cured. Note that it was important to avoid touching the painted surface at any time since body oils could adversely affect the behavior of the luminescent coating.

## **2. Experimental Procedure**

Setting the video resolution for the framegrabber to the maximum (752 x 480) resulted in 11 frame buffers being available to store for image data. The controlling software for the framegrabber was capable of capturing a sequence of images, digitizing them, and storing each image of the sequence in consecutive image buffers, the number of buffers used in the sequence (from one up to the number of available buffers) being specified by the operator. Because of the limitation of collecting only 11 images for each execution of the sequence algorithm, and the fact that averaging one hundred images was desirable to obtain noise-free data, for each of the wind-on and wind-off conditions, ten runs were executed. (10 frame buffers vice 11 buffers were utilized). Since the underexpanded free jet was a steady and repeatable event, this method of collecting data was a feasible solution for the limited memory of the frame-grabber board.

The data for the wind-off condition was collected first. The flat plate was illuminated with the tungsten-halogen light source while the laboratory lights were turned off, preventing any spurious wavelengths from entering the camera and offsetting the



image data. A real-time image of the plate was displayed on the image monitor so that the camera output could be adjusted for the best quality picture using a combination of focus, manual gain, and lens iris. Manual gain was necessary because of the low light condition, but care had to be exercised because with an increase in gain there was an accompanying increase of noise introduced into the image. The shutter speed for the camera was set to off.

After the first sequence of images was captured and stored in the frame buffers, the light source was switched off to minimize the degradation to the paint. The light source was such that the line voltage applied to the lamp housing was adjustable; however, power was ultimately controlled with an on/off switch. Thus, the same illumination intensity was maintained each time the lamp was turned on.

The ten images were averaged together to form a single image. The single image was saved to a floppy disk. The light source was again switched on in preparation for the second sequence of images, allowing time for the luminescent coating to reach its maximum intensity. (This is referred to as the "induction period", which is explained in Appendix B). The second sequence of images was then captured and stored, and the tungsten-halogen lamp shut-off. The images were averaged to give a single image and again saved to floppy disk. This routine was executed until ten averaged images for the wind-off condition had been saved to floppy disk. Each sequence of capturing the data took less than one minute.



The procedure for obtaining images for the wind-on condition was similar. With the light source on and the plate properly illuminated, the underexpanded-jet apparatus was started. Once the desired pressure was set using the plenum control valve, and the pressure was stabilized, the imaging sequence was executed. When the software had completed its routine, the jet was shutdown and the light source turned off. The jet apparatus was equipped with a shutoff valve so that the jet could simply be turned on and off without disturbing the setting of the plenum control valve. This ensured repeatability of the event for each sequence of 10 images.

It is important to note that throughout these events, the camera and light source had to remain fixed, spatially, with respect to the plate. In addition, no adjustments of any kind could be made to the instruments or equipment. Any deviations would introduce errors into the results.

Conventional pressure data were obtained concurrently with the luminescent paint data using the CALSYS2000 data acquisition system [Ref. 17]. Twenty samples per port using a data collection rate of 33 Hz were obtained and averaged together. These pressure data would be used later in the calibration process. Ambient pressure and temperature were also recorded.

### **3. Image Data Reduction**

#### ***a. Image Processing***

Several image-processing techniques were used to manipulate the data in order to obtain the desired result. The techniques are described individually below.

Appendix C provides a summary of the steps used in operating the EPIX software for acquiring, processing, analyzing, and reducing the data.

Round-off error from the image processing routines was a concern. To ensure against loss of accuracy due to round-off error, the system hardware had to be capable of doing at least 16 bit arithmetic. The EPIX frame grabber board was capable of conducting 32-bit operations. When the image was processed, the 8-bit intensity values for each pixel in the image were first converted to 32 bit words. Once the processing was complete, the modified values of each pixel were converted back to an 8-bit format for display. If the mathematical operations were conducted with anything less than 16-bit precision, all significant digits would be truncated.

(1) Averaging. The emission of photons from any source is a random process following a Poisson distribution, and the number of photogenerated carries collected in a potential well of the camera array (see Appendix D for an explanation on the operation of a CCD camera) in time "t" is thus a random variable. The standard deviation of this random variable is referred to as photon (shot) noise. This noise is a fundamental limitation in all imaging applications since it is a property of light itself, not of the image sensor.

By averaging a sequence of images, the signal-to-noise ratio of the data has been found to be significantly improved. This process has the effect of reducing the scatter in the luminous intensity measurement [Ref. 6:p. 8]. McDonnell-Douglas [Ref. 6]

has found that as few as eight images averaged together showed a marked reduction of noise on the signal.

The reason for choosing one hundred images for each of the wind-on and wind-off conditions was the prior experience in the work conducted by NASA-Ames, the University of Washington, and McDonnell-Douglas. In each case, one hundred images was adopted in all work done to date.

The ten averaged images of the wind-off condition were loaded into ten frame buffers of the EPIX framegrabber board. As with the initial averaging of the raw image data, the ten buffers were averaged together to form a single image. This single image, a result of averaging one hundred "raw" images together, was then saved to floppy disk. The corresponding wind-on images were averaged in a similar manner, and the resultant image saved with its wind-off counterpart.

The procedure used in averaging the data in the present work was slightly different than used at NASA-Ames, the University of Washington, and McDonnell-Douglas. In those cases, one hundred images were collected and then averaged in one step. In the present work, ten averaged images were averaged to form the final image. Again, this is a result of the limited memory available on the frame grabber board. However, since each image has a random distribution of data associated with it, the averaging technique used will have little effect on the outcome of the result.

The significance of image averaging can be seen in Figures 28 through 30. In each figure, an image and a graphical distribution along a single line of pixel values in

the image is shown. Figure 28 shows a single raw image of the wind-on condition at 80 psig. Figure 29 shows the effect of averaging ten wind-on images together and Figure 30 shows one hundred images averaged together. In each figure, an image and a graphical distribution along a single line of pixel values in the image are shown.

(2) Dark Current. Appendix D details what dark current is and how it affects the storage of photogenerated carriers in the potential well of a photo-sensitive array element. The effect of the dark current on an image is that it produces an offset in which the zero incident light condition does not correspond to the zero grey level. To correct for this offset, a "dark" image was acquired and then subtracted from the wind-off and wind-on conditions.

To acquire a dark image, a lens cover was placed on the lens prohibiting any light from striking the CCD array, and then an image was acquired. One hundred images were taken and averaged as was done with the wind-on and wind-off conditions. A dark image was generated after each of the wind-on runs. Analysis of the dark current image showed that 1 to 2 grey levels were present, which were the levels subsequently subtracted from the wind-off and wind-on images.

(3) Registration. When a pixel-to-pixel comparison of two images of the same object field taken from the same sensor at different times is desired, it is necessary to spatially register the images to correct for relative translational shifts, rotational shifts, and geometrical distortions. In the general case, this is accomplished in the software



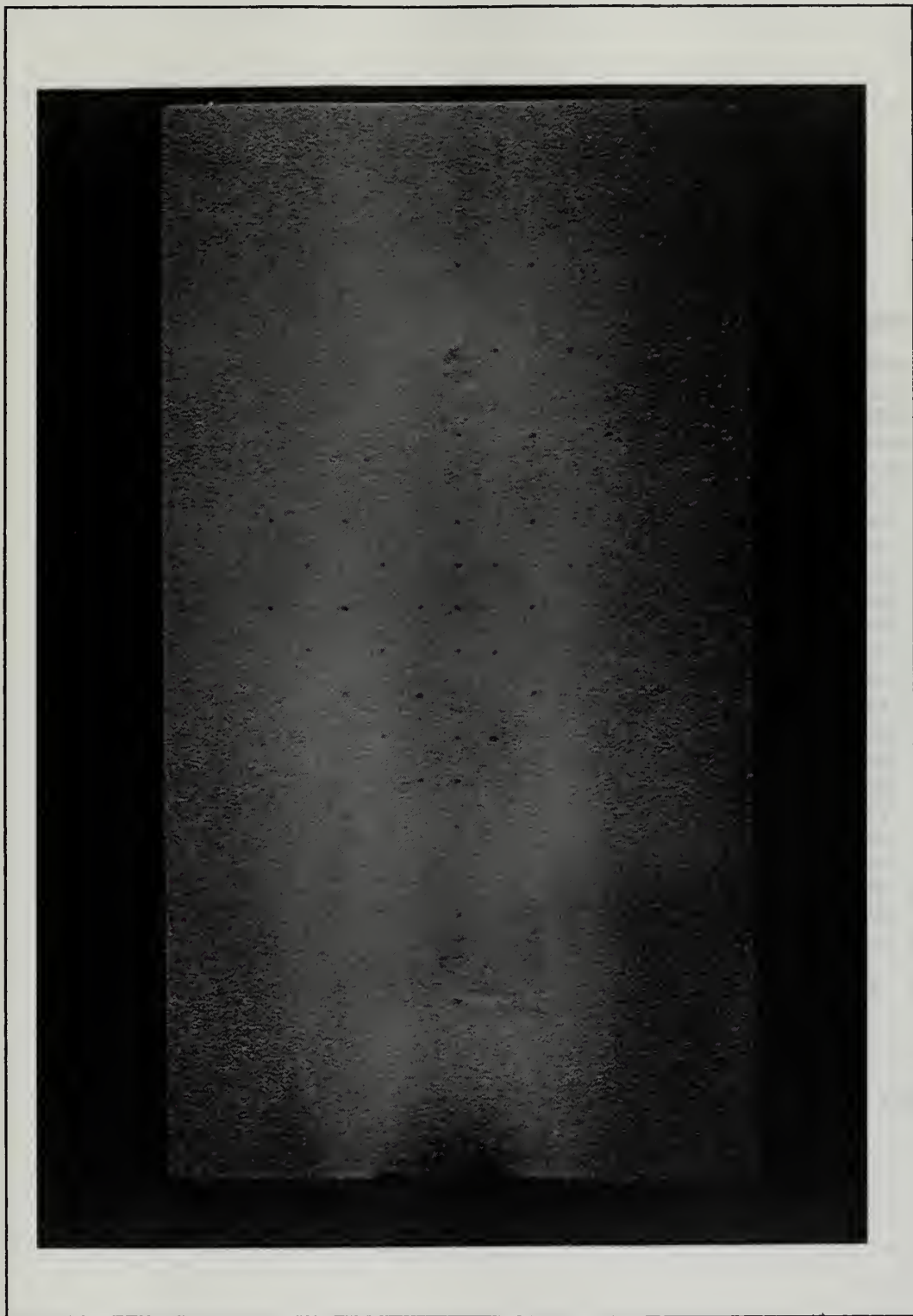


**Figure 28a.** Single Image of the Underexpanded Jet Across the Flat Plate at 80 psig



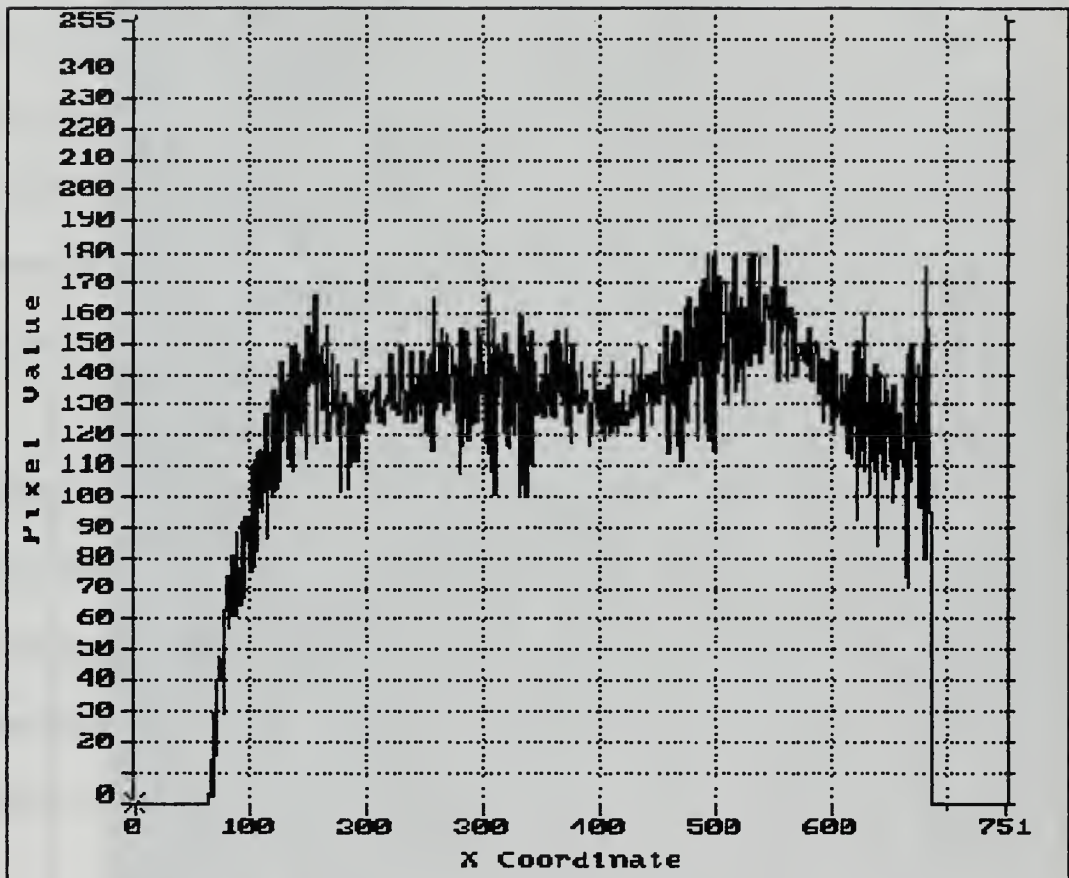


Figure 28b. Graphical Representation of a Single Line of Pixels of a Single Image



**Figure 29a.** Ten Averaged Images of the Underexpanded Jet Across the Flat Plate

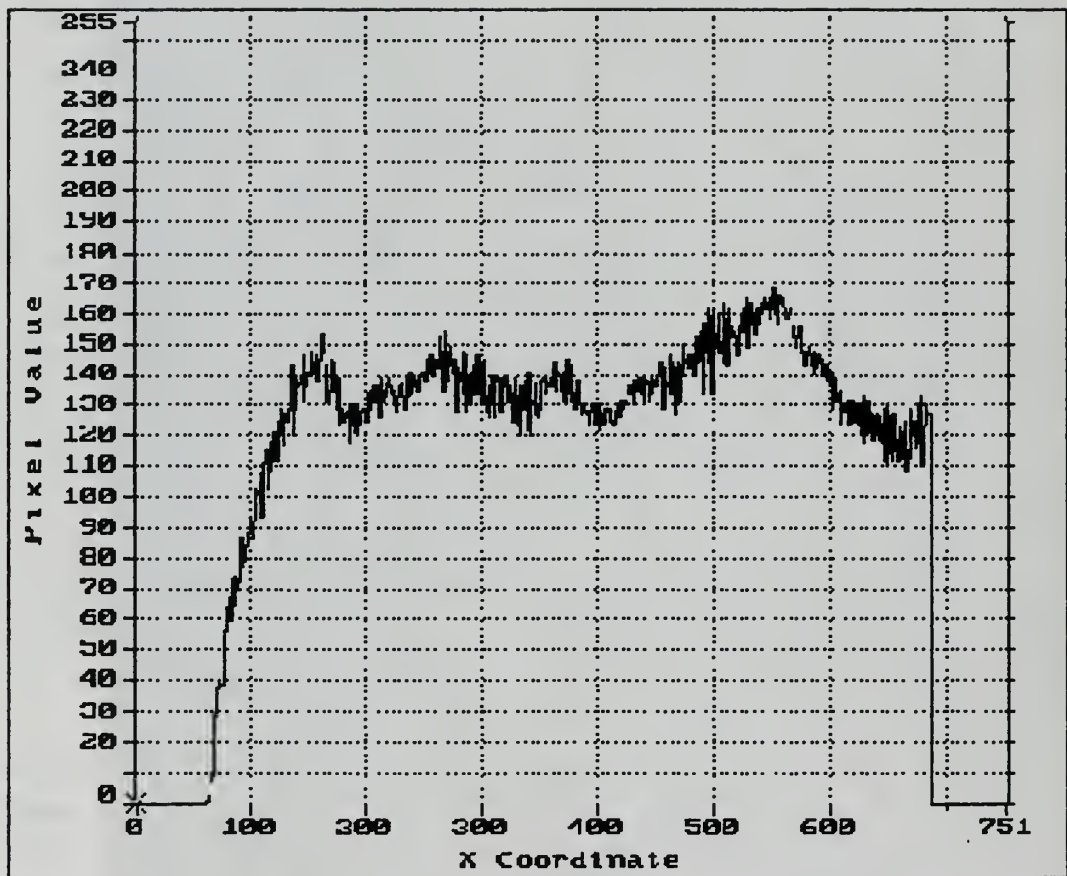


Figure 29b. Graphical Representation of a Single Line of Pixels of Ten Averaged Images



**Figure 30a.** One Hundred Averaged Images of the Underexpanded Jet /Flat Plate

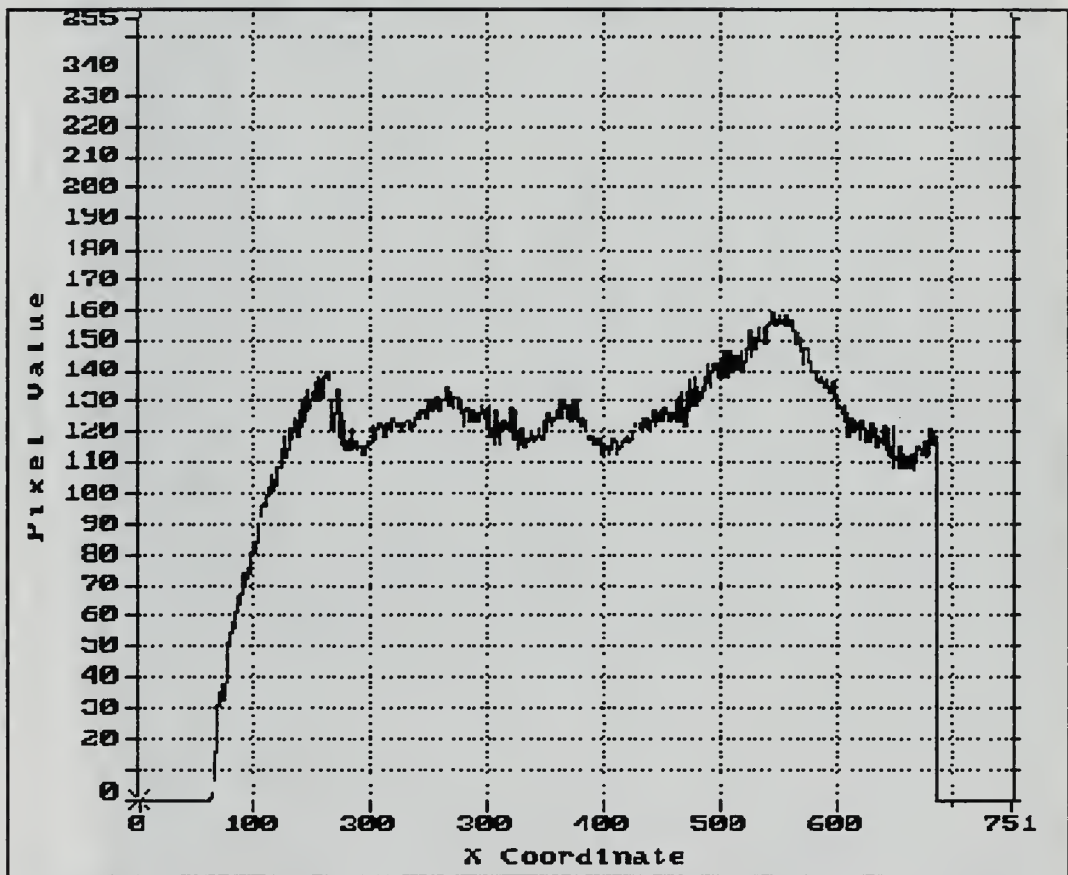


Figure 30b. Graphical Representation of a Single Line of Pixels of One Hundred Averaged images



using a pair of transformation equations relating the new coordinates to the old coordinates. An example set of transformation equations, termed the *affine projection*, are

$$x' = (a_{11}x + a_{12}y + a_{13})/(a_{31}x + a_{32}y + 1)$$

and

$$y' = (a_{21}x + a_{22}y + a_{23})/(a_{31}x + a_{32}y + 1)$$

where  $x, y$  are the old coordinates and  $x', y'$  are the new coordinates. The eight unknown coefficients in the two equations can be determined if the coordinates of four points, called control points, can be determined from each of the two images involved. [Ref. 21:p. 71]

In the jet/plate interaction experiment, the stiffness of the plate was expected to be sufficient to withstand the forces imposed on it by the jet so that any deformation that did occur would be insignificant, making registration unnecessary. However, comparison of the wind-on and wind-off images showed that the plate did experience a horizontal translation when the jet was on. It was found that the thrust produced by the jet caused a deformation in the structure supporting for jet apparatus. Thus, the jet apparatus and flat plate in combination experienced a displacement relative to the camera.

Examination of the wind-off and the corresponding wind-on images showed that for the 65 and 80 psig cases, the images had shifted one pixel width in the direction of the thrust, and two pixel widths for the 90 psig case. The image-registration algorithm in the EPIX software was found to be unsuitable for this correction. In

addition, the lack of "natural" features on the plate to serve as control points did not allow the use of the software. [When the object lacks such features and image registration is anticipated, artificial marks such as black circles can be distributed on to the surface. In the present case, registration was not expected to be needed, the plate was not so equipped.]

The registration between the wind-off and wind-on images was a relatively simple issue involving rigid body motion in one dimension. For this particular situation the images were aligned using the "Copy and Shift Image" function in the EPIX software which allowed an image to be shifted in its buffer up or down, left or right by an operator- specified number of pixels. The registration scheme was accomplished by first loading the wind-on and wind-off images into consecutive image buffers. The wind-on condition was considered the "warped" image and the wind-off image the "reference" image to which the warped image would be registered. A cursor overlay was simultaneously displayed on the image monitor with the wind-off image. The cursor was adjusted so that its horizontal character overlaid the pressure ports along the centerline of the plate while the vertical character of the cursor overlaid the pressure ports along the vertical centerline of the plate. The cursor remained fixed relative to the screen of the monitor; this served as a reference for comparison of object feature location when shifting between the wind-on and wind-off buffers. The wind-on image was then shifted relative to the vertical-cursor character until the vertical centerline pressure ports were overlaid by the vertical cursor character. When complete, the images were considered registered.

The accuracy of using this approach was judged to be similar to that of registration software since the registration software normally requires the operator to manually locate the control points in each image. In addition, since the body moved relative to the light source, consideration must be given to whether changes in brightness were due to the pressure variations, or were caused by the motion of the plate.

McClachlan *et al* [Ref. 22:p. 3] indicate that this is of greatest concern when model deflections and distortions are extreme. Since the flat plate motion consisted of rigid body translation, the magnitude of which was extremely small, this concern was considered to be insignificant.

(4) Ratioing. While the reason for ratioing the wind-off image with the wind-on image was to satisfy the Stern-Volmer relation and produce a pressure map, there were other benefits which arose from the procedure. In Figure 31 it is easy to discern the gross features of the pressure distribution in the wind-on image. The ratioing process had the affect of enhancing the finer detail in the image that would otherwise be too subtle for detection. [Ref. 7:p. 7]

Examination of the wind-off image in Figure 32 shows the evident brightness variations from point to point across the surface. This was due to a combination of differences in illumination, paint thickness variations, and features in the model itself. Figure 33 shows a three dimensional graphical representation of the wind-off intensity values across the surface of the plate. This illustrates the variations that exist across the plate. The result of ratioing was the elimination of these non-uniformities.



**Figure 31.** Wind-on Image of the Underexpanded Jet at 80 psig Across a Flat Plate



**Figure 32.** Wind-off Image for the 80 psig Condition



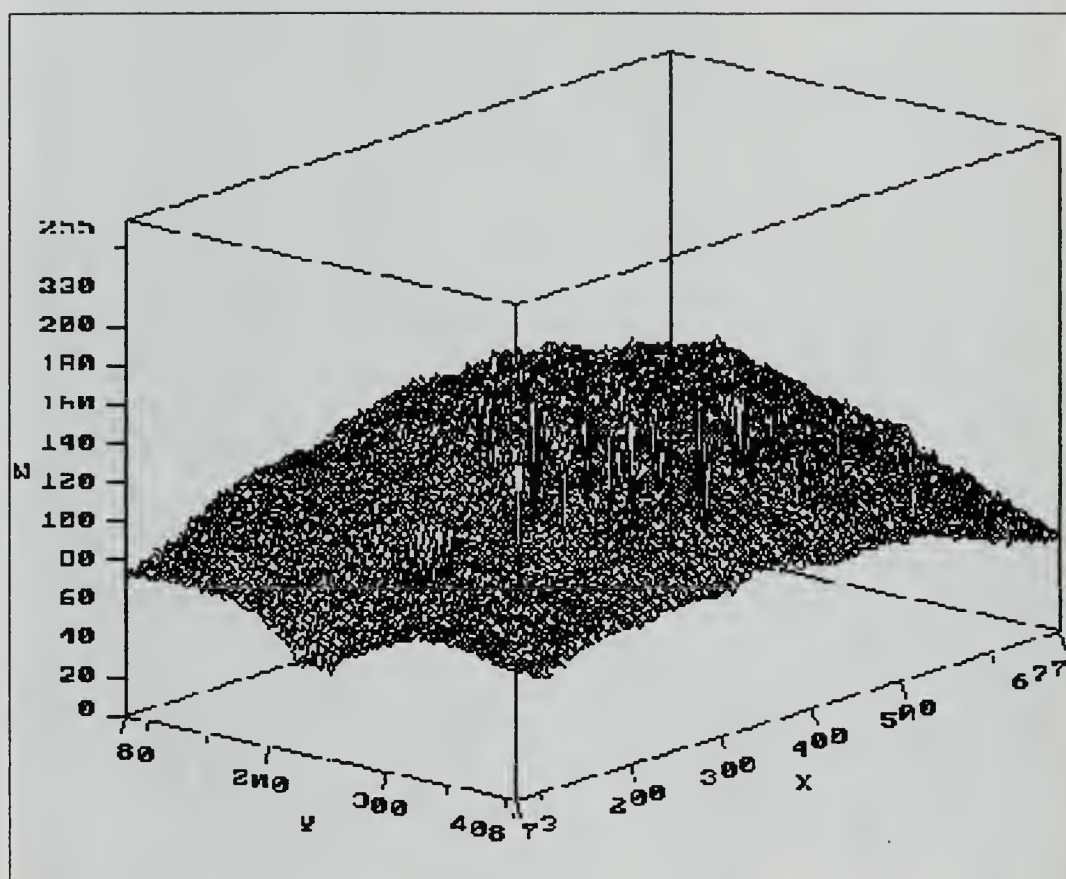


Figure 33. Three Dimensional Intensity Plot of the Wind-off Condition of the Plate

The "Ratio Image Operation" under the "Two Image Arithmetic" menu of the EPIX software formed the weighted ratio of corresponding pixels. The operation is mathematically expressed as

$$(c0 * \text{PixB} + c1)/(c2 * \text{PixA} + c3)$$

where the coefficients  $c0$ ,  $c1$ ,  $c2$ , and  $c3$  are modifiable. For the current work,  $\text{PixA}$  was designated the wind-on image while  $\text{PixB}$ , the wind-off image. In addition, the coefficient  $c0$  was assigned the value of 100 while the coefficients  $c1$ ,  $c2$ , and  $c3$  were assigned the values 0, 1, 0 respectively. The reason for assigning  $c0$  the value of 100 was to scale the resultant ratioed intensity map such that differences of the grey values between neighboring pixels could be discerned.

Figure 34 illustrates the ratioed image for the underexpanded jet across the flat plate at 65 psig plenum pressure. The importance of proper registration of the wind-on and wind-off images prior to ratioing cannot be overstated. To illustrate the effect of improper registration, the images used to form the resultant image in Figure 34 were modified where the wind-on condition was shifted an additional five pixel widths in the direction of the thrust. The result of ratioing these two images is shown in Figure 35. A reduction in fine details, as compared to Figure 34, is clearly evident.

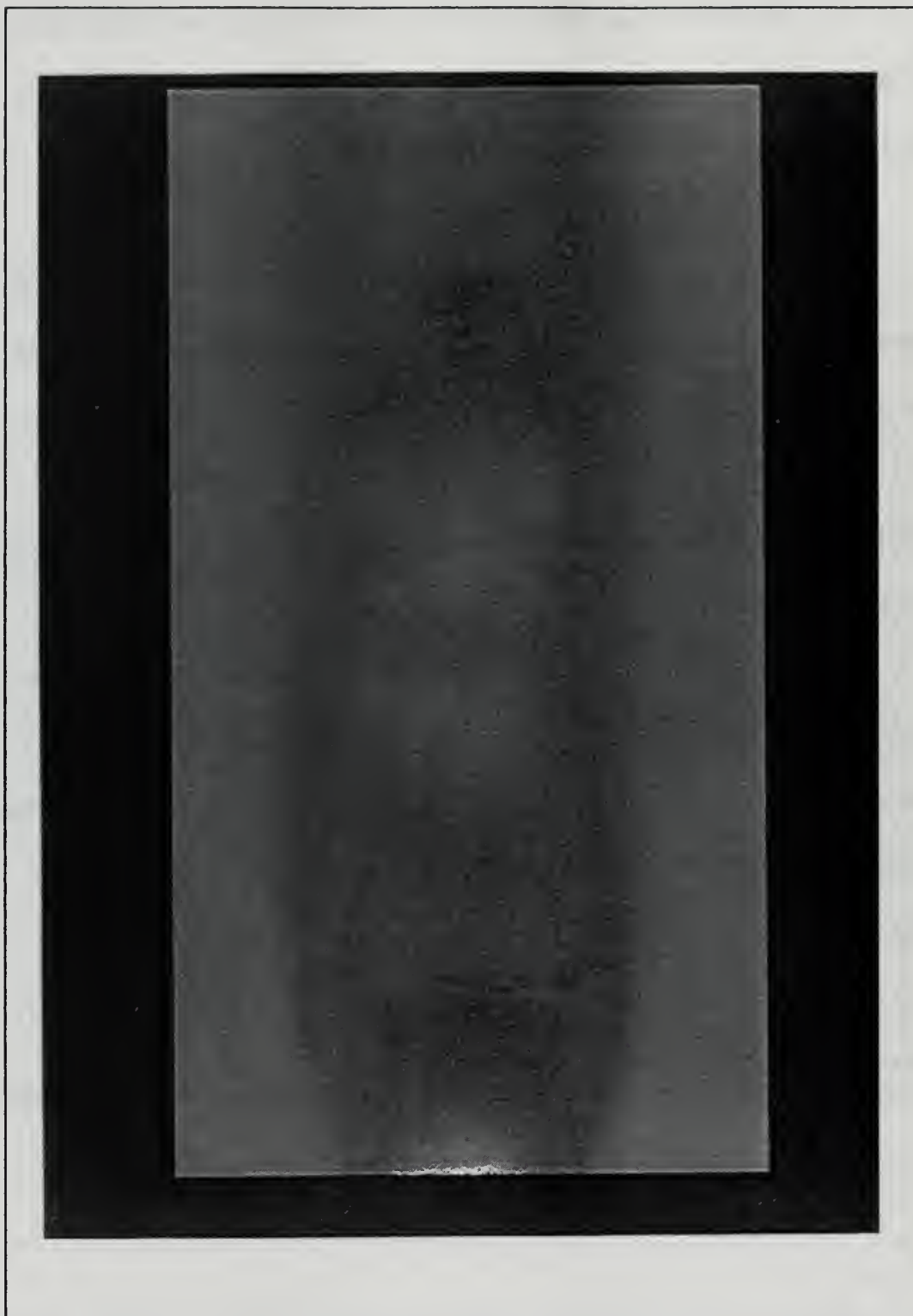


**Figure 34.** Ratioed Image of the Wind-off and Wind-on Images for the Flat Plate /Jet Interaction at 80 psig



**Figure 35.** Result of a Ratioed Image Following Improper Registration Technique

## ***b. Calibration***

Two methods were available to calibrate the intensity ratio map, the intent of which was to obtain the sensitivity coefficients for the Stern-Volmer equation and establish the pressure map.

The first method, termed "*a priori*", involved calibrating a paint sample in a controlled pressure and temperature chamber. Using the data obtained from the chamber, and knowing the temperature of the model surface, the appropriate values for the Stern-Volmer coefficients could be found [Ref. 7:p. 7].

The second method, termed "*in situ*", which was the method employed in the present work, used the pressure obtained using a conventional pressure tap in the model surface and compared this with the intensity from the luminescent paint adjacent to the tap. Using data from a number of taps, the sensitivity coefficients were obtained by a least-squares linear fit. The coefficients A and B, being functions only of temperature, were good over that portion of the surface which was at the same temperature as the area containing the pressure taps. [Ref. 7:p. 10]

The approach used to produce pressure data from the ratioed image was similar to that used by Kavandi [Ref. 9:p. 94]. This entailed averaging the data from five adjacent rows of pixels near the pressure taps to produce a single row of data. (This, has the effect of averaging a total of five hundred images together.)

To do this, the ratioed image was loaded five times into consecutive frame buffers of the frame-grabber board. Each successive image was then vertically offset by



one pixel row with respect to the previous image, i.e., the first image remained unmodified, the second image was shifted one pixel row down in its frame buffer with respect to the first image, the third image shifted two pixel rows down with respect to the first image, etc. The five buffers were then averaged. Each row of pixels in the resultant image, with the exception of the first five and the last five rows of the image, was then an average of the corresponding row in each of the five images. A row of pixels close to the pressure taps was then selected to serve as calibration data. Figure 36 shows the data from the selected line of pixels for the flat plate in the underexpanded jet at 80 psig, prior to averaging with four adjacent lines of pixels. Figure 37 shows the data for the same line after the averaging procedure. [It is noted that the "spike" on the left side of the graph is due to paint that has separated from the leading edge of the plate]. From an examination of Figure 36 and Figure 37 it can be concluded that the five-row averaging procedure had the effect of reducing the noise level in the distribution with negligible effect on the distribution itself.

The calibration curves that resulted from plotting intensity values against the measured surface pressure at jet stagnation pressures of 65, 80 and 90 psig, are shown in Figures 38, 39 and 40, respectively. All data were obtained using the line of pixels and the line of pressure taps along the centerline of the jet. Two separate linear fits are shown in each of the figures. This was done when it was realized that the data were poorly represented by a single curve, and that large variations in temperature over the surface of the plate was the probable cause. It is possible that the groups of points which correlate

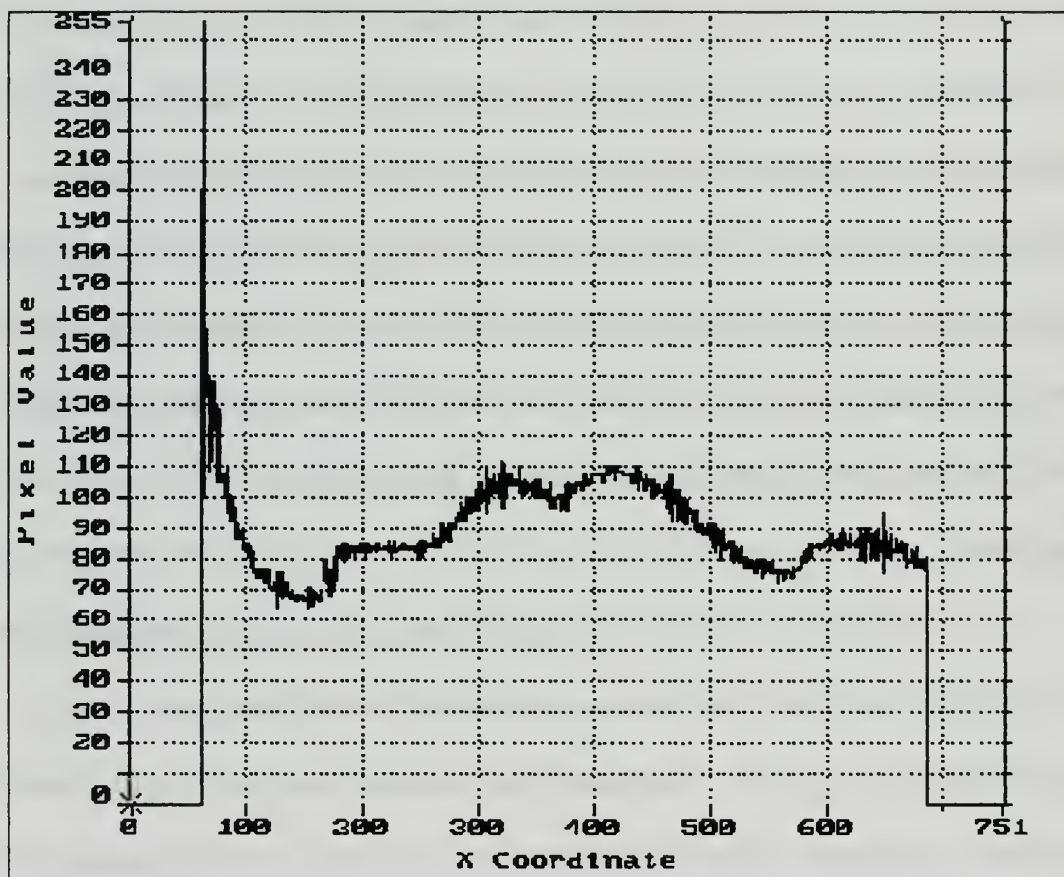


Figure 36. Calibration Line of Pixels for the 80 psig Case Prior to Spatial Averaging

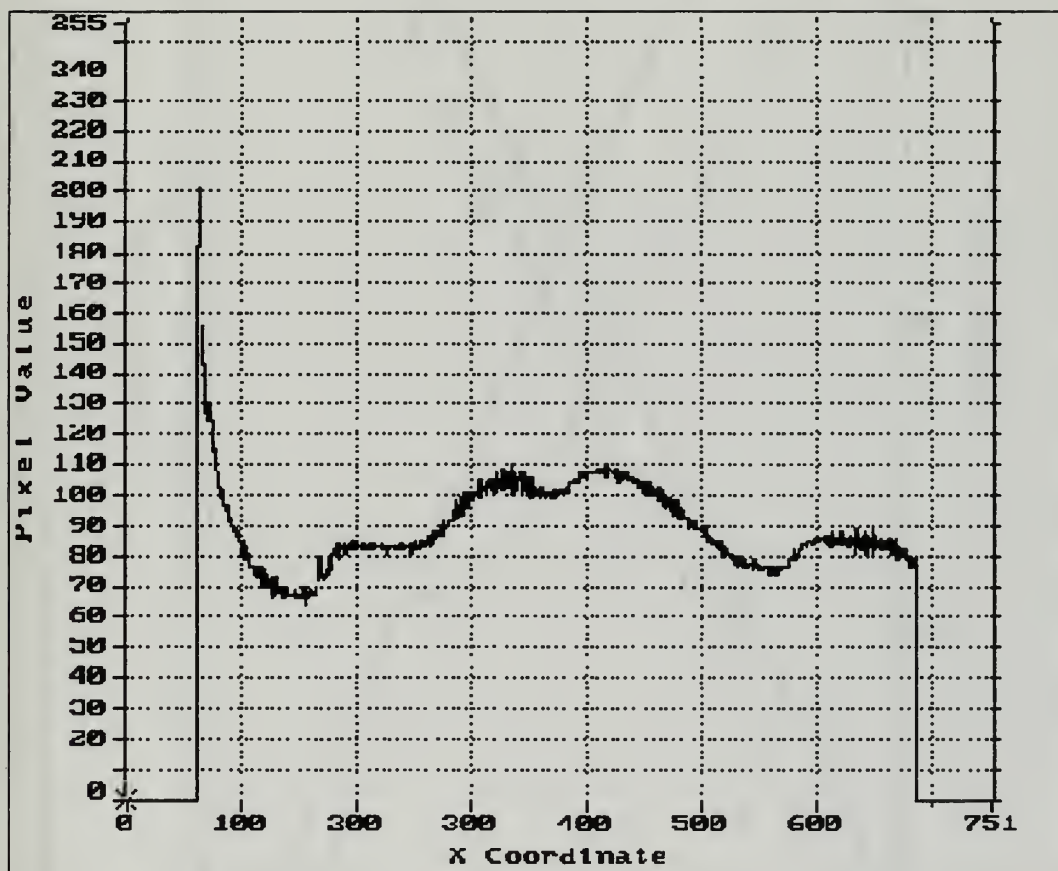
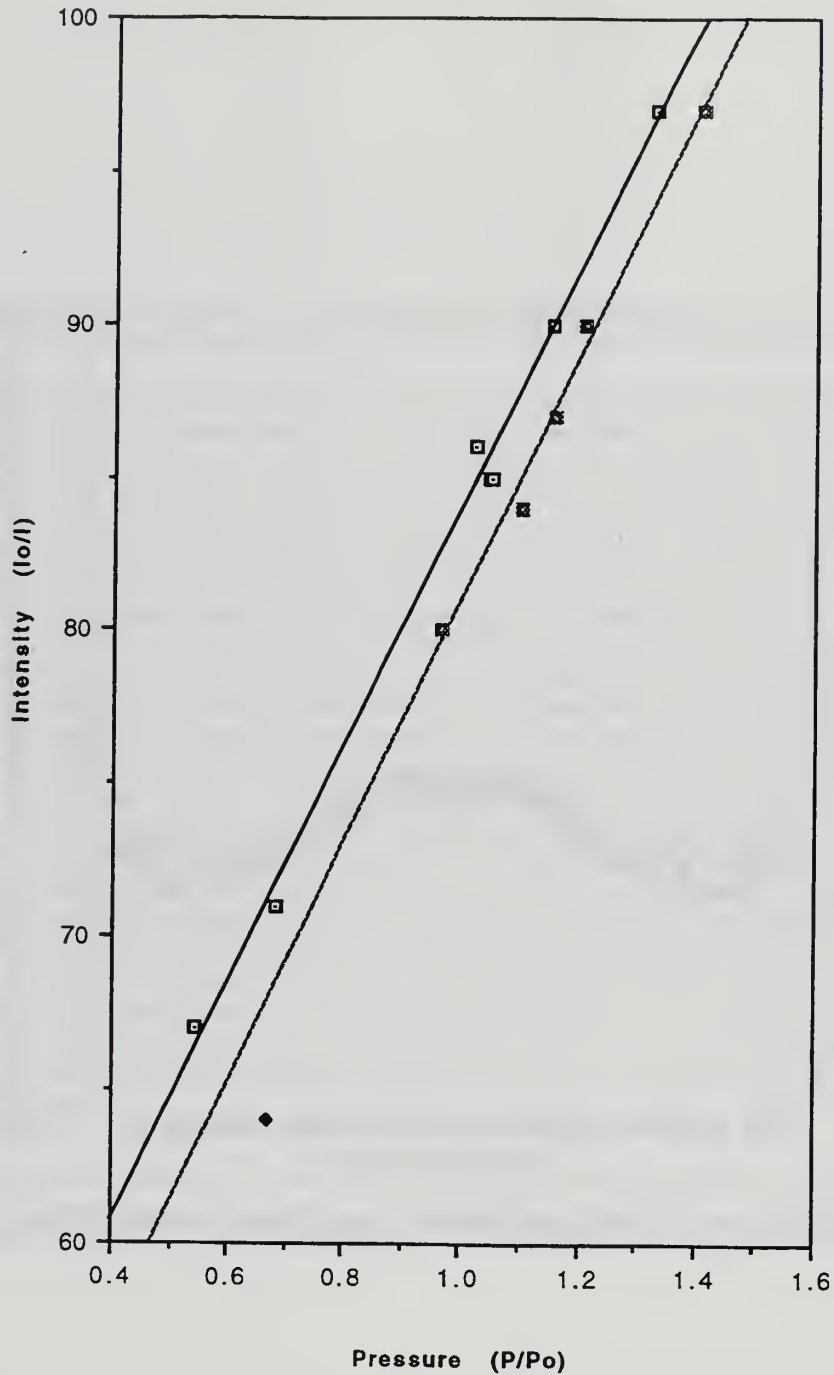


Figure 37. Calibration Line of Pixels for the 80 psig Case After Spatial Averaging

Calibration Curve For The Underexpanded  
Jet Nozzle Across A Flat Plate  
(65 psig Plenum Pressure)



**Figure 38.** Calibration Curve for the Underexpanded Jet/Flat Plate at 65 psig

Calibration Curve For The Underexpanded  
Sonic Jet Across A Flat Plate  
(80 psig Plenum Pressure)

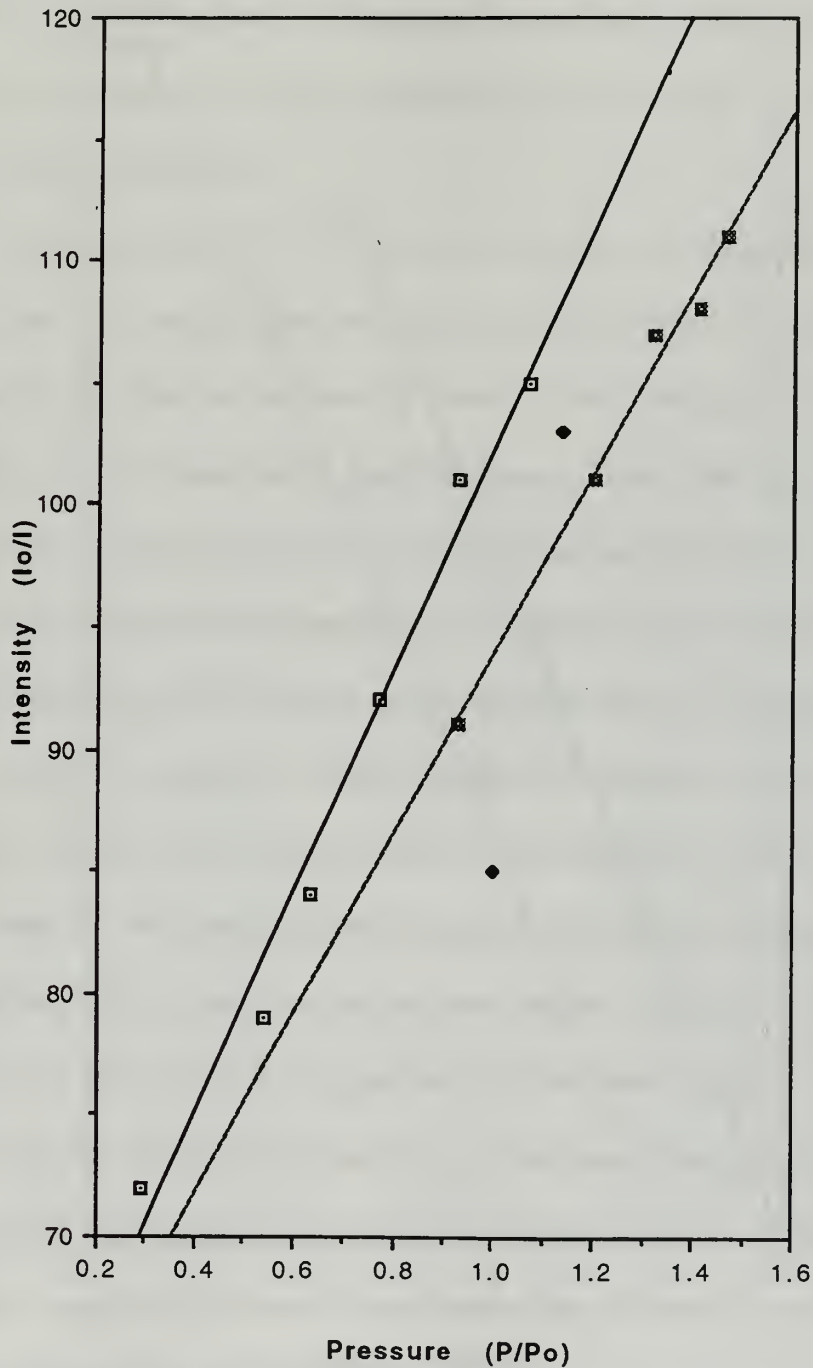


Figure 39. Calibration Curve for the Underexpanded Jet/Flat Plate at 80 psig



Calibration Curve For The Underexpanded  
Sonic Jet Across A Flat Plate  
(90 psig Plenum Pressure)

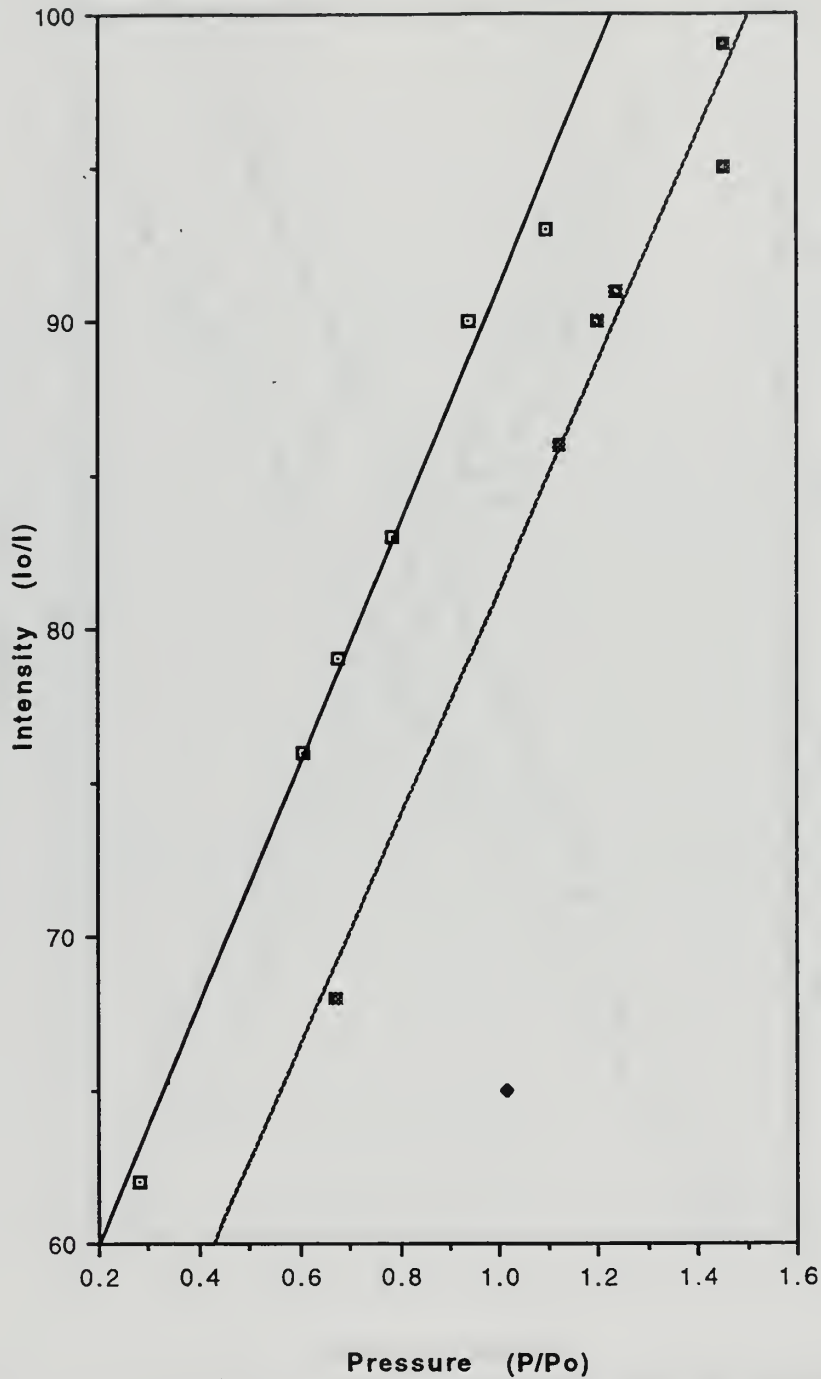
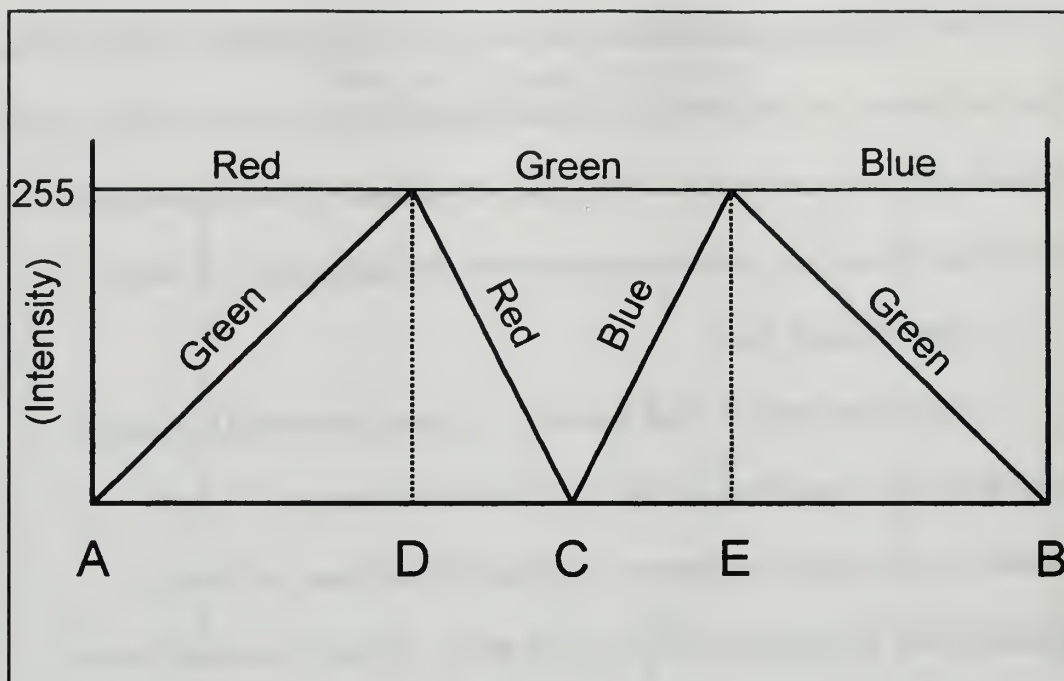


Figure 40. Calibration Curve for the Underexpanded Jet/Flat Plate at 90 psig

linearly are from regions of similar surface temperatures. However, the complexity of the flow over the plate surface, with a three-dimensional separation contained within it, makes the estimation of surface-temperature distribution very difficult. These results clearly indicate the need to measure surface temperature if *in-situ* calibration is to be used.

### ***c. Field Pressure Map***

Pseudo-coloring (or "false coloring") of a gray scale image was used to accentuate areas of an image that are not easily discerned by the eye. This was accomplished by providing an assignment of amounts of red, green and blue to a corresponding value of intensity in the gray-scale image. Through the use of look-up tables, the software allowed specification of linear ramps, logarithmic curves, polynomials, gamma correction, inversion and transposition in a pattern or sequence of a non-specific nature. For a gray-scale image the index value is synonymous with its intensity value. Reference 23 may be consulted for further information concerning the manipulation of lookup tables. The color map or sequence that was developed for the present work is shown in Figure 41. The constants A and B represent the minimum and maximum index values of the interval over which the color map was defined. All other index values were assigned the pixel value of zero in the color map. The minimum and maximum index values were found by conducting a histogram on the gray-scale image which gave a breakdown of the pixel intensity values and the frequency of occurrence in the image. The intensity values associated with the pressure-sensitive paint images are usually grouped in an interval between the 0 to 255 index value range.



**Figure 41.** Graphical Representation of the Red, Green, and Blue Lookup Tables

The constant C represents the mid-point of this interval. The constants D and E were varied to obtain the desired bandwidth of the green lookup-table input which influenced the mid portion of the color spectrum.

The final pressure maps for the 65, 80, and 90 psig plenum conditions are given in Figures 42, 43, and 44 respectively. Although quantitative information is not available, the results in Figures 42, 43, and 44 show good qualitative agreement with their schlieren counterparts in Figures 12, 13, and 15 respectively.

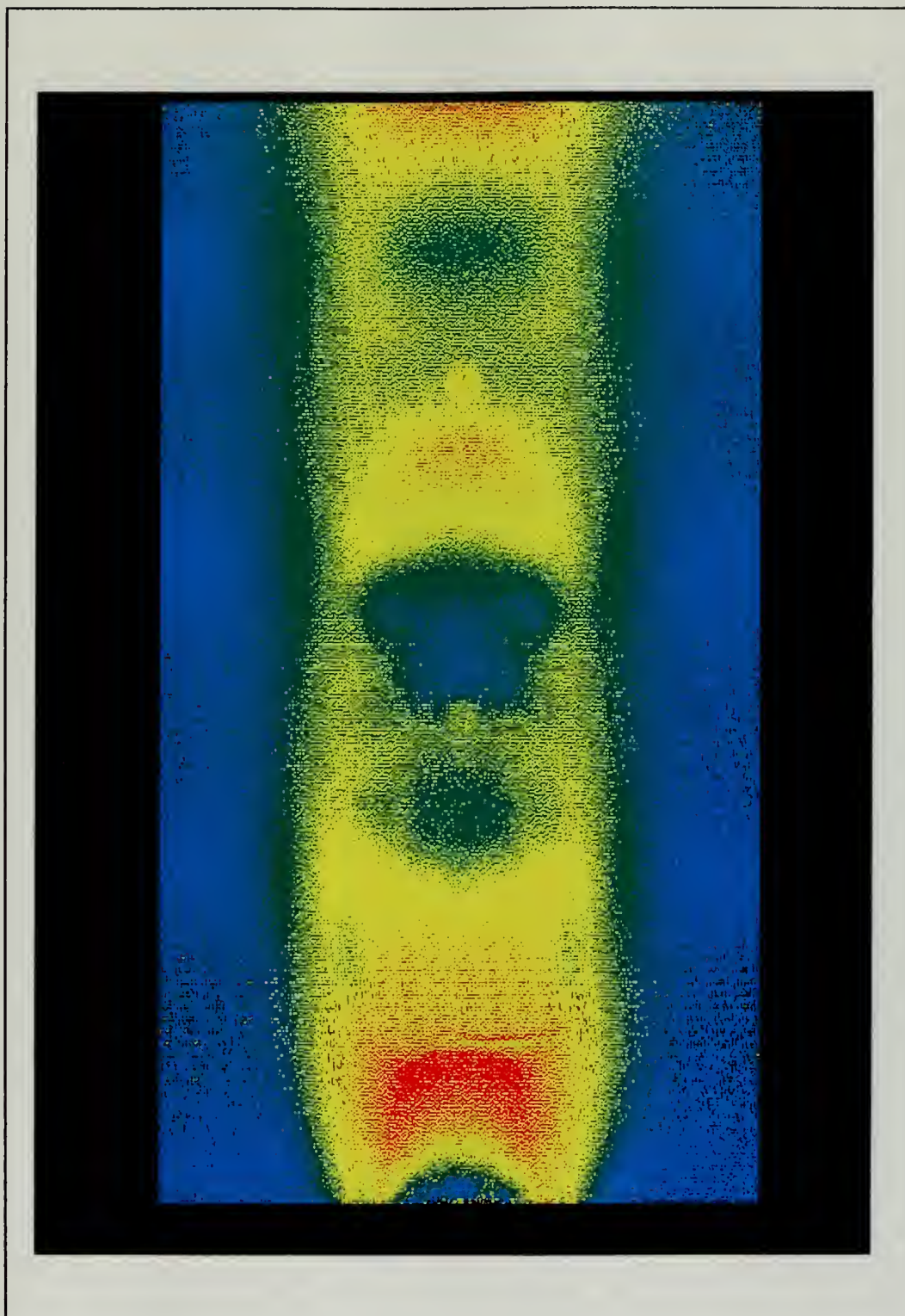


**Figure 42.** Pressure Map of the Underexpanded Jet at 65 psig Across a Flat Plate





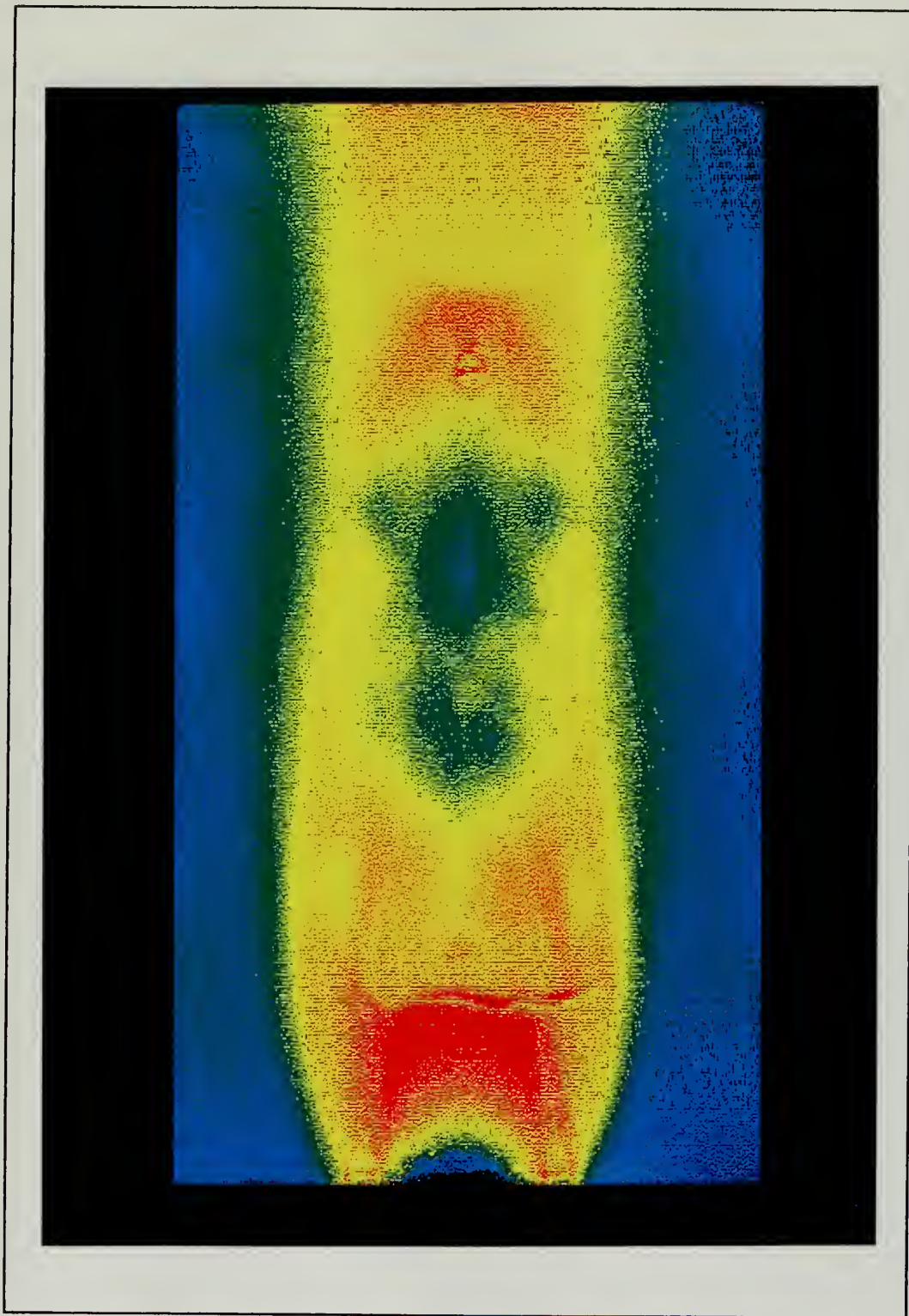


**Figure 43.** Pressure Map of the Underexpanded Jet at 80 psig Across a Flat Plate



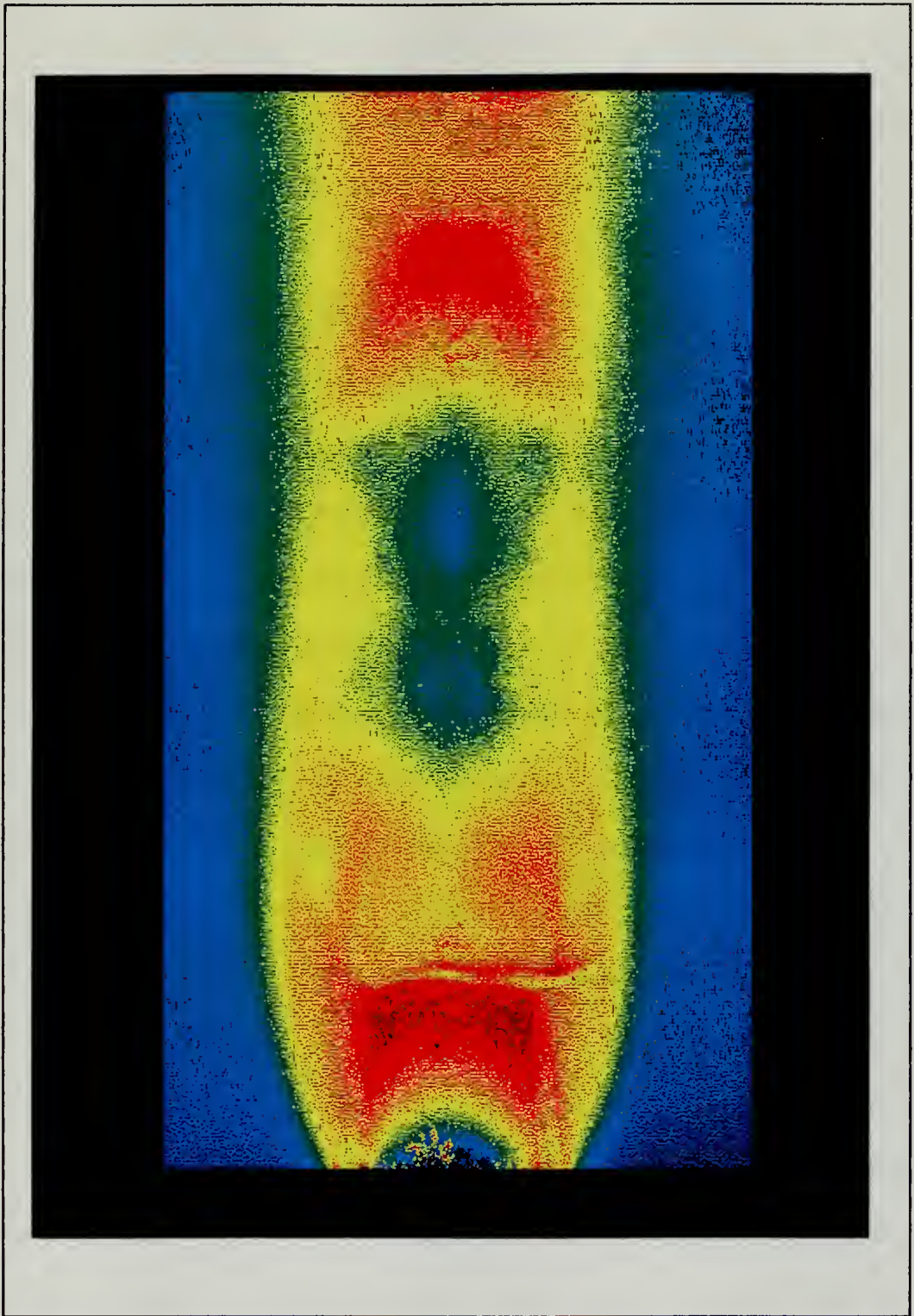


**Figure 44.** Pressure Map of the Underexpanded Jet at 90 psig Across a Flat Plate



## **IV. APPLICATION TO SHOCK-BOUNDARY LAYER INTERACTION IN A SUPERSONIC WIND TUNNEL**

### **A. DESCRIPTION OF FACILITY**

The supersonic wind tunnel, located in Bldg. 216 of the Gas Dynamics Laboratory [Bldg. 216] at the Naval Postgraduate School, was of the blow-down type. Supply air was produced by the same supporting facility as the underexpanded sonic jet apparatus. A schematic of the tunnel and supporting facility is shown in Figure 45 while Figure 46 shows a photograph of the wind tunnel.

Air to the tunnel, from a maximum pressure of 300 psi, was controlled by a pneumatic control valve. The control valve used a diaphragm actuator. Regulated instrument air from the supply system was routed to one side of the diaphragm and the controlled pressure, from a tap on the plenum, was connected to the other. This allowed precise control of the plenum pressure. A pressure gauge installed on the plenum provided pressure readout.

The plenum chamber was cylindrical with an internal diameter of approximately 20 inches. With the exception of a splash plate mounted perpendicular to the flow near the entrance of the chamber, the plenum was empty. The flow exited the chamber through a contraction and circular-to-rectangular transition section, into the convergent-divergent



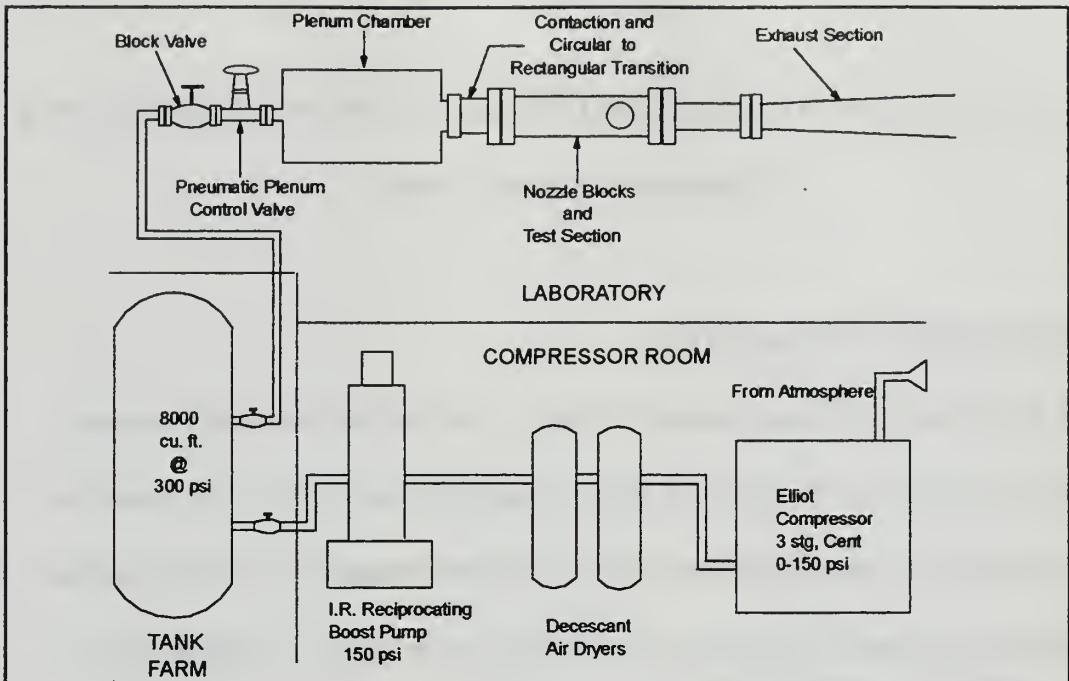


**Figure 45.** Schematic of the Supersonic Wind Tunnel and Supporting Facility

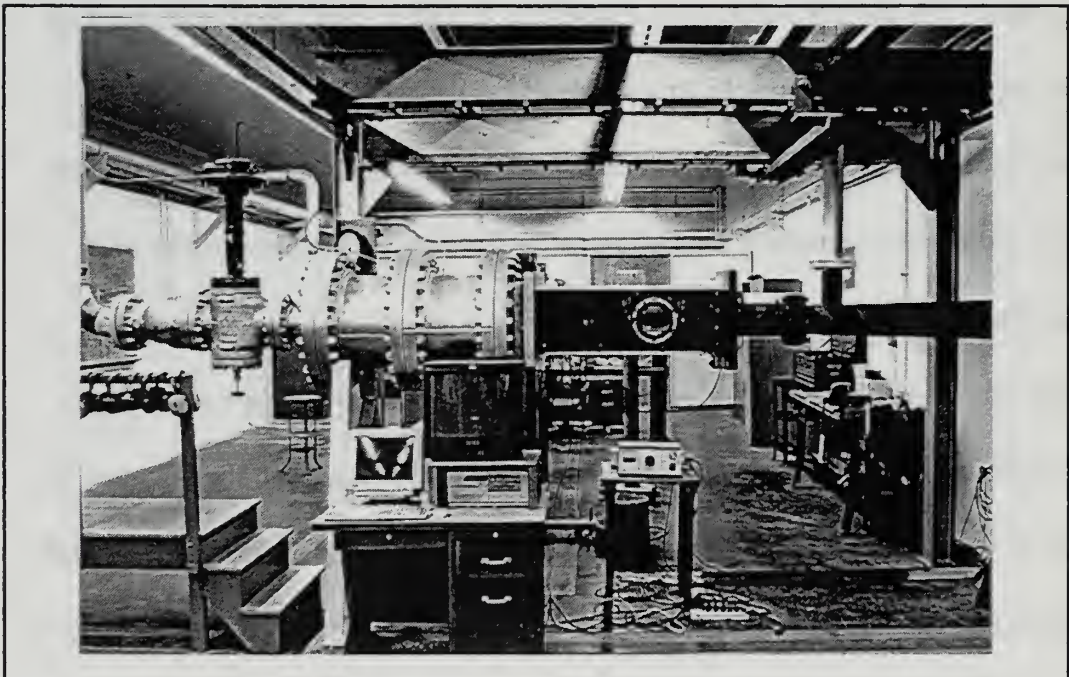


**Figure 46.** Supersonic Wind Tunnel Apparatus

nozzle. The nozzle and test section, shown schematically in Figure 47, were comprised of a set of two (interchangeable) aluminum blocks forming the contour and two flat plates forming the side walls and enclosing the constant-width section.

The test section was nominally four inches in width and four inches in height. Six-inch diameter circular glass windows on each side of the test section provided optical access. Two small gate valves were mounted on each of the side walls just downstream of the test section. They were used to allow "bleed" and thus control back pressure in order to position the "starting" normal shock in the test section. The flow exited the test section into an exhaust duct which vented to the atmosphere outside the building.

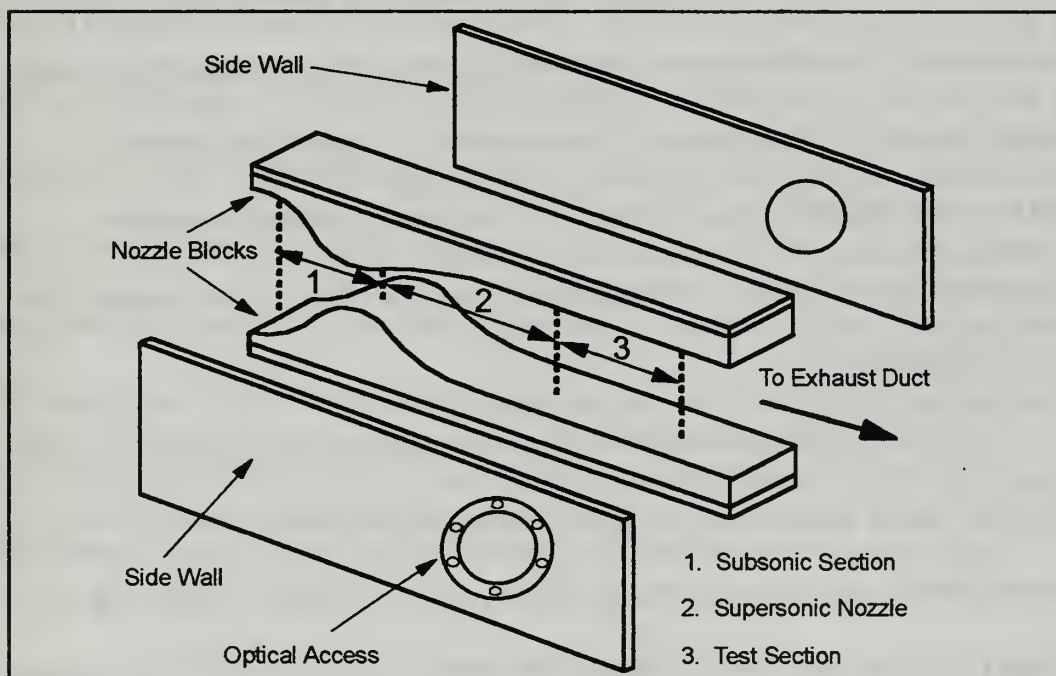


**Figure 47. Nozzle Blocks and Test Section Exploded View**

## **1. Nozzle Blocks**

The interchangeable pairs of nozzle blocks were each designed to produce a specific Mach number in the test section. For the present study, two Mach numbers, 1.4 and 1.7, were used, since this was the range of Mach number of interest in the proposed study of control of shock-boundary layer interaction. A set of blocks for  $M=1.4$  existed. However, it was necessary to design and manufacture a set of blocks to provide  $M=1.7$ . The program described in Appendix E was used to derive the contour for the  $M=1.7$  nozzle. The new blocks were otherwise similar to the existing blocks and were manufactured to the original drawings using the new contour.

### ***a. Performance Evaluation of the Mach 1.7 Nozzle Blocks***

To evaluate the new nozzle blocks, several runs at varying plenum pressures were conducted. A series of pressure taps along one side of the tunnel allowed pressure data to be collected. The taps extended approximately four inches upstream of the nozzle throat and downstream to the entrance of the test section. A metal blank containing additional taps was installed in place of one of the test section windows to measure pressures through the test section. One tap downstream of the test section measured the pressure of the exiting flow.

The data acquired indicated that the normal shock associated with the nozzle starting process rapidly passed through the test section into the exhaust duct as soon as the operating pressure ratio decreased below the first critical condition. Unlike with the  $M=1.4$  blocks, the bleed valves on the sides of the tunnel could not be used to position the

shock. It was realized that some form of blockage would have to be introduced into the passage at some point downstream of the test section in order to "set" the shock in the test section.

The mounting points for the gate valves, which were located three inches downstream of the test section and were aligned such that their centerlines coincided with each other, were adapted so that circular rods of varying diameter could be installed across the tunnel. A total of four rods was used. Operating the tunnel at 75 psi plenum pressure, the static pressure distribution was recorded for each configuration. The effect of rod diameter on shock position is clearly seen in Figure 48.

The 3/8 inch diameter rod was found to place the shock just prior to the test section. To position and control the shock precisely in the center of the test section, a means of bleeding off mass flow was developed. The solid rod was replaced by a 3/8 inch outside diameter tube. A series of 11/64 inch holes was drilled through the tube wall, in a line along its 4-inch length. The tube was then mounted between the gate valves with the holes aligned with the flow. This arrangement allowed a controlled mass flow to pass through the holes into the tube and out of the tunnel via the gate valves. The gate valves could be adjusted to vary the amount of outgoing mass, thus moving the shock to the desired position in the test section. A schematic of this arrangement is shown in Figure 49 while Figure 50 shows a photograph of the bleed-off tube mounted in the tunnel.



# Pressure Distribution Along Tunnel Wall Mach 1.7 (75 psi Plenum Pressure)

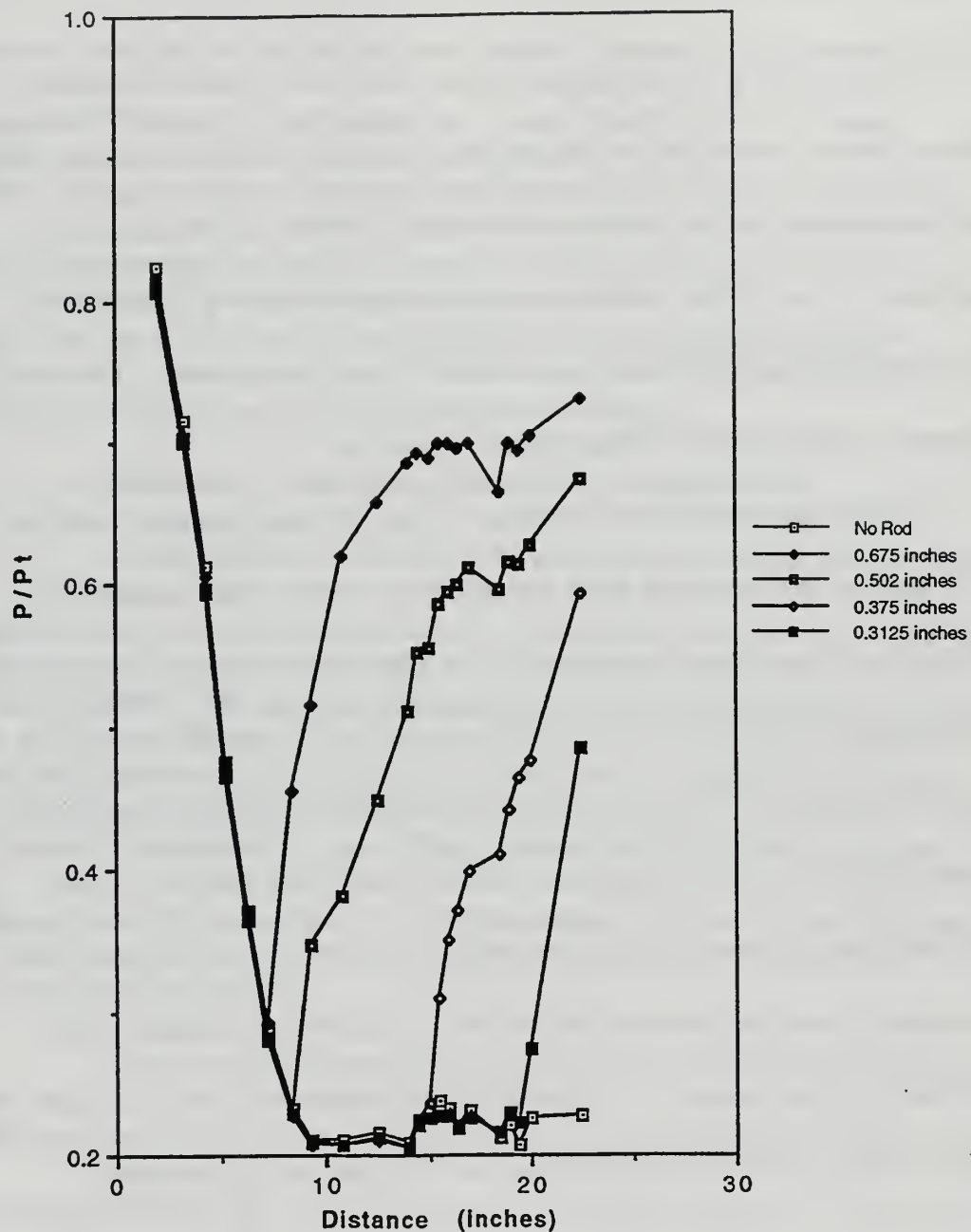
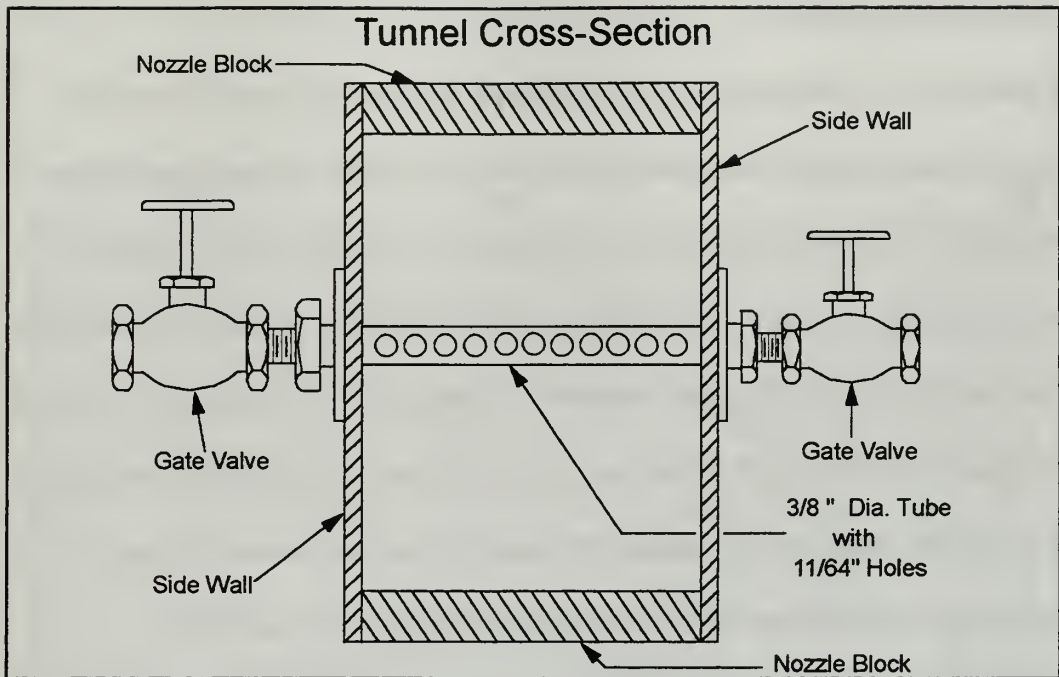
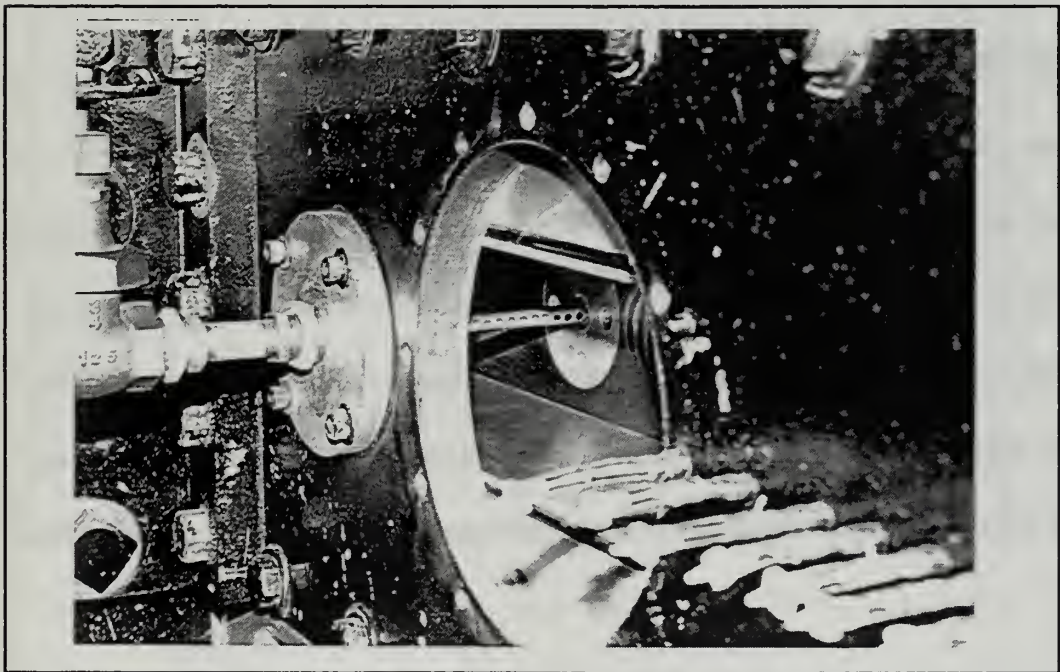


Figure 48. Tunnel Pressure Distributions as a Result of Varying Rod Diameters





**Figure 49.** Cross-Sectional View of the Mass Bleed-Off System



**Figure 50.** Mass Bleed-Off Tube Mounted in the Tunnel

## **B. INSTRUMENTATION**

The metal blank, containing eleven pressure taps, and used as described above to measure the pressure distribution in the test section, was used as the model surface on which to observe the interaction between the starting normal shock and the nozzle boundary layer using pressure-sensitive paint. The metal blank was installed on one side of the test section and a six inch glass window was installed on the other. Concern for the spectral transmittance of the glass window led to an analysis of the glass for the range of 350 nm to 700 nm using a spectrometer. The results of the test, shown in Figure 51, indicated that the transmittance levels were satisfactory for the current work.

The optical measurement system was the same as was used for the underexpanded jet study described in chapter three. A schematic of the setup is shown in Figure 52.

## **C. EXPERIMENTAL PROCEDURE**

It was found that the shock-boundary layer interaction in the test section was inherently unsteady. This precluded the use of the procedure outlined in chapter three for acquiring the wind-on data. That method required the event of interest to be steady and repeatable, thus enabling one hundred images to be taken over a series of ten runs. The approach taken for the unsteady process was simply to create as many image buffers as possible for a single sequence, and to execute this sequence in the shortest period of time.

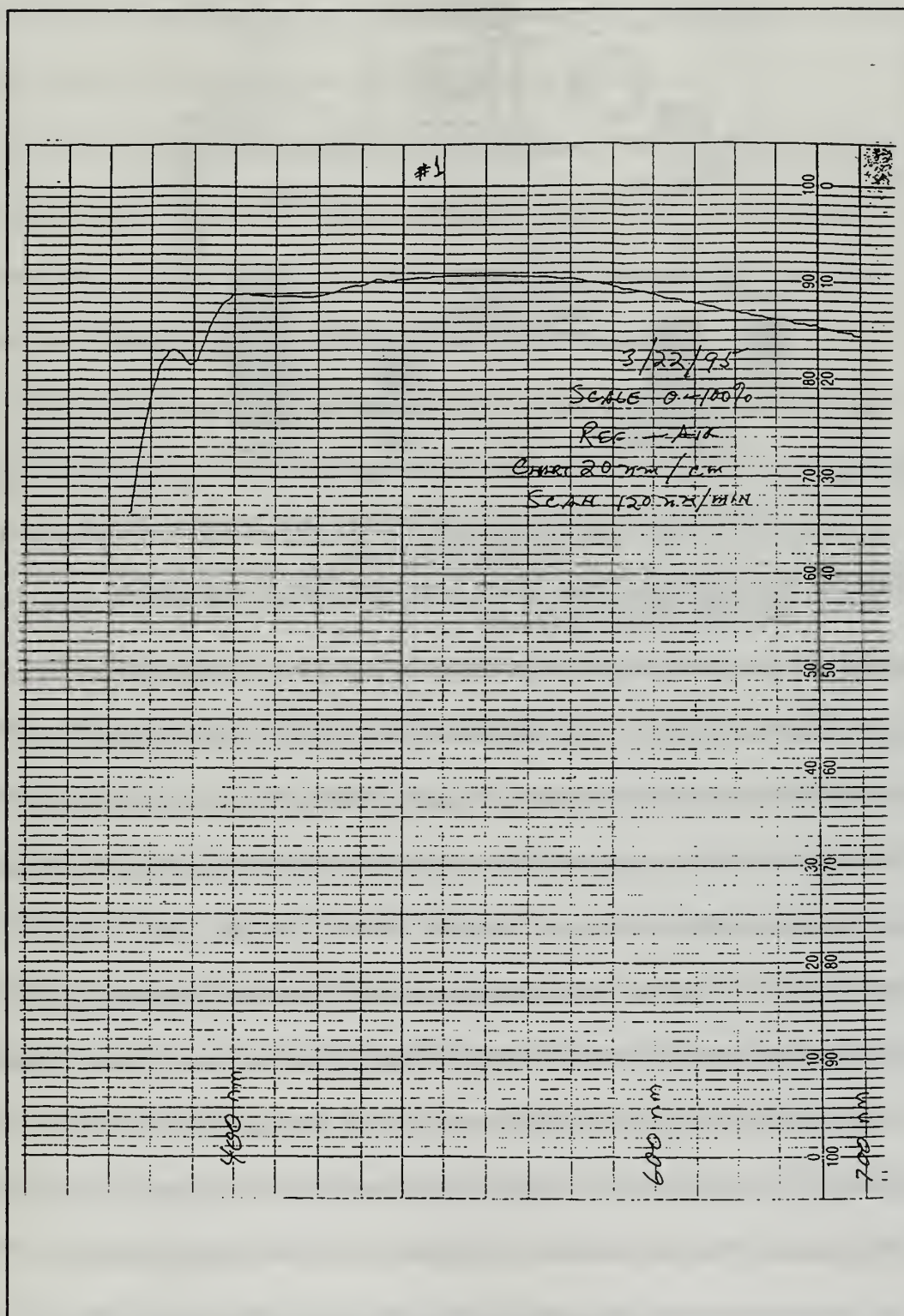
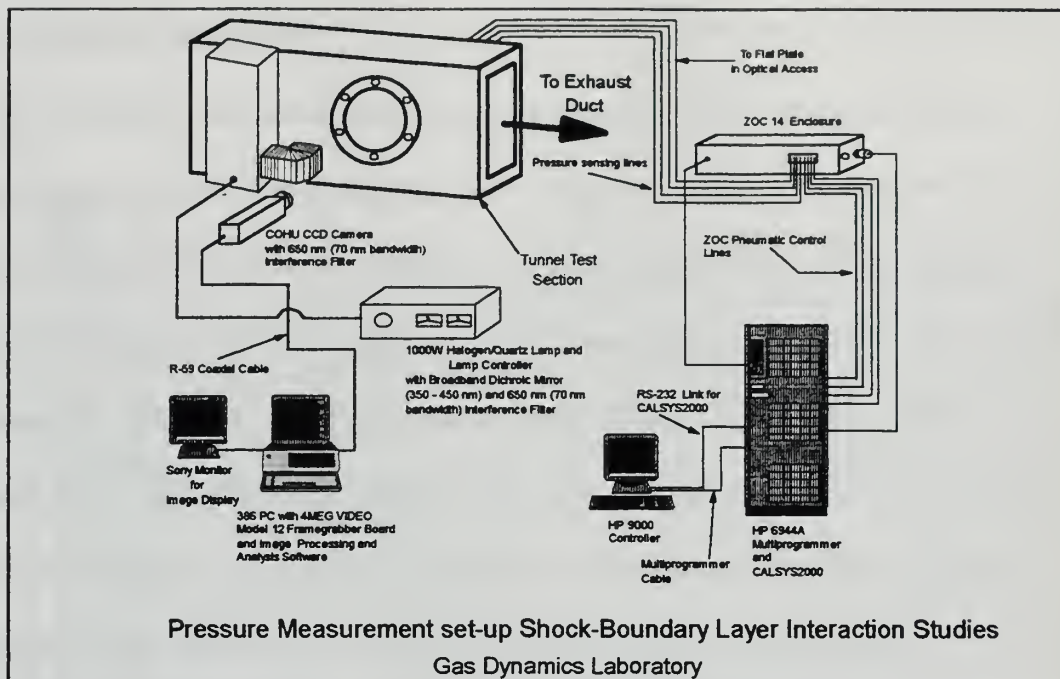


Figure 51. Spectrometer Results for the Optical Window





**Figure 52.** Instrumentation Setup for the Supersonic Wind Tunnel, Shock-Boundary Layer Experiment

The maximum number of image buffers that could be created for image capture was a function of video resolution. To maximize the number of available buffers it was necessary to minimize the video resolution. To accomplish this, the camera was focused on the test section so that the surface of the metal blank was clearly displayed on the video monitor. The video resolution was set at maximum (752 x 480) at this point. With the video resolution menu displayed on the computer screen, the parameters controlling the numbers of pixels and pixel lines were iteratively decreased until the camera's field of view shown on the video monitor exhibited only the test surface, the rest of the field of view being deleted. The resulting resolution was 600 pixels per line and 340 lines of video or 600 x 340 (assuming "Interlace: Use Distinct (2) Fields?" is active) which allowed 21 image buffers to be available for image capture. Since McDonnell-Douglas [Ref. 6:p. 8]

had shown that averaging data from as few as eight images significantly reduced the noise on the signal, it was concluded the 21 images would be sufficient.

The period required for a sequence to be completed was based on the time interval specified between consecutive samples, the shortest interval being 1/30 of a second. Since a video frame was generated every 1/30th of a second by the camera, the total time to execute a sequence containing 21 image buffers was 1.37 seconds.

The experiment began with the Mach 1.4 blocks installed in the tunnel. Using the shadowgraph technique, the normal shock was positioned in the test section by adjusting the backpressure through the gate valves, while the plenum pressure was set at 30 psi. When the valves were properly adjusted the tunnel was shut down, the metal window blank with pressure sensitive paint applied was installed, and the camera and illumination system were located eight inches away from the optical glass window. A real-time image of the test section was displayed on the image monitor, and the parameters to execute the desired sequence described above, were input into the computer. A cover was placed over the test section to prevent photodegradation of the paint, the light source was turned on and allowed to "ramp up" and stabilize. The wind tunnel was then started, the plenum pressure set at 30 psi, and the laboratory lights were turned off. The wind-on data were captured while pressure data were taken simultaneously using the CALSYS2000 data acquisition system. Twenty samples per port were taken at a sampling rate of 10,000 Hz. Three such runs were conducted. Between each run, wind-off and dark-current images were collected. Temperatures for the tunnel and the test plate were not available.



The Mach 1.7 nozzle blocks were then installed with the mass bleed-off system described earlier. With the plenum pressure set at 70 psi the shadowgraph was again used to position the normal shock. With the test plate installed, three runs were conducted in a similar manner to that described for the  $M=1.4$  blocks. The data were post-processed using the techniques described in chapter three.

#### **D. DISCUSSION AND RESULTS**

The flow structure expected to be produced by the interaction between a normal shock and a turbulent boundary layer is shown schematically in Figure 53. The pressure-sensitive paint technique was to be used to measure the surface pressure through the interaction region. Previous work by Perretta [Ref. 24] involved a study of the flow across the shock structure shown in Figure 53, and the resulting separation, for the given  $M=1.4$  tunnel configuration used in the present study.

For the  $M=1.4$  case, the pressure map obtained is shown in Figure 54. It can be seen that the interaction was nearly two-dimensional. To illustrate the distribution of the pressure rise, a line of pixel intensity values taken along the plate is shown in Figure 55. The profile resembles those of Kooi [Ref. 25:p. 30-8] for turbulent boundary layer separation on a flat plate due to normal shock interaction. The steepest slope of the curve indicates the start of the interaction, according to Kooi's work. The separation point can be identified as that point in the curvature where either a discontinuity in the curvature

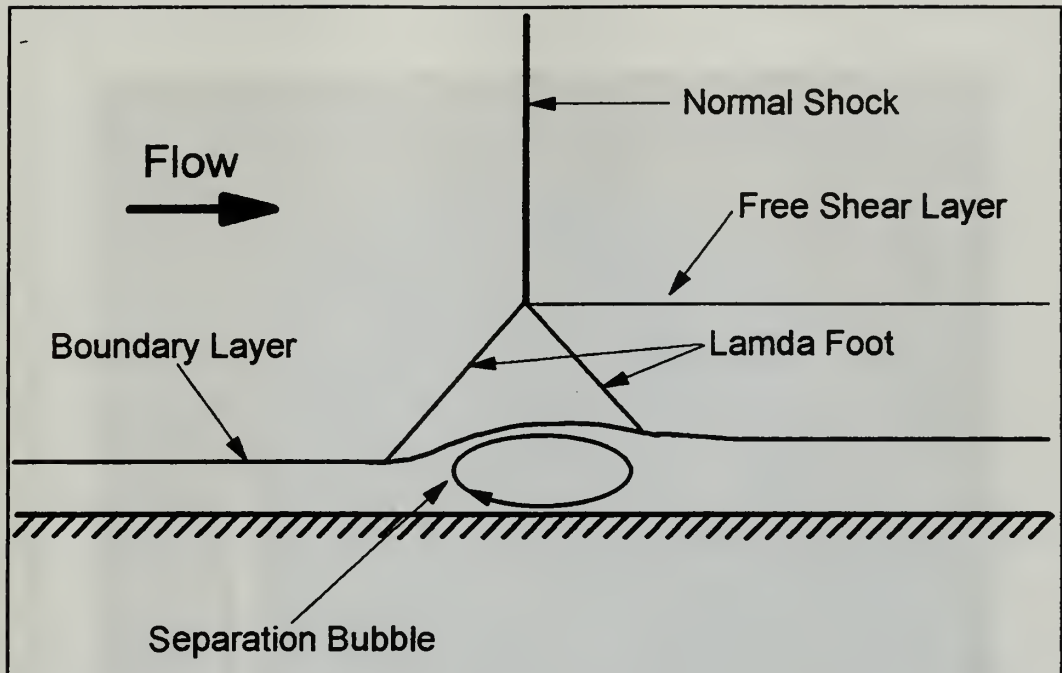


**Figure 53.** Schematic of the normal shock-boundary layer interaction

exists or the degree of change in curvature is much less compared to that of the start of the interaction, indicating a much slower rise in pressure. From the distribution of the intensity values, this point is difficult to determine. This can be attributed to oscillations of the normal shock, and the pressure-sensitive paint's poor dynamic response to these changes, causing an averaging effect and eliminating changes in curvature from the curve. Also, the time to execute the data collection sequence was much longer than the oscillation period of the shock, adding to the error in the results. The absence of a plateau in the intensity distribution suggests that the separation region was very short.

In the case of  $M=1.7$ , the determination of separation is more definite. The pressure map is shown in Figure 56 while the corresponding streamwise line of pixel-intensity



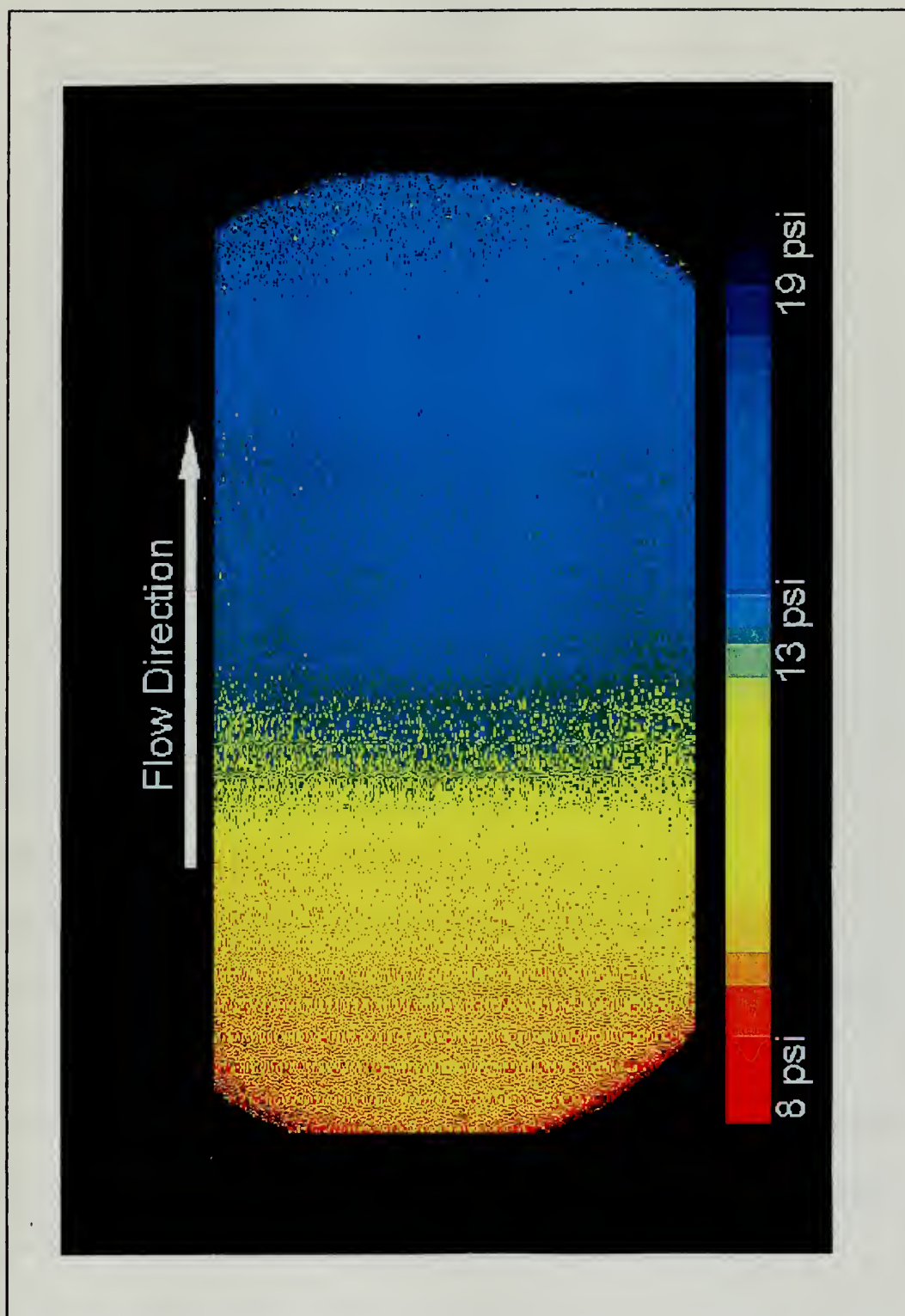


**Figure 54.** Mach 1.4 Pressure Map of the Shock-Boundary Layer Interaction





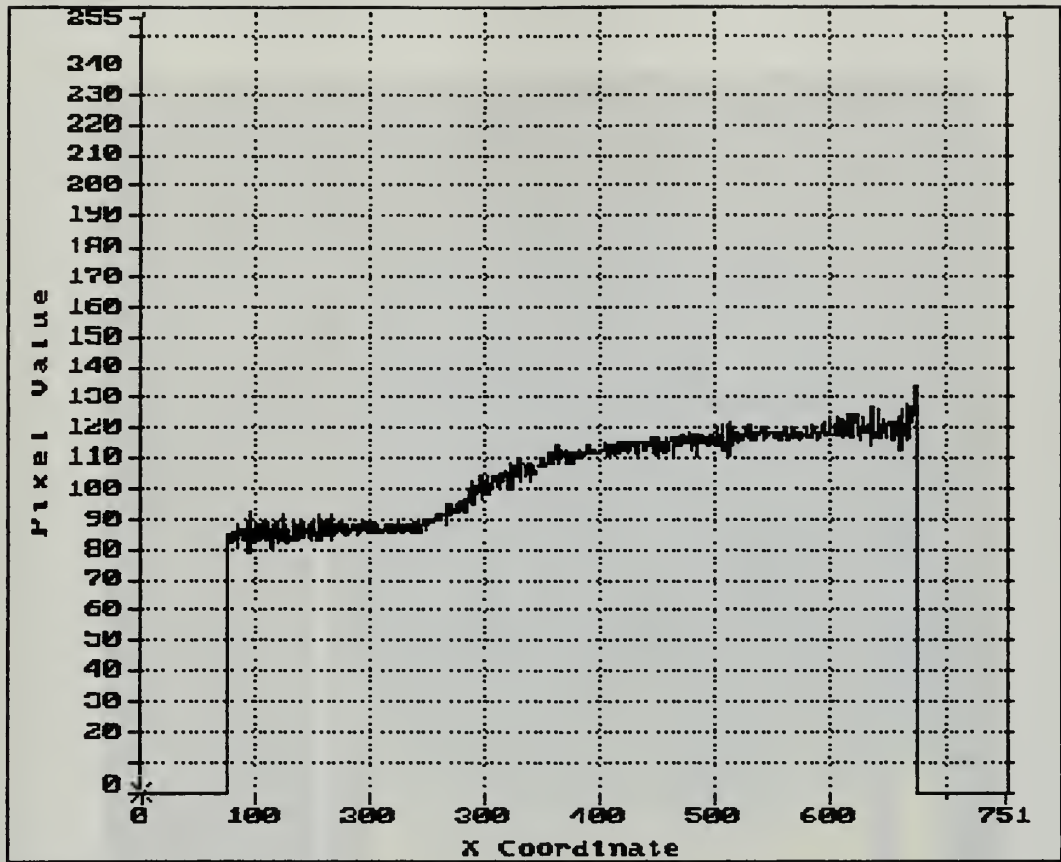


**Figure 55.** Graphical Representation of the Pressure Distribution of the Shock-Boundary Layer Interaction at Mach 1.4

values is displayed in Figure 57. The intensity curve here shows a definite plateau, a region of nearly constant pressure, which is an indication of an extended length of separation. This region corresponds to the area illustrated by the narrow green band in the pressure map of Figure 56.

The calibration curves for the  $M=1.4$  and  $M=1.7$  data are given in Figures 58 and 59 respectively. In contrast to the calibration curves developed for the underexpanded jet/flat plate data, areas of similar temperature are more easily identified in the shock-boundary layer experiment. The data points upstream and downstream of the normal shock have been linearly approximated separately since there was a near



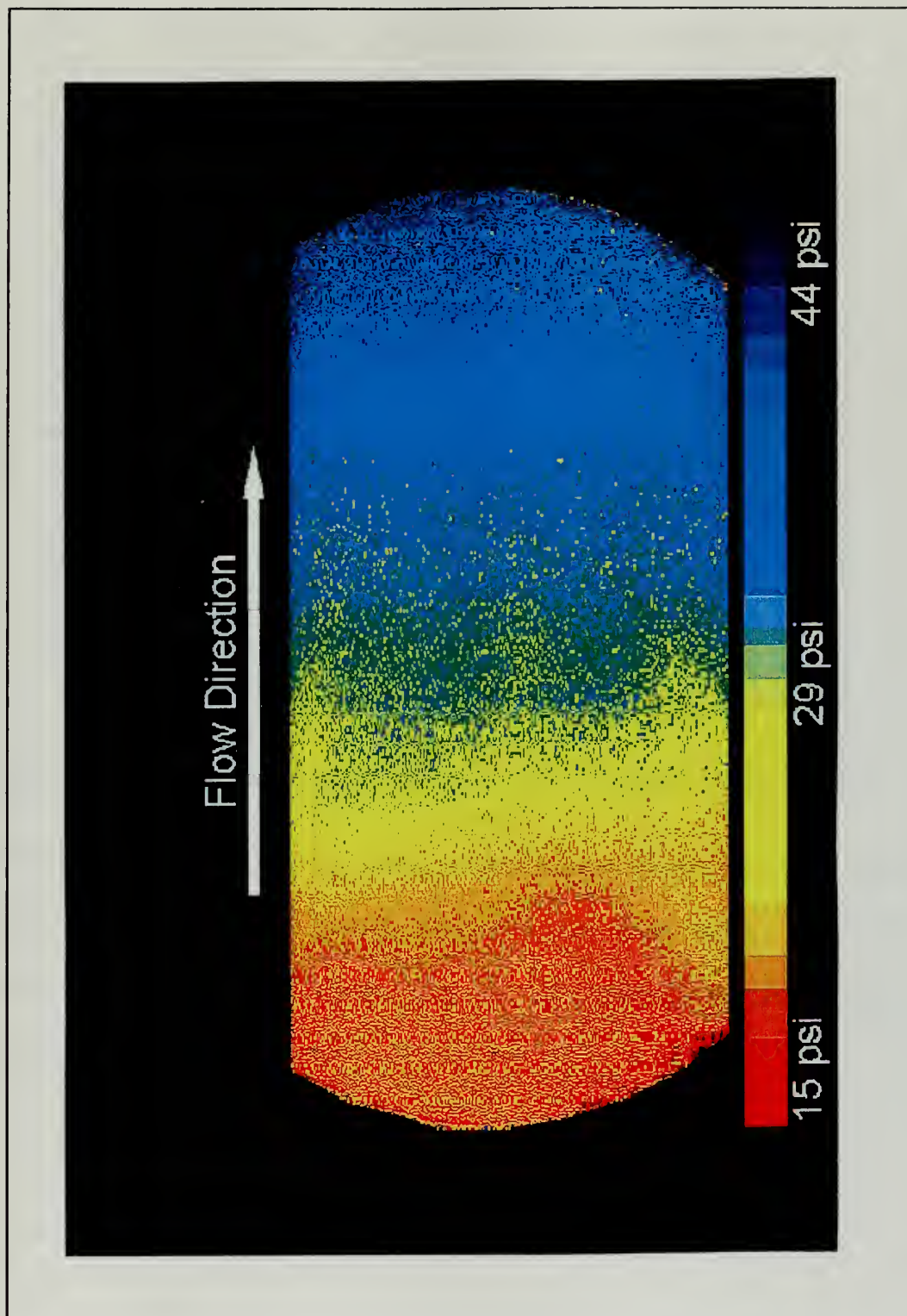


**Figure 56.** Mach 1.7 Pressure Map of the Shock-Boundary Layer Interaction



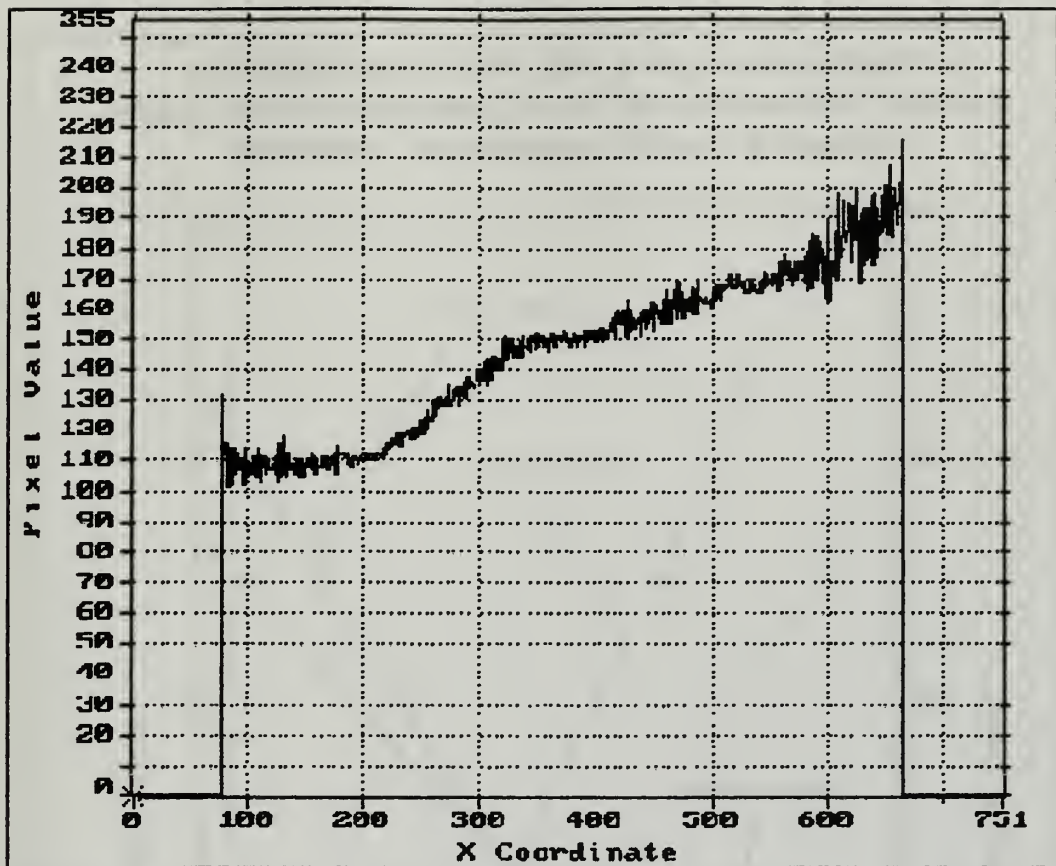


**Figure 57. Graphical Representation of the Pressure Distribution of the Shock-Boundary Layer Interaction at Mach 1.7**

discontinuity in temperature and heat transfer at the shock impingement location. There is seen to be a change in the sensitivity of the paint to pressure change which occurs at the shock. The paint is more sensitive downstream of the shock, which is consistent with the occurrence of higher temperature.



**Calibration Curve For The Shock-Boundary  
Layer Interaction In The Supersonic Windtunnel  
(Mach 1.4 -- 30 psig Plenum Pressure)**

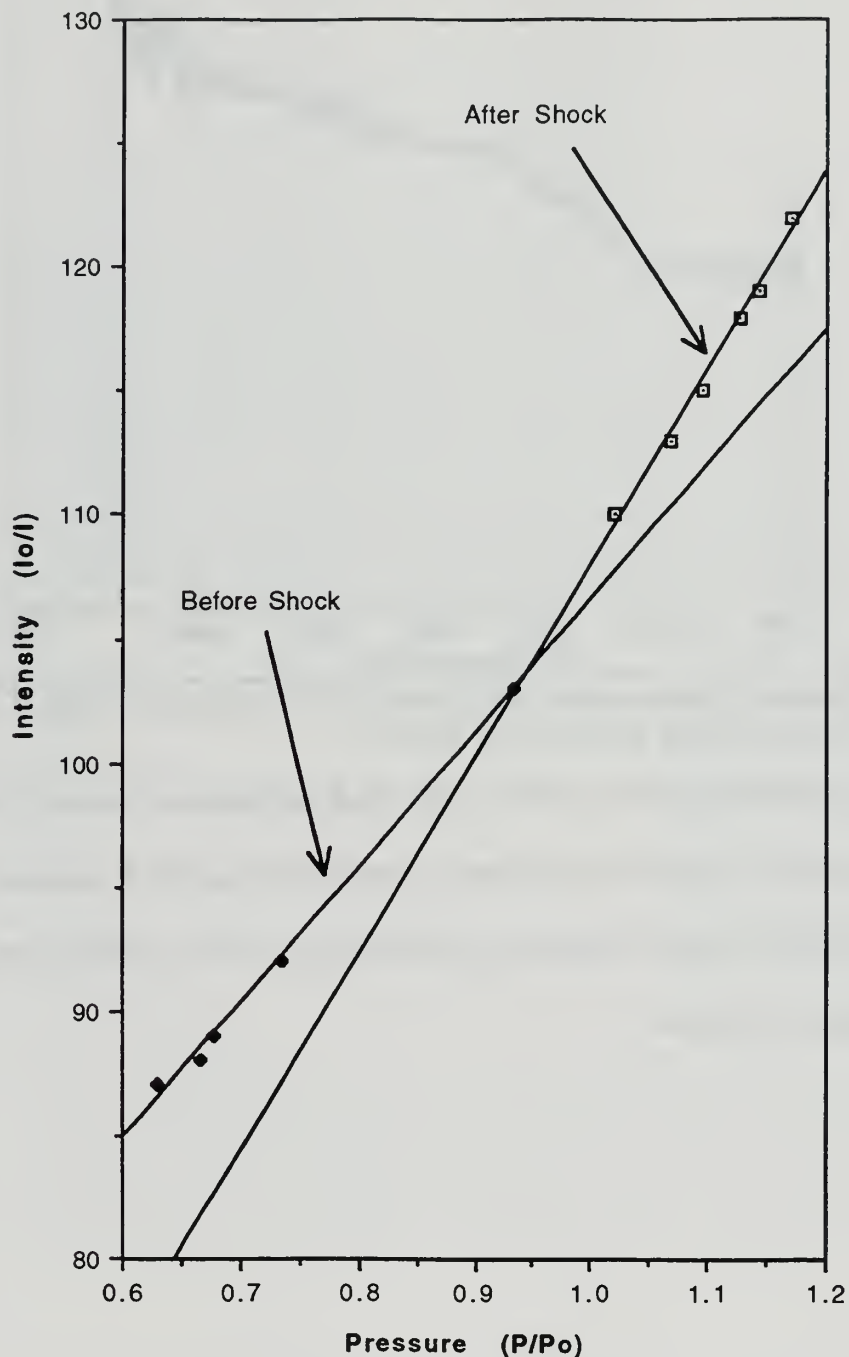


**Figure 58. Calibration Curve for the Mach 1.4 Interaction**

# **Calibration Curve For The Shock-Boundary Layer Interaction In The Supersonic Windtunnel (Mach 1.7 -- 75 psig Plenum Pressure)**

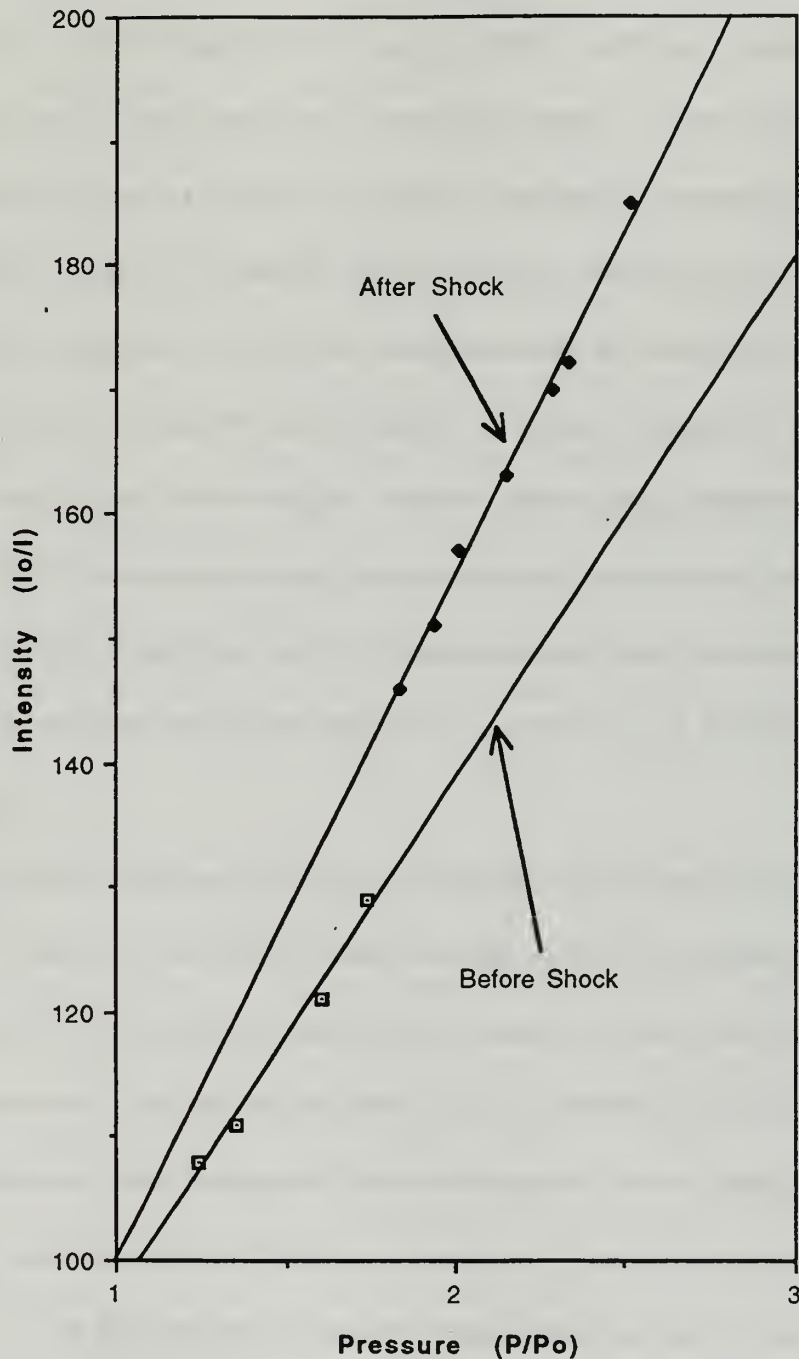


**Figure 59. Calibration Curve for the Mach 1.7 Interaction**



## V. CONCLUSIONS AND RECOMMENDATIONS

The pressure-sensitive paint (PSP) technique offers a flexible and convenient method for measuring surface static pressures in aerodynamic testing. Its most significant feature is the non-intrusive manner in which it provides a mapping of a continuous pressure field over a surface. Because of its detailed spatial resolution (when compared to conventional pressure taps), a complete picture of the events occurring on the surface is available, including details not necessarily anticipated prior to testing. It appears to be highly suitable as a technique to use to validate results calculated using computational fluid dynamics (CFD). In the present study, pressure-sensitive paint was applied successfully in two experimental configurations involving shock-boundary layer interaction. The conclusions drawn from the present application are relevant to any first-time application of the technique.

The luminescent technique, although conceptionally simple, required learning. It was important to understand the entire process, including each of the components comprising the pressure measurement system (paint, optics, camera, software), the limitations of the system (particularly of the luminescent paint), and the interpretation of the measurements through calibration, before meaningful data were acquired. Several attempts to progress through the entire process were found to be necessary. Thus, the initial experimental arrangement (a flat plate immersed in an underexpanded jet) served well as a test bed for building experience before more complicated experimental geometries were attempted.

The components that comprised the current measurement system were adequate for initial experience, system development, and measurements. However, in order to make highly quantitative measurements routinely, some refinements are recommended. The camera and the digitizer combination are, by far, the most critical components in the PSP measurement system. The accuracy and precision of the measurements is highly dependent upon the dynamic range and signal-to-noise ratio of these components. The camera and digitizer used had a grey-scale resolution of eight bits giving a dynamic range of 256:1. Since many measurements, such as in shock-boundary layer interaction experiments, may generate changes in the luminescent intensity as little as two percent, it is crucial that the camera and digitizer be sensitive enough to these changes and to assign a gray-scale value that is appropriate for the given intensity level. Recommendations from NASA Ames Research Center and McDonnell Douglas have suggested a minimum of 14 bits for gray level resolution.

With a relatively low signal being detected, the signal-to-noise ratio at high light levels is limited by the photon shot noise. The accuracy of measurement is contingent upon the highest possible full-well potential of the CCD element, which requires a minimum generation of dark current. Active cooling of the CCD array would maximize the signal-to-noise ratio of the array. Such developments in CCD cameras can be expected [For example, Princeton Instruments Inc. currently offers a Penta Max camera that uses air circulation to cool its CCD array, which achieves -45 degrees Celsius]. Similarly,



system noise can be reduced by combining the digitizer with the camera, thereby reducing electrical noise, and then feeding the signal directly into a memory buffer in the computer.

The EPIX 4Meg Model 12 frame grabber and memory buffer and its associated software was limited in data collection. Since the board was limited to capturing only 11 images per sequence (assuming maximum resolution), the acquisition of one hundred images was far too slow to avoid inaccuracy of the results due to photodegradation of the paint. The EPIX 48Meg Model 12 frame grabber, for example, would provide the ability to capture up to 132 images per sequence. Not only would this reduce or eliminate the error associated with photodegradation, but image processing time would be significantly reduced. Data acquisition speed is mandatory in experiments in which the flow is not completely steady.

A similar issue concerns the present image-processing software. Designed for general applications, it is not the most efficient, or the most suitable, for the PSP applications. Although single-function algorithms such as registration software to spatially align two images together, to compensate for temperature sensitivity and apply the calibration to the data, and routines to pseudo-color the results must be written, consideration should be given to automating the entire process, from acquisition of the data to production of the calibrated pressure field map.

The temperature sensitivity of the paint and its effect on the results is a major concern if pressure measurements are to be made in the compressible flow regime. To accurately measure the pressures on a surface, it will be necessary to know the surface distribution of

temperature so that the calibration curves can be adjusted accordingly. Although temperature measurements could be made using thermocouples, this approach raises the same issues as those associated with using pressure taps to make pressure measurements. A possible solution is to use, concurrently, a high-performance infrared camera to record a high-resolution, continuous image of the temperature distribution on the surface. Since the results from infra-red cameras are produced using a digital process similar to that used in PSP, it is possible that the techniques could be combined to produce a temperature-compensated pressure map.

Finally, the applicability of the present technique to more complicated model configurations with more limited optical accessibility of the surface of interest, has yet to be attempted here. The combination of curved surfaces with significant temperature variations, and with limited optical access, will provide a significant challenge to the successful quantitative use of PSP.

## APPENDIX A. RUSSELL-SANDERS COUPLING

Associated with the angular momentum of an electron is a magnetic moment. When the electron is placed in a magnetic field, the interaction of the field with the magnetic moment of the electron causes the angular-momentum vector to precess about the direction of the external field, much the same way a toy top precesses in a gravitational field. However, in contrast to the top, which can have an infinite number of momentum-vector orientations with respect to the field direction, the angular-momentum vectors of the electrons in an atom (or molecule) are allowed only certain orientations. The solutions of the Schrödinger equation dictate permitted orientations; not every orientation is allowed. The only allowed directions are those at which the components of the angular momentum along the direction defined by the magnetic field have certain quantized values. This behavior is called *space quantization*. [Ref. 10:p. 491]

Each orientation of the momentum vector with respect to the external field direction corresponds to a unique energy state. Since the angular motion of the electron is equivalent to an electromagnet, the energy of the interaction between the magnetic moment it possess and an external field can be expressed as  $E = \mu H \cos \theta$ , where  $H$  is the strength of the external field,  $\theta$  is the angle between the field and momentum vector, and  $\mu$  is the magnetic moment. [Ref. 26:p. 25]

Now consider what happens when a single unpaired electron is not in the presence of a magnetic field. Here, the orbital angular momentum of the electron creates the magnetic

field, defining a specific direction in space. Thus the angular momentum associated with the intrinsic spin of the electron is oriented with respect to this magnetic field. According to space quantization principles, the spin angular-momentum vector of the electron can have two orientations with respect to the direction defined by the magnetic field; this corresponds to the doublet line structure observed for the spectra of an atom, and is the basis for the spin quantum number ( $+1/2$  and  $-1/2$ ) assigned to the electron. [Ref. 26:p.27]

In an atom with several electrons, the orbits are usually oriented first with respect to each other, giving a resultant orbital magnetic moment. Similarly, there is a resultant spin moment which is oriented with respect to the resultant magnetic field due to the orbital motion. With space quantization, the resultant spin vector may have several orientations, each corresponding to a different energy level. Thus, the atom (or molecule) may have several energy levels for a single configuration. [Ref. 27:p. 79] These multiple energy levels for a single configuration of an atom (or molecule) is the basis for Russell-Sanders coupling which impacts the multiplicity of state that an atom or molecule can possess.



## APPENDIX B. LUMINESCENCE COATING CHARACTERISTICS

The luminescent coating used in the present work possessed several undesirable characteristics of which the user must be aware if accurate results are to be obtained. A summary of these is presented below. For a more in-depth discussion, the reader may refer to the references mentioned.

### A. TEMPERATURE SENSITIVITY

The photoluminescence process is temperature sensitive by nature. The coating used in the present work exhibited a non-linear response, and intensity decreased with increasing temperature. This response at a constant pressure is shown graphically in Figure B1. [Ref. 1:p36] The temperature dependence has a significant effect on the calibration curves of intensity vs. pressure. As is shown in Figure B2a, the variations in slope can be significant [Ref. 1:p. 62].

An interesting property displayed by the calibration curve for the coating is the condition where the coating-sensitivity coefficients add to unity (i.e.  $A + B = 1$ , in the Stern-Volmer equation). This occurs when the data taken for  $I$  and  $I_0$  are taken at the same temperature. If this is not the case, the coefficients add to other than one,  $A + B \neq 1$ . The consequences are illustrated in Figure B2. In Figure B2(a) only the 23.7 °C curve exhibits the property that  $A + B = 1$  while the 50 and 6 °C calibration curves were calculated with  $I$  and  $I_0$  at different temperatures. In Figure B2(b), the 50 and 6° C



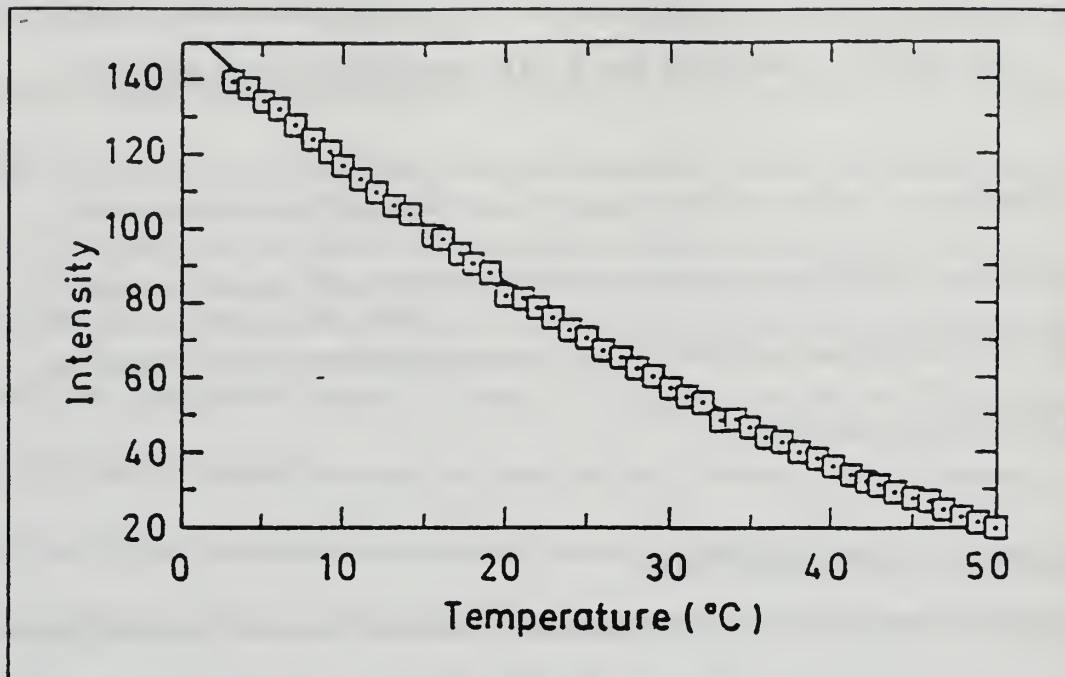


**Figure B1.** Luminescence Intensity as a Function of Temperature [From Ref. 1:p. 36]

calibration curves have been replotted using data for both  $I$  and  $I_0$  obtained at similar temperatures. Clearly, the slope and zero intercept have been significantly altered. [Ref. 1:p.37]

## B. PHOTODEGRADATION

When subjected to ultraviolet light, the luminescent coating undergoes photodegradation, resulting in a decrease of its response with time of exposure. A representative example of this is shown in Figure B3 where intensity is plotted as a function of time of exposure. In this case the coating lost 46% of its response after one hour of exposure. [Ref. 1:p. 36 ]

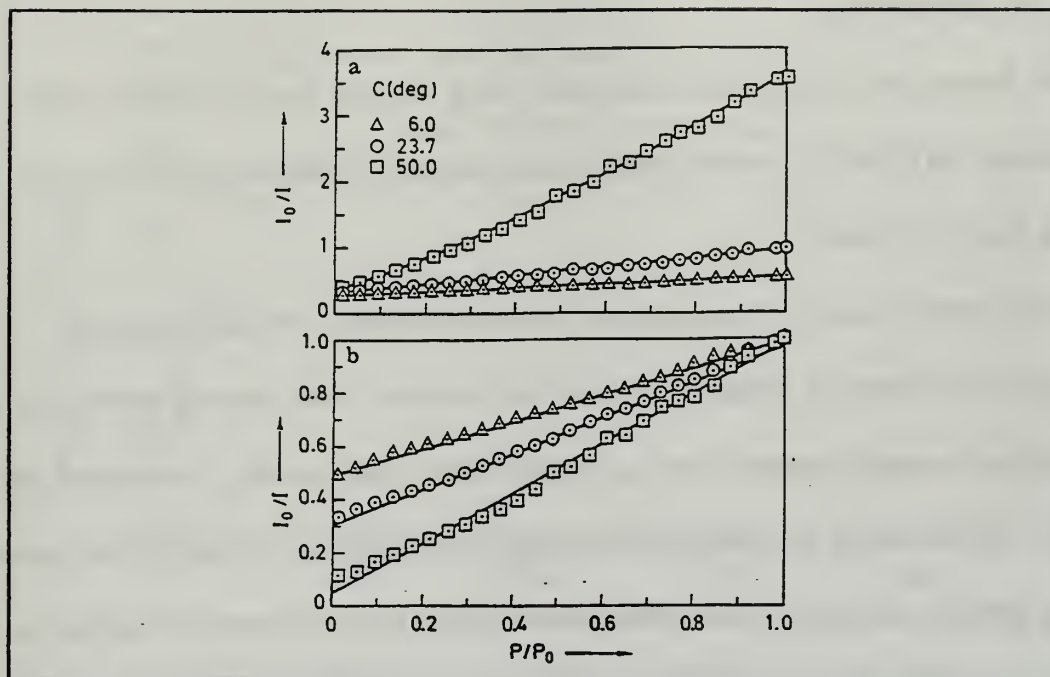


**Figure B2.** Effect of Temperature on Coating Calibration Curves [From Ref. 1p: 37]  
 (a).  $I_0$  for Curve Measured at 23.7° C  
 (b).  $I_0$  for Curve Taken at its Respective Temperature

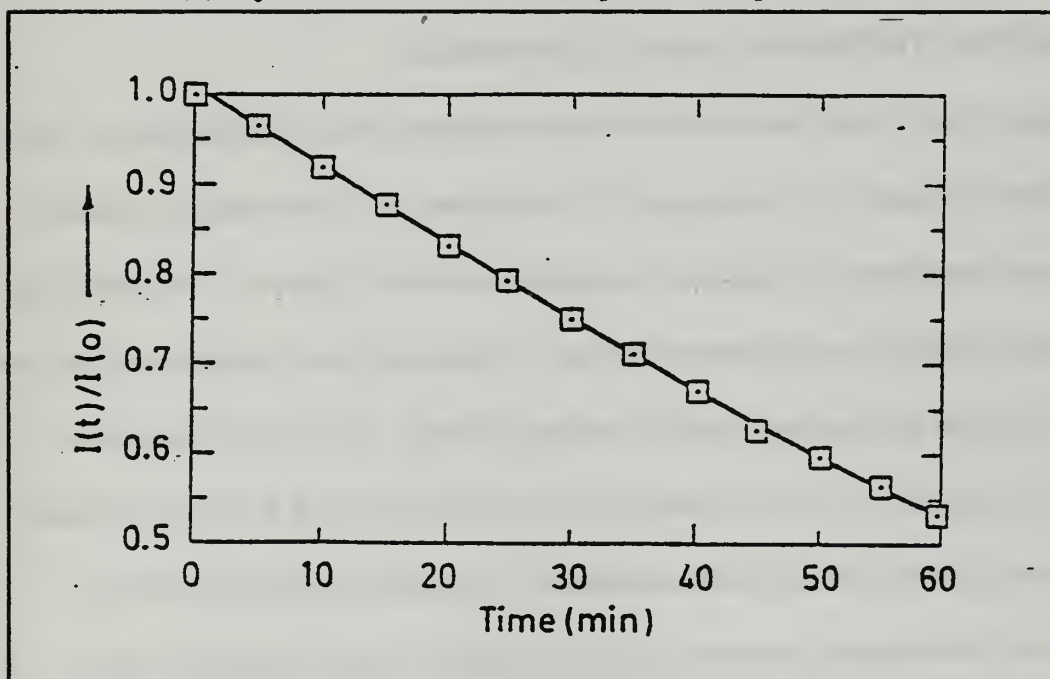


**Figure B3.** Illustrative Example of the Effect of Photodegradation on Response Time [From Ref. 1p:36]

### **C. TIME RESPONSE**

The luminescent coating used in the present work has been found to exhibit a time response on the order of 1 second limiting measurements of pressure fluctuations to no greater than 1 Hz. [Ref. 8:p. 3]

This limitation is not a characteristic of the active molecule. In theory, the time response of the coating to pressure transients may be as fast as the decay of luminescence. For platinum octaethylporphyrin this is approximately 0.1 milliseconds. The problem lies with the polymer matrix in which the active molecule is embedded. By limiting the rate of oxygen diffusion, the polymer slows the optical response to surface pressure fluctuations. [Ref. 1:p. 41]

### **D. COATING THICKNESS / INDUCTION PERIOD**

Kavandi [Ref. 9:p.86] has conducted tests to determine if film thickness has any effect on calibration results. Over the range of 5.5 micrometers to 17 micrometers, consistent with normal application, no significant variations were noted. However, a noticeable lag, or "induction period", existed between the time excitation light was turned on and the time that the detected luminescence reached maximum intensity. The period of maximum intensity was observed to be in the range of 30 to 45 seconds and it is therefore advisable to allow this period to elapse before taking data. A graph of absolute intensity as a function of time following exposure to the exciting light is shown in Figure B4. [Ref. 9:p.89]

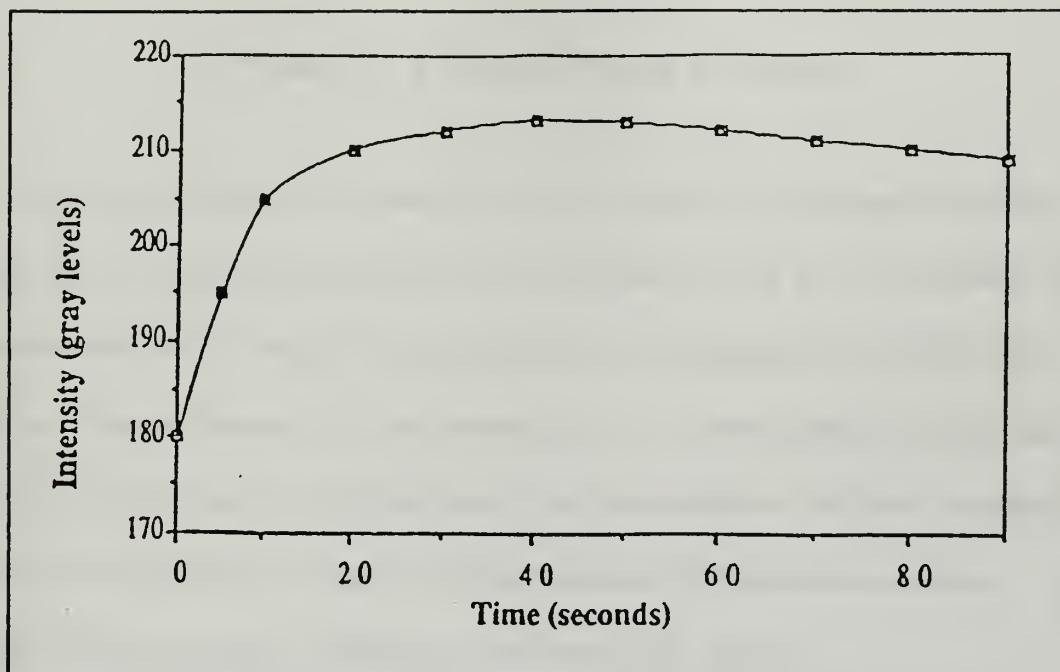


**Figure B4.** Induction Period of the Luminescent Coating with Thicknesses in Excess of 17 Micrometers [From Ref. 9:p. 89]





## **APPENDIX C. EPIX SOFTWARE SUMMARY**

This appendix outlines the software steps used in acquiring, processing and reducing image data. All information discussed here may be found in [Ref. 23]. The appendix is intended to serve as a user guide but is not meant to be a substitute for the EPIX user's manual. The user's manual is vital to developing a sound understanding of the software in order to be able to use it to its fullest extent. The data acquisition and image processing system is set up such that the menus and commands are displayed on the computer monitor while the images are displayed on the Sony image monitor.

### **A. IMAGE DATA ACQUISITION**

The main menu for the EPIX 4MIP-4MIPTOOL software is shown in Figure C1. Prior to data collection, the video resolution is set. Selecting "Video Resolution" from the main menu, the video resolution sub-menu will be displayed as in Figure C2. Check to insure that the "Interlace: Use Distinct (2) Fields ?" is set to "ON". The sampling resolution is considered next and it is application dependent. The sampling resolution sets the size of the video window displayed on the image monitor, allowing the selection of a smaller field of view. The maximum resolution is 752 pixels per line by 480 lines per frame or image (Two fields make up one frame; however the number of lines selected is based on each field, the maximum number being 240. For both fields to be active, the interlace function must be on). Upon setting the desired sampling resolution, the

4MIP V2.8	4MEG VIDEO Image Acquisition, Display, Processing, Analysis Copyright (C) 1984-1993 EPIX, Inc. All rights reserved	
! COMMAND >>		< Quit Menu
> Video Formats		? Help Key Usage
> Video Resolution		> Image Test Patterns & Sequences
> Video Digitize/Display		> Image Processing
> Motion Sequence Capture/Display		> Image Printing
> Special Operations & Modes		> Image File Load/Save
> Contrast & Lookup Tables		> Image Measurements
> Pixel Peek, Poke & Plot		> Paint, Draw & Text Overlay
> Image Zoom & Pan		> Feature Finders
> MIPX Scripts		> DOS Escape
> Custom Menu		> Obscure Menus

**Figure C1. "Main Menu" for EPIX Interactive Image Analysis Software**

> Video Resolution			
! COMMAND >>		< Quit Menu	
! Interlace: Use Distinct (2) Fields ?		ON	
! Horz: Pixels Sampled per Line	752	! Vert: Lines Sampled per Field	240
! Horz: Pixel Width	1	! Vert: Line Height	1
! Horz: Left Edge	8	! Vert: Top Edge	0
! Horz: Right Edge	761	! Vert: Bottom Edge	240
! Horz: Set L/R Centering	ON	! Vert: Set Top/Bot Centering	ON
! Horz: Set Max Samples per Line	OFF	! Vert: Set Max Samples per Field	OFF
Variable Sampling (Pixel Width or Line Height) Parameters:			
! Horz: Width Multiple at Edge	1	! Vert: Height Multiple at Edge	1
! Horz: Width Unaffected Center	1	! Vert: Height Unaffected Center	1
Split Digitize/Display Screen Parameters:			
! Horz: Division Position	2	! Vert: Division Position	2
! Horz: Division Spacing	8	! Vert: Division Spacing	0
! Pixels in each Image	360960	! Image Buffers in Memory	11

**Figure C2. "Video Resolution" Sub-Menu**

number of frame buffers available for capturing images is displayed in the lower right corner of the menu. For 752 x 480 resolution, 11 frame buffers are available. After setting the resolution, return to the main menu by selecting "Quit Menu".

From the main menu, select the "Video Digitize/Display"; this menu is shown in Figure C3. Select the function "Digitize", the result of which is a real-time video display of the camera's field of view. Adjustments to the camera can be performed, such as focus, gain, iris setting, etc., to achieve the desired image. When complete, return to the main menu; the real-time image will remain displayed on the monitor.

Next select the "Motion Sequence Capture/Display" sub-menu; this menu is illustrated in Figure C4. The first step here is to choose the length of the sequence, and which buffers are to be used, by selecting the sequence starting and ending buffers. For example,

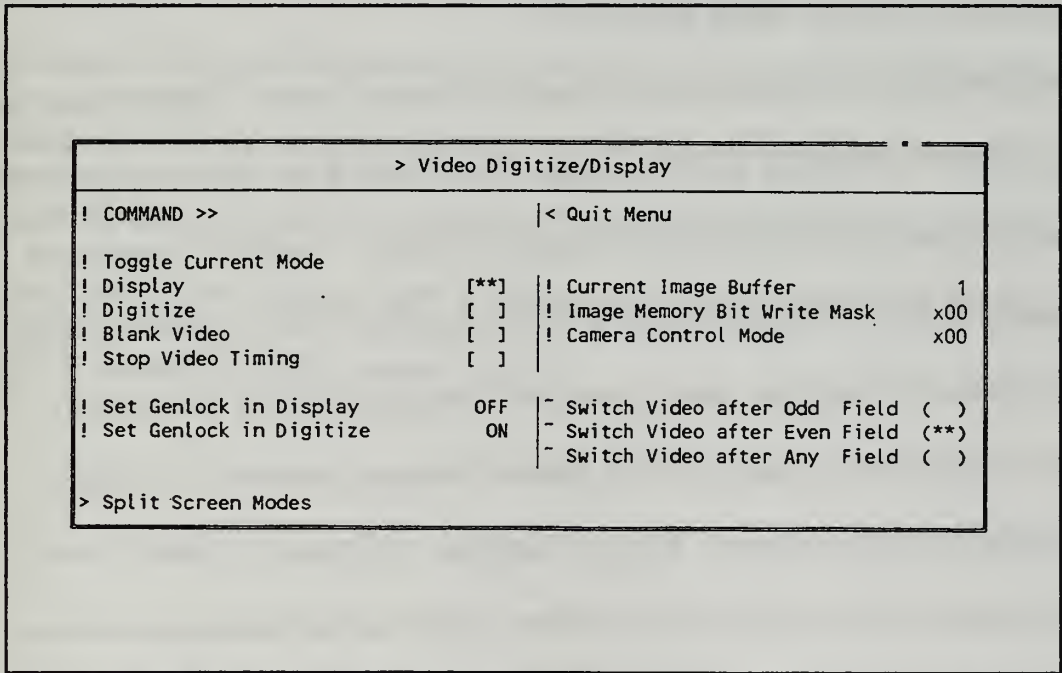


**Figure C3. "Video Digitize/Display" Menu**

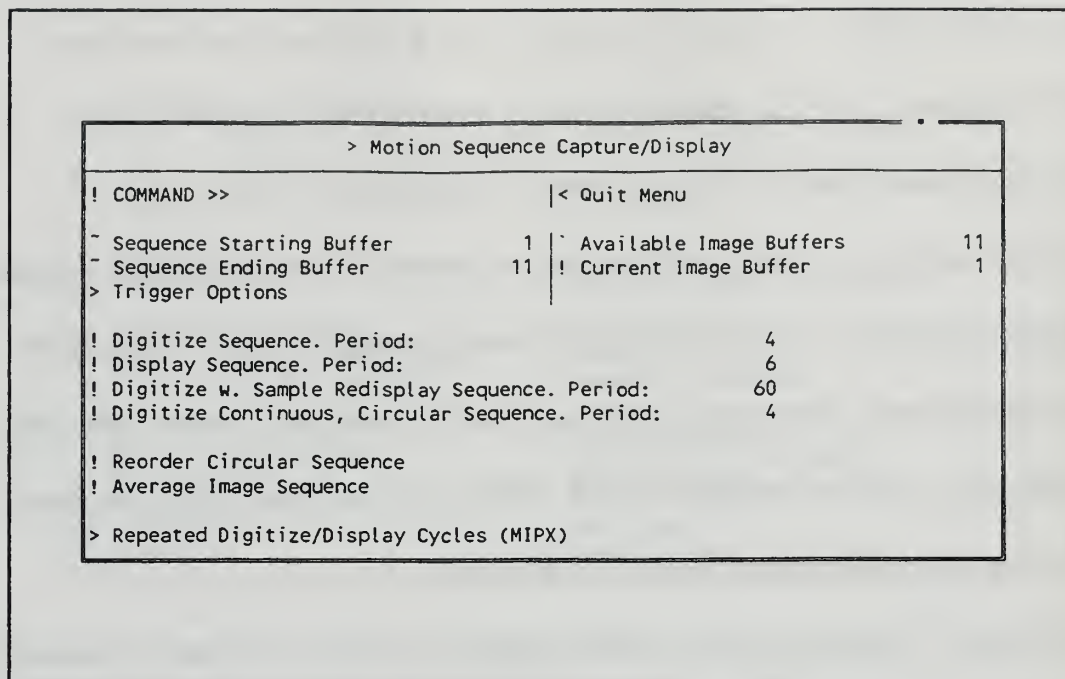


**Figure C4.** "Motion Sequence Capture/Display" Sub-Menu.

in the flat plate/jet interaction work only 10 of the 11 buffers were used; thus the starting buffer was set to 1 and the ending buffer to 10.

The time interval between consecutive samples is then set with the "Digitize Sequence. Period:" function. The period is based on units of video fields if the video is not interlaced (1/60 sec) or video frames if the video is interlaced (1/30 sec). The COHU camera was set internally to send an interlaced image to the frame-grabber board. Since the incoming signal to the board is interlaced, the software can be programmed using the interlace function to store either an image with both fields of the image (interlaced) or an image with a single field (non-interlaced). With the "Interlace: Use Distinct (2) Fields ?" set to active, the period will be based on units of frames. For the jet/plate interaction experiment collection, the period was set to the default value of 4 frame periods between each



captured image or  $4/30 = 2/15$  of a second between each captured image. For the supersonic wind tunnel experiment the period was set to 1 or  $1/30$  of a second between each captured image.

One note concerning this function; to enter the desired period, the mouse or arrow keys are first used to position the cursor on the function. The period is entered using the numeric keys, the program responding to the entry by "highlighting" it red. The entry is then entered into memory by either strobing the left mouse button or striking the "enter" key. This action, however, also starts the execution of the algorithm for sequence image capture. When complete, all designated buffers will contain a captured image. If the image buffer used to display the real-time image lies between the starting and ending sequence buffers, it too will contain a captured image. Therefore, until the desired event is being displayed on the monitor in the real-time format, the entry for the period should not be strobed or the above sequence of events will have to be repeated to redisplay the real time image. It is, of course, not necessary to display a real-time image to capture a sequence of images. By simply re-strobing the "Digitize Sequence. Period:" a new set of images is stored in the designated buffers. Displaying a real-time image of the desired event on the monitor is simply a matter of choice.



## **B. IMAGE PROCESSING**

### **1. Averaging**

The procedure outlined in Chapter III for data collection of the wind-on, wind-off, and dark-current conditions involved executing the above-described steps ten times, i.e., ten images per sequence, executing the motion-sequence algorithm ten times, for a total of one hundred images. After each sequence run, the images in the designated buffers were averaged together to form a single image. This was done by strobing the function "Average Image Sequence" in the "Motion Sequence Capture/Display" sub-menu. The averaged image is stored in the buffer designated as the starting sequence buffer.

The hard drive of the 80386 PC used in the present work contained software applications used in other research, which presented inadequate memory space for image-data storage. Therefore, all data was transferred from the frame-grabber board to floppy disk. The command to store data to disk is found in the main menu and is designated as "Image File Load/Save". From the resulting sub-menu, select the option "File Load/Save, Tiff Format w. AOI". The sub-menu for this option is brought up onto the computer screen. Position the cursor on the option, "Save Image to File. Name", and type "b:filename.tif". Striking the "enter" key will bring up the menu "Select IMAGE BUFFER and/or AREA OF INTEREST" to appear; select the option "Image Area Of Interest: Full Image". The image will then be sent to the floppy. "Full Image" refers to the image size that is set in the "Video Resolution" sub-menu; thus if the image resolution is set to 752 x 480, this will be the image size that is stored on the disk.

Once ten averaged images have been saved to disk, they can be loaded back into ten frame buffers on the frame-grabber board using "Image File Load/Save" function. Again, select "File Load/Save, Tiff Format w. AOI" and then position the cursor on "Load Image from File . Name:". Type "b:filename.tif" and strike "enter". In the "Select IMAGE BUFFER and/or AREA OF INTEREST" sub-menu, select "Image Area Of Interest: Full Image" and strike "enter". The image will be loaded into the current image buffer. The current image buffer is selected by simply toggling the Pg Up/Pg Dn keys.

With all ten averaged images loaded into the frame grabber, return to the main menu and select the "Motion Sequence Capture/Display" function. Insure the "Sequence Starting and Ending Buffers" reflect the sequence of buffers that the averaged images are stored in (See Figure C4). This complete, the images are averaged together using the "Average Image Sequence" option, the resultant image being stored in the buffer designated the sequence-starting buffer. This image represents either the wind-on and wind-off images that will eventually be ratioed or the averaged dark-current image that must first be subtracted from these two images. The three resultant images are again stored on floppy disk.

## **2. Subtraction**

The averaged wind-on, wind-off, and dark-current images are loaded back into consecutive buffers of the frame-grabber board using the steps for loading files that were discussed above. From the main menu select "Image Processing", from which the image-processing sub-menu is displayed on the screen as in Figure C5. Choose the "Two Image

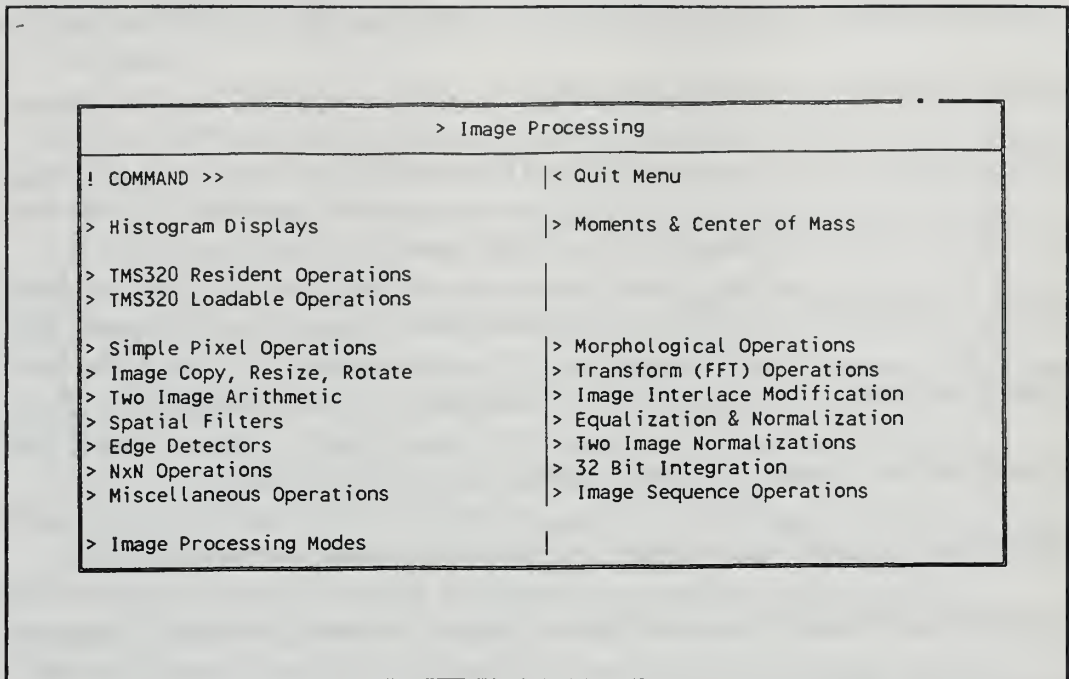


**Figure C5. "Image Processing" Sub-Menu**

Arithmetic" option, which sub-sequently displays the options available for conducting operations involving two images, this menu being illustrated in Figure C6. Four subtraction options may be selected; the option " $\text{Abs}(\text{PixB} - \text{PixA})$ " was used in the present work, where the absolute value of an intensity value is taken if it is less than zero. When this function is selected, the "Select IMAGE BUFFER and/or AREA OF INTEREST" for PixA menu is displayed. Before selecting anything from this sub-menu, ensure that the current-image buffer that is being displayed on the image monitor is that containing the dark current image; this represents PixA. From the "Select IMAGE BUFFER and/or AREA OF INTEREST" menu, choose the option "Full Area of Interest: Full Image". When this step has been completed, the "Select IMAGE BUFFER and/or AREA OF INTEREST" for PixB is displayed. Here, ensure the current image buffer

```

> Two Image Arithmetic

! COMMAND >>                                     |< Quit Menu

! Add Images:      PixB <- PixB + PixA MOD 256
! Add Images:      PixB <- Min(PixB + PixA, 255)
! Subtract Images: PixB <- 128+(PixB-PixA)/2
! Subtract Images: PixB <- PixB - PixA MOD 256
! Subtract Images: PixB <- Max(PixB - PixA, 0)
! Subtract Images: PixB <- Abs(PixB - PixA)
! AND Images:      PixB <- PixB & PixA
! Exclusive OR Images: PixB <- PixB o PixA
! Average Images:  PixB <- (PixA + PixB) / 2

! Product Images:  PixB <- (c0*PixA+c1) * (c2*PixB+c3) / c4
! Product Coefficient: c0      1      | Product Coefficient: c3      0
! Product Coefficient: c1      0      | Product Coefficient: c4      64
! Product Coefficient: c2      1

! Ratio Images:    PixB <- (c0 * PixB + c1) / (c2 * PixA + c3)
! Ratio Coefficient: c0      1      | Ratio Coefficient: c2      1
! Ratio Coefficient: c1      0      | Ratio Coefficient: c3      0

! Function on Images: PixB <- f(PixB, PixA). Expression:

! UnInsert Images: If (PixB = PixA) PixB <- 0. Eps #:      0
! Insert Images: If (PixB == 0) then PixB <- PixA

```

**Figure C6. "Two-Image Arithmetic" Sub-Menu**

being displayed on the monitor is either the wind-on or wind-off image; this represents PixB. Again select "Full Area of Interest: Full Image" from the sub-menu. Execution will begin, the modified image residing in the frame buffer that originally contained PixB. Conduct this operation on both the wind-on and the wind-off images.

### 3. Registration

Registration of images will be unique to every application. As discussed in Chapter III, the registration procedure between the wind-on and wind-off images for the jet/flat plate interaction involved solid body motion, a relatively simple registration problem. Registration between images that involve more complex scenarios such as translational shifts, rotational shifts, and geometric distortions, will require more complicated software procedures than were used here.



If the extent of distortion between the images is simply solid body translation, then the following procedure can be used: Load the wind-on and wind-off images into consecutive buffers. From the main menu, select the "Pixel Peek, Poke & Plot" option; this sub-menu is shown in Figure C7. When this menu is displayed, the cursor will be overlaid on the image monitor, and can be controlled with the left button on the mouse is depressed. The cursor coordinates remain the same as the image buffer is changed, allowing examination of feature registration among image sequences. Thus using the wind-off image as the reference image, the vertical and horizontal characters of the cursor are aligned on a feature or control point that is distinctive in both images. By shifting back and forth between the buffers containing the images, using the Pg Up/Pg Dn keys and not disturbing the cursor location, an indication of the magnitude of distortion is obtained.

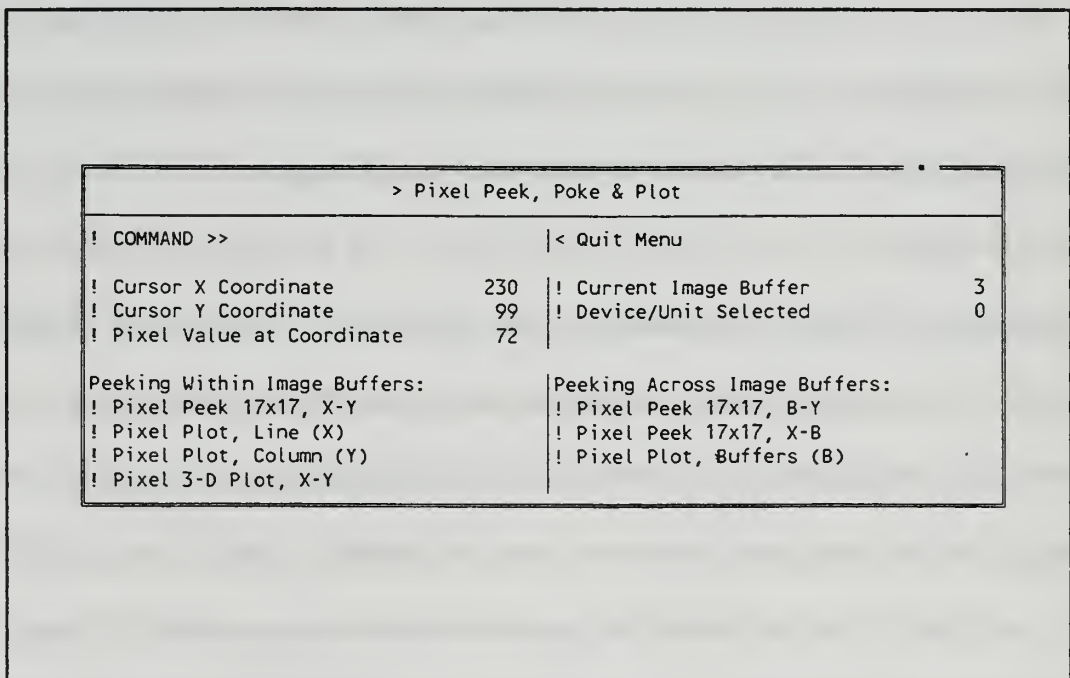


**Figure C7.** "Pixel Peek, Poke and Plot" Sub-Menu



Return to the main menu and select "Image Processing", followed by the option "Image Copy, Resize, Rotate"; this sub-menu is shown in Figure C8. The function "Copy & X,Y Shift" copies an image, shifting the image left or right and up or down in its buffer. The *Left(-X) Right(+X) Shift* parameter specifies the number of pixels the image is to be shifted left or right; the *Up(-Y) Down(+Y) Shift* parameter specifies the number of pixels the image is to be shifted up or down. When the parameters have been entered, strobe the "Copy & X,Y Shift" function using the left button of the mouse or the "enter" key. (Ensure that the wind-on image is in the current image buffer prior to this step). The "Select IMAGE BUFFER and/or AREA OF INTEREST" for image A menu will appear from which the "Image Area of Interest: Full Image" option is selected; when this is done the "Select IMAGE BUFFER and/or AREA OF INTEREST" will re-appear for image B

> Image Copy, Resize, Rotate			
! COMMAND >>		< Quit Menu	
! Copy Image			
! Copy & X,Y Shift			
- Left(-X) Right(+X) Shift:	0	! Copy & Flip Left/Right	
- Up(-Y) Down(+Y) Shift:	0	! Copy & Flip Top/Bottom	
		! Copy & Flip Top/Bottom & Left/Right	
! Copy & Skew Left/Right			
- Skew at Top Edge:	0	! Copy & Skew Up/Down	
- Skew at Bottom Edge:	0	- Skew at Left Edge:	0
		- Skew at Right Edge:	0
Following operations require nonoverlapping source and destination:			
! Copy & Resize w. Bilinear Interpolation			
! Copy & Resize w. Nearest Neighbor Interpolation			
- Interpolate: Top->Up	[**]		
- Interpolate: Top->Down	[ ]		
- Interpolate: Top->Left	[ ]		
- Interpolate: Top->Right	[ ]		
- Interpolate: Top Flipped	NO		
! Copy & Resize w. Linear Area Interpolation			
! Copy & Resize w. Gaussian Area Interpolation			
! Copy & Resize w. Pixel Replication			
- Pixel Replication, X	2		
- Pixel Replication, Y	2		
! Copy & Rotate w. Bilinear Interpolation. Angle:			
			45.0
! Copy & Rotate w. Nearest Neighbor Interp. Angle:			
			45.0
- Rotation Correction for Aspect Ratio (X/Y):			
			2.33

Figure C8. "Image, Copy, Resize, Rotate" Sub-Menu

where again the option "Image Area of Interest: Full Image" is chosen. When this selection is made the operation will then be executed. The current image buffer containing the wind-on image will be replaced with the modified wind-on image. Return to the "Pixel Peek, Poke & Plot" sub-menu and use the cursor to determine if the wind-on and wind-off images are properly registered. Several iterations may be necessary until the images are aligned.

#### **4. Ratioing**

With the images correctly registered, the ratioing process can now be executed, i.e., the wind-off may be divided by the wind-on images. Proceed to the "Two Image Arithmetic" sub-menu as previously done when the dark current image was subtracted from the wind-on and wind-off images. Under the "Ratio Images" option, set the ratio coefficients, that are used for "gain and offset", as follows:  $c_0 = 100$  (or 128),  $c_1 = 0$ ,  $c_2 = 1$ ,  $c_3 = 0$ . Next strobe the "Ratio Images" function which will cause the "Select IMAGE BUFFER and/or AREA OF INTEREST" menu for PixA to be displayed. Ensure the current image buffer is displaying the wind-on image. Select "Image Area of Interest: Full Image". This will cause the "Select IMAGE BUFFER and/or AREA OF INTEREST" to be re-displayed for PixB. Now shift the buffer containing the wind-off image such that it becomes the current image buffer. Again select "Image Area of Interest: Full Image". The ratioing process will then commence replacing the image designated as PixB, i.e., the wind-off image, with the modified image.

## 5. Thresholding

A black background is usually added to the ratioed image to provide contrast and enhancement to the resultant image. From the main menu chose "Image Processing" and then the option "Simple Pixel Operations". Under the function "Threshold Pixel Values" set the values as follows:

- Threshold: Lowbound                      0
- Threshold: Highbound                    255
- Threshold: NewValue                    0

Stroke the "Threshold Pixel Values" function with the left mouse button; the "Select IMAGE BUFFER and/or AREA OF INTEREST" menu will appear. The boundary shape of the painted surface depicted in the ratioed image will dictate which area of interest to select for this image processing operation, i.e., "Interactive Rectangular", "Interactive Elliptical", "Interactive Freehand", and "Interactive Polygon". The area of interest includes the area of the image that the painted surface does not occupy; for the flat plate, since the sides were parallel to the image axis, the "Interactive Rectangular Region" was selected as the region of interest. The area of the flat plate image not occupied by the plate was broken down to four areas of interest, that is, the area above the plate, below the plate, left of the plate, and to the right of the plate. Using the mouse with the right button depressed, these areas were outlined individually with the cursor. Once the areas had been outlined, the thresholding process was executed.

## 6. Pseudocoloring

To add false coloring or pseudocoloring to the gray-scale image, select the "Contrast & Lookup Tables" option from the main menu. This menu is illustrated in Figure C9. Each of the primary colors, red, green, and blue are set by selecting the "Numerically Set & Show" option for the individual colors. The option displays the sub-menu illustrated in Figure C10. Using the function "Set Partial Linear Ramp" any configuration of linear ramps may be constructed. A graphical display of the inputs can be shown on the computer screen by selecting the "Plot Table" option in the menu illustrated in Figure C10.

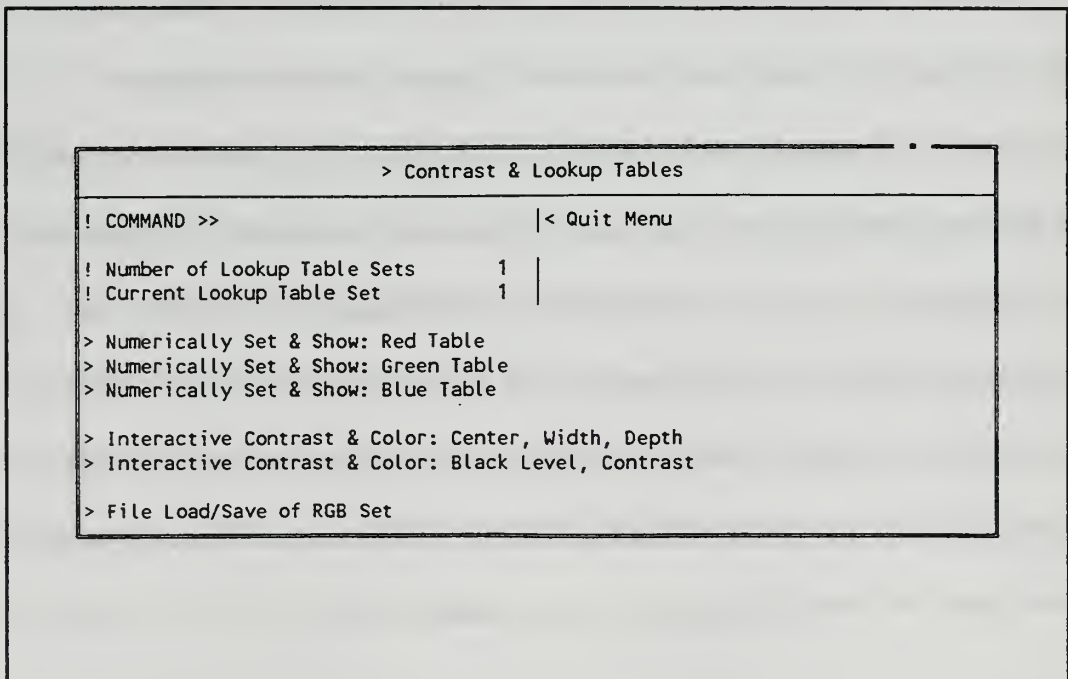


**Figure C9.** "Contrast & Lookup Table" Sub-Menu

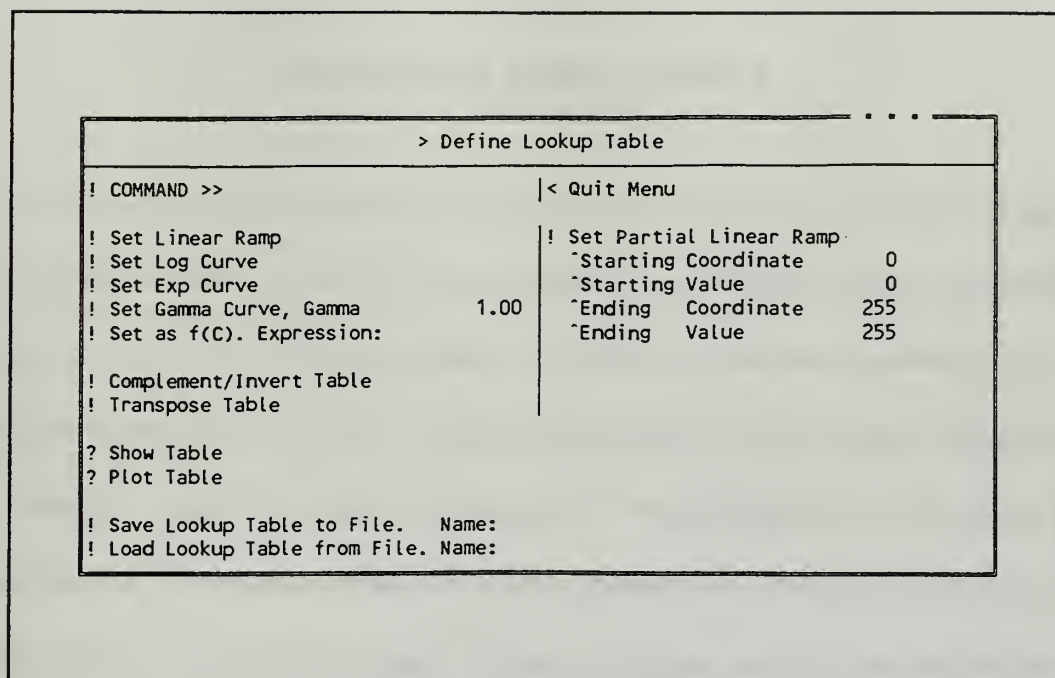


**Figure C10. "Define Lookup Table" Sub-Menu**





## APPENDIX D. DARK CURRENT

Thermal generation of electrons or "dark-current" is a naturally-occurring consequence of using semiconductor devices for photo reception. To understand dark-current effects on pressure-sensitive paint measurements, it is necessary to review the operation of a charged-coupled device (CCD). A schematic illustration of a CCD is shown in Figure D1.

Consider a single CCD electrode in Figure D1. Absent the application of a bias to the gate electrode, a uniform distribution of holes or majority carriers exists in the p-type semiconductor. As a positive voltage is applied to the gate, the holes are repelled from the semiconductor immediately beneath the gate, forming a depletion layer or potential well. An increase in the voltage causes the depletion region to extend further down into the bulk semiconductor, causing an increasing positive potential known as a surface potential to exist at the semiconductor and insulator (oxide) interface. Eventually a gate bias is reached at which the surface potential becomes so positive that the minority carriers (in this case electrons) are attracted to the surface where they form an extremely thin but very dense inversion layer. [Ref. 28:p. 6 ]

In image-sensing applications of CCD's, the minority carriers are generated when photons entering the silicon substrate excite the valence electrons of the material into the "conduction band", becoming free electrons. The electrons are then collected under the

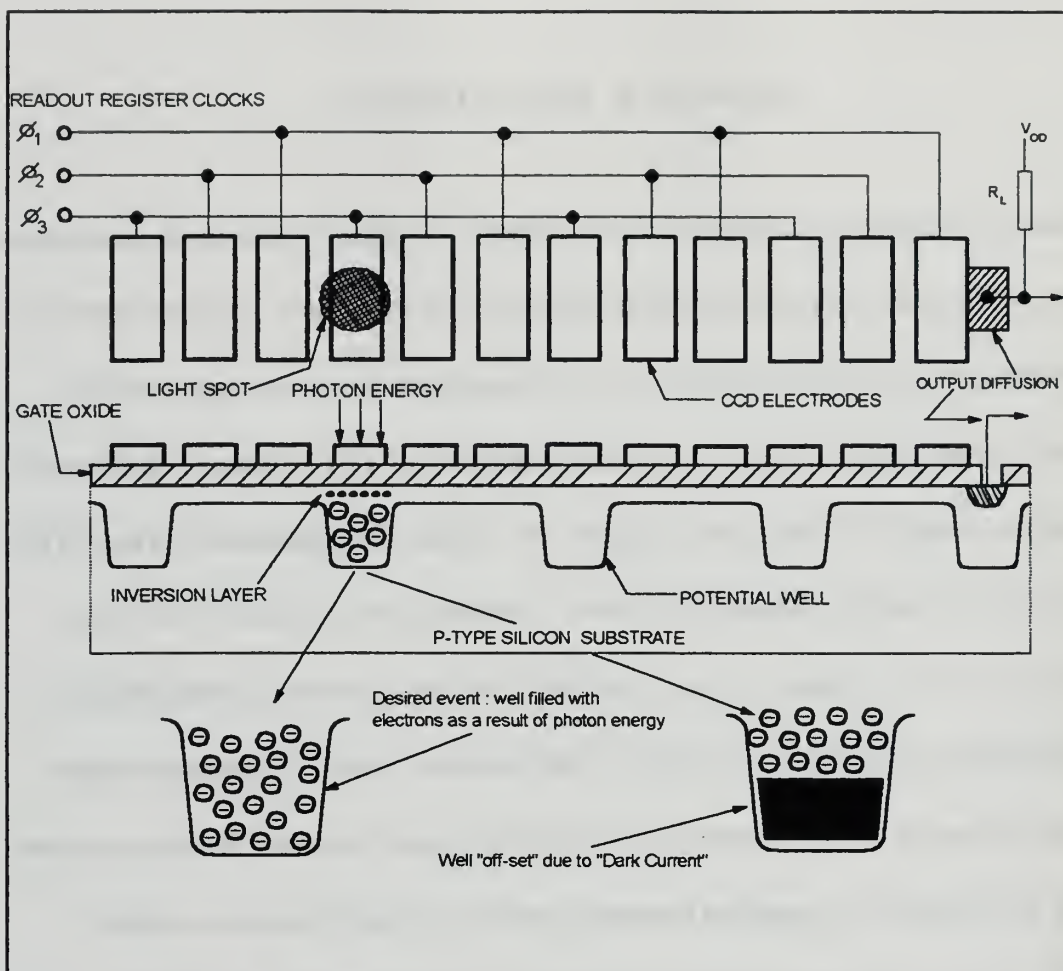


**Figure D1.** Representation of the Effect of Dark-Current on the Creation of Charge electrode of the applied bias. The number of electrons under the electrode within a given period of time is proportional to the local light intensity.

In addition to the photoelectric effect described above, free electrons can also be produced by thermal energy, of which the rate of generation increases exponentially with temperature for a pure semiconductor. Thus, the presence of thermally generated minority carriers limits the maximum possible usefulness of the potential well by displacing optically generated carriers. This produces an "offset" in the measurement image such that the

zero-incident light level does not correspond to a zero gray-level pixel index. Thus, the dark image must be removed from the measurement images. To do this, a dark image is acquired by prohibiting any light from striking the CCD array and sampling an image. Several of these images are taken and time averaged together. This is necessary because dark current generation tends not to be uniform over a whole array. The resulting averaged dark current is then eliminated from the measurement images using image processing techniques discussed in Chapter III.





## **APPENDIX E. SUPERSONIC NOZZLE DESIGN PROGRAM**

Software for the design of two-dimensional supersonic nozzles was acquired from the Naval Surface Warfare Center (NSWC), White Oak, Maryland. The software package is comprised of two programs; the first program is concerned with establishing the isentropic contour of the nozzle while the second corrects for the viscous effects of the fluid and adjusts the contour accordingly.

Support documentation for the software from a user's standpoint is not available. In addition, the early fortran code is not well structured, making it difficult to interpret the algorithm and follow its logic. It is difficult to recognize many of the variables, and there are no comment statements. However, enough information has been deduced such that the program may be operated effectively. The intention of this appendix is to document what is now known about the software.

Modifications have been made to the original software primarily involving the manner in which program input entries are made and data storage accomplished. Originally, the program was designed to access punch-card readers and magnetic-tape drives for data input and output management. Entries are now made directly to the program through interactive software in a format that is more flexible and user friendly. Output data are stored in a file structure compatible with hard drive systems. A listing of the modified software is given in Section C of Appendix E.

## A. INVISCID CONTOUR SOFTWARE (Program char6)

The program "char6" generates the isentropic contour of the supersonic nozzle using the method of characteristics. Initiation of the program will depend on the filename assigned to the object code at the time of compiling and linking of the source code. Once started, the program first displays an introductory summary as shown in Figure E1. As indicated by these remarks, the storage of the output data is currently limited to the data for one run. A successive run will overwrite the data storage files from the previous run.

Entries made by the user through the interactive sequence of prompts for input data have been sub-divided into two categories; the first category identifies the "characteristic" lengths and nozzle type that will be used to define the configuration; the second specifies dimensions and flow characteristics to which the nozzle will be designed.

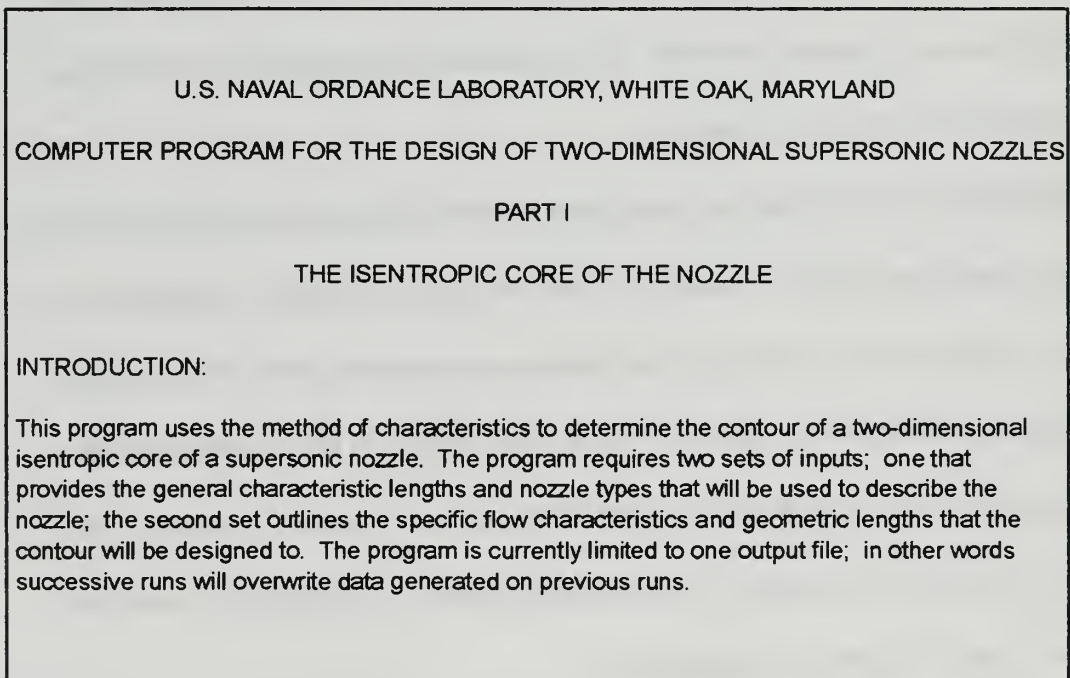


**Figure E1.** Illustrative Example of the Introductory Remarks for Program char6

## **1. Category 1: Characteristic Lengths and Nozzle Types**

### **1. INPUT A DESCRIPTION OF THE PROJECT**

Allows a short summary of the project to be recorded as part of the final output summary. The description is limited to 80 characters.

### **2. INDICATE TYPE OF NOZZLE, 1-SHORT, 2-REGULAR, 3-EXPONENTIAL**

Provides the option of choosing a specific contour shape. The methodology the program uses to generate the contour begins by first determining the centerline Mach number distribution based on the choice of contour. The method of characteristics is then used in conjunction with the centerline distribution in determining contour geometry.

### **3. INDICATE THROAT OR EXIT HEIGHT TO BE READ, 1-EXIT, 2-THROAT**

Irrespective which is used; the program calculates the option not selected using simple isentropic relations. Both heights are employed in the program in computing the contour.

### **4. INDICATE CHARACTERISTIC HORIZONTAL LENGTH TO BE READ, 1-EXIT LENGTH, 2-START OF TEST RHOMBUS**

Refer to Figure E2 for clarification of the horizontal lengths discussed. The exit length is defined as the distance between the nozzle throat and the nozzle exit.

The characteristic network created by the method of characteristics is such that the last two characteristic lines in the grid complete the expansion process by turning the flow parallel to the centerline of the nozzle and thus expanding it to the desired test section Mach number. These two characteristic lines can also be thought of as forming half of an imaginary rhombus as shown in Figure E2. This is known as the test section rhombus. The distance between the nozzle throat and the intersection formed by the two characteristic lines defines the horizontal length referred to above.

### **5. INDICATE OUTPUT, 1-STEP-BY-STEP, 2-WALL POINTS ONLY**

Generally, the approach used in applying the method of characteristics can be summarized in a three step process: Step 1 -- the determination of the characteristic lines in the  $xy$  space using

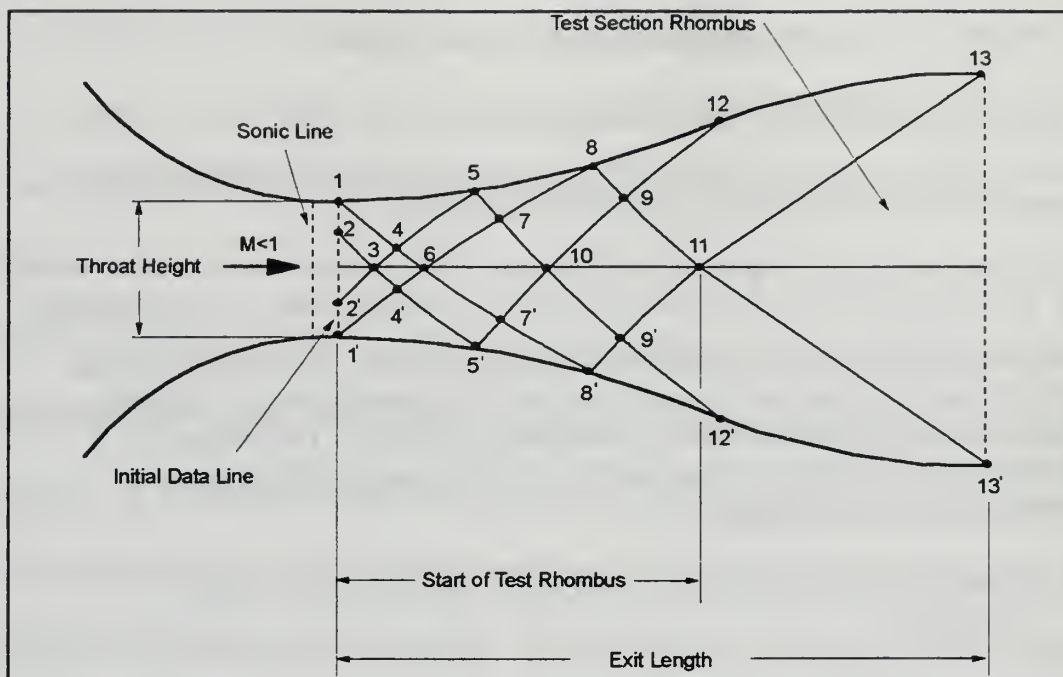


**Figure E2.** Schematic of Supersonic Nozzle Design by the Method of Characteristics

$$\left(\frac{dy}{dx}\right)_{\text{char}} = \tan(\theta \pm \mu)$$

where  $\theta$  is the angle between the streamline of the flow and the horizontal and  $\mu$  is the angle between the streamline and the characteristic line; Step 2 -- the determination of the compatibility equations

$$\begin{aligned} \theta + v(M) &= \text{const} = K_- && \text{(along the right characteristic)} \\ \theta - v(M) &= \text{const} = K_+ && \text{(along the left characteristic)} \end{aligned}$$

where again  $\theta$  is the angle between the horizontal and the streamline, and,  $v(M)$  is the Prandtl-Meyer function, the compatibility equations holding along the characteristics; Step 3 -- the solution of the compatibility equations point by point along the characteristics.

**Note:** The initial data line used in starting the computation of the method of characteristics in this program begins with the assumption that the sonic line at the throat is straight. A point  $\Delta M$  downstream of the sonic line along the centerline Mach number distribution is chosen as the initial point for the characteristics procedure. With the combination of this initial point, the centerline distribution, and the radius of curvature at the throat, the method of characteristics is carried out in a marching fashion.



Choosing the option step-by-step will instruct the program to include in the final output all "steps" used in calculating the characteristic net, including local data pertaining to the nodal points comprising the turning angle, the x and y coordinates of the grid points and the Mach number. If in turn the option "wall points only" is exercised, the data associated with the grid points that decide the contour or wall geometry are included in the final output.

Once the last selection for the first category of inputs is chosen and the "enter" key is subsequently struck, the selections made are then displayed in the following format:

NOZZLE = SHORT (REGULAR, EXPONENTIAL)

HEIGHT TO BE READ = EXIT (THROAT)

LENGTH TO BE READ = LENGTH TO EXIT (LENGTH TO RHOMBUS)

OUTPUT FORMAT = STEP-BY-STEP (WALL POINTS)

The question, "Are input values correct?, 1-Yes, 2-No", follows immediately, allowing the opportunity to make changes to the inputs if necessary. Selecting "Yes" causes the following menu to be displayed:

INPUT VALUES TO BE CHANGED (1, 2, 3, 4):

1- TYPE OF NOZZLE: A. SHORT, B. REGULAR, C. EXPONENTIAL

2 - HEIGHT TO BE READ: A. EXIT, B. THROAT

3 - LENGTH TO BE READ: A. EXIT, B. TEST RHOMBUS

4 - TYPE OF OUTPUT: A. STEP-BY-STEP, B. WALL POINTS ONLY

By selecting a value from one to four a sub-menu of the descriptors to the right of the colon of the input chosen is listed. For example, selecting the value of 2 (Height to be read) from the above menu yields

1 - EXIT, 2 - THROAT



prompting a choice of height designation. After hitting the "enter" key, the program will again display the first-category input selections, showing the latest modifications. An opportunity to make additional alterations is also afforded when the question, "Any other changes?, 1-Yes, 2-No", immediately follows. Selection of "No" initiates the sequence of events for data input associated with the second category.

## **2. CATEGORY 2: NOZZLE FLOW AND GEOMETRY SPECIFICATIONS**

Commencement of the sequence of prompts for the second category of inputs is denoted by the statements

**"THE NEXT SET OF INPUTS SPECIFY FLOW CHARACTERISTICS AND  
SPECIFIC GEOMETRY DIMENSIONS FOR THE NOZZLE"**

**\*\*\*\*\* PLEASE UTILIZE DECIMAL POINTS FOR THESE INPUTS \*\*\*\*\***

It is necessary to use decimal points when specifying numeric data; the program is formatted to read the input data in scientific notation, though numeric values may be entered into the program as real numbers. If a decimal point is not explicitly stated, the exponent field in the scientific notation format will reflect this with zeros, resulting in an ambiguous input. Thus, if the real number "14" is the desired input, it must be entered as "14."; this results in the scientific notation representation "0.14000E+02". If the number is entered as "14", the resulting representation will be "0.14000E+00".

The inputs for the second group are outlined as follows:

### **1. INPUT RATIO OF SPECIFIC HEATS**

Self-explanatory.

## 2. INPUT TEST SECTION MACH NUMBER

The Mach number of the uniform flow that is required at the exit plane of the nozzle.

## 3. INPUT EXIT LENGTH (INCHES) OR INPUT BEGINNING OF TEST RHOMBUS (INCHES)

The choice made in the first category of inputs concerning the horizontal length will dictate which prompt will be displayed. Refer to Figure E2.

## 4. INPUT HALF HEIGHT OF EXIT (INCHES) OR INPUT HALF HEIGHT OF THROAT (INCHES)

Again dependent on the selection made in the first category of inputs with reference to the height to be read.

## 5. INPUT RADIUS OF CURVATURE AT THROAT (INCHES)

Self-explanatory.

## 6. INPUT MULTIPLICATIVE FACTOR FOR "X" INCREMENT

Influences the spacing between consecutive contour points. A range between 1.0 (representing 150 points to describe the contour) to 0.5 (representing 400 points) is available.

Note: Generation of the cubic centerline Mach number distribution, which is associated with the regular nozzle contour, is dependent upon the result of a "feasibility expression" involving the second category values input by the user. If the outcome of the expression does not fall into a pre-determined interval, the program halts execution and displays the message,

\*\*\* CUBIC CENTERLINE MACH NO. DISTRIBUTION IS  
NOT APPROPRIATE FOR INPUT GIVEN \*\*\*

At this point, the program must be re-initialized and the process of re-entering the input started over. One of the input values, gamma, test section Mach number, exit length or length to test rhombus, exit or throat height, or the radius of curvature, or a combination thereof

must be changed such that the compatibility requirements set forth by the feasibility expression are satisfied.

When the data for the multiplicative factor has been entered and the "enter" key struck the second category of inputs are displayed in the following fashion:

```
GAMMA = 0.14000E+01
SMT = 0.17000E+01
XEXXT = 0.11500E+02
YTHEX = 0.19500E+01
RCT = 0.11500E+01
DELMUL = 0.70000E+00
ARE INPUT VALUES CORRECT ?, 1 - YES, 2 - NO
```

where

```
GAMMA = Ratio of specific heats
SMT = Test section Mach number
XEXXT = Exit length or length to the beginning of test
        rhombus depending on the choice in first category
        of inputs
YTHEX = Half height of exit or half height of throat depending
        on the choice in the first category of inputs
DELMUL = Multiplicative factor for "x" increment
```

As in the first category of inputs, the option to make changes to the input data is available. When changes are desired a listing of the input descriptors is displayed:

```
INPUT VALUE TO BE CHANGED: 1 - GAMMA, 2 - SMT,
3 - XEXXT, 4 - YTHEX, 5 - RCT, 6 - DELMUL
```

A selection will exhibit a directive prompting the user to input the new value. For example, choosing gamma (1) results in,

```
INPUT NEW VALUE FOR GAMMA
```

Fulfilling this and subsequently striking the "enter" key causes the second category of inputs to be re-displayed showing the recent modifications. Additional changes may also be conducted at this point if necessary.

If the second category of inputs have been reviewed with satisfaction, the program will begin calculation of the isentropic contour at this point. Conclusion of the routine is indicated by the remarks,

**OUTPUT ISENTROPIC DATA FOR NOZZLE CONTOUR  
STORED IN FILENAME "outpt1"**

**DATA FROM THIS FILE TO BE USED IN THE VISCOUS  
PROGRAM "nbl6.f" IS STORED IN FILENAME "outpt2"**

The file "outpt1" contains a systematic breakdown of the data calculated by the program which are then available to the user for review. A complete explanation and an example of the format are presented in the following section. The file "outpt2" contains the data that are to be utilized in the program "nbl6" and are in a format that is convenient for file processing.

### **3. "outpt1" EXAMPLE AND DESCRIPTION**

Figure E3 shows the format in an example of the file "outpt1". It has been sub-divided into its major components and labeled for reference below.

1. Introductory Header - Self-explanatory.
2. Descriptive Comments - Refers to the comments made in the first category of inputs when prompted by the program for a description of the project.
3. User Inputs - Encompasses all the inputs into the program made by the user. The input identifiers associated with the first category of inputs are defined as follows:

INDSR = Nozzle Type  
INDYTH = Characteristic Height (Throat or Exit)  
INDXTE = Characteristic Length (Exit or Test Rhombus)  
INDOUT = Output Mode (Step-by-Step or Wall Points)



U.S. NAVAL ORDNANCE LABORATORY, WHITE OAK, MARYLAND							INTRODUCTORY HEADER
COMPUTER PROGRAM FOR THE DESIGN OF TWO-DIMENSIONAL SUPERSONIC NOZZLES							
PART I							DESCRIPTIVE COMMENTS
THE ISENTROPIC CORE OF THE NOZZLE							
1.7 MACH NOZZLE							USER INPUTS
INPUT DATA							
CARD NO. 1	INDSR = 2 INDYTH = 1 INDXTE = 1 INDOUT = 1 INDCAL = 0 INDTAP = 0 INDCRD = 0						NOZZLE PARAMETERS
CARD NO. 2	GAMMA = 0.14000E+01 SMT = 0.17000E+01 XEXT = 0.11500E+02 YTH = 0.19800E+01 RCT = 0.11500E+02 DELMUL = 0.70000E+00						
NOZZLE PARAMETERS							CENTERLINE DISTRIBUTION
MACH NO.	YTH	YEXT	XEXT	XT			
0.17000E+01	0.14803E+01	0.19800E+01	0.11500E+02	0.87780E+01			
	RCT	B					
	0.11500E+02	0.35425E+00					
CENTERLINE MACH NUMBER DISTRIBUTION USING CUBIC EQUATION							METHOD OF CHARACTERISTIC RESULTS
	N	X	MACH NO.				
	1	0.534600E-03	0.100010E+01				
	2	0.732600E-03	0.100014E+01				
	3	0.930600E-03	0.100017E+01				
	.	.	.				
	.	.	.				
	.	.	.				
CHARACTERISTICS MANIPULATION ( *INTERPOLATED WALL VALUES)							CONTOUR OUTPUT
N	K	X(INCHES)	Y(INCHES)	MACH NO.	STREAM ANGLE		
2	3	0.629684E-03	0.6428261E-02	0.000000E+00	0.136713E-04		
2	2	0.828632E-03	0.5607560E-02	0.000000E+00	0.156680E-04		
3	3	0.718964E-03	0.1198140E-01	0.000000E+00	0.293399E-04		
.	.	.	.	.	.		
.	.	.	.	.	.		
.	.	.	.	.	.		
FINAL OUTPUT TO PART I, ISENTROPIC CORE CONTOUR							
I	X(INCHES)	Y(INCHES)	CL MACH NO.	WALL MACH NO.	WALL ANGLE	RAD OF CURV (IN)	
1	0.435619E+00	0.149273E+01	0.107887E+01	0.114198E+01	0.220395E+01	0.000000E+00	
2	0.462758E+00	0.149380E+01	0.108359E+01	0.114598E+01	0.228777E+01	0.188330E+02	
3	0.490391E+00	0.149492E+01	0.108838E+01	0.115003E+01	0.237073E+01	0.193154E+02	
.	.	.	.	.	.	.	
.	.	.	.	.	.	.	
.	.	.	.	.	.	.	

Figure E3. Example Showing the Format of File "outpt1"



INDCAL, IND TAP, and INDCRD are no longer user-accessible. These variables were used in the original software and controlled the medium to be used to record the output data, i.e., magnetic tape or punch cards. The variables have been "hardwired" in order to accommodate the current software modifications for data output management.

The input descriptors for the second category of inputs have been previously defined.

4. Nozzle Parameters - These include, in addition to those dimensions supplied by the user, the "related" values calculated by the program using isentropic relationships or simple geometric relations. Thus, given the input of the throat height the program calculates the exit height, or, given the horizontal length from the throat to the exit plane the program calculates the length from the throat to the test rhombus. The parameters are defined as,

Mach No. = Nozzle exit Mach number

YTH = Half height of nozzle throat

YEXIT = Half height of nozzle exit

XEXIT = Length between nozzle throat and exit

XT = Length between nozzle throat and test rhombus

RCT = Radius of curvature at throat

\* B = Indicates result of "Feasibility Expression"

\* Note: The result of the feasibility expression, to determine if the cubic centerline Mach number distribution may be calculated with the given nozzle dimensional inputs, must fall in the interval  $-2.0 < B < 1.0$ .

5. Centerline Mach Number Distribution - Denotes the centerline location (relative to the throat) and corresponding Mach number. The function used to generate the distribution, i.e., cubic, exponential, etc., is dependent upon the choice of nozzle type (regular, exponential, short).
6. Method of Characteristic Results - Describes the characteristic manipulation used to generate the wall values along the contour.

N = Characteristic line (From left to right)

L = Nodal points along characteristic line

X (inches) = X-coordinate of nodal point

Y (inches) = Y-coordinate of nodal point

Mach No. = Local Mach number at nodal point

Stream angle = Local velocity angle at nodal point with respect to the horizontal

7. Contour Output - Final output of the isentropic core.

X(INCHES) = X - coordinate of isentropic core

Y(INCHES) = Y - coordinate of isentropic core

CL MACH NO. = Centerline Mach number

WALL MACH NO. = Mach number along contoured wall

WALL ANGLE = Wall angle relative to centerline

RAD. OF CURV. (IN) = Radius of curvature

## **B. MODIFICATION FOR VISCOUS EFFECTS (Program nbl6)**

The program "nbl6" modifies the contour of the nozzle to account for the boundary layer formation. Originally, this software considered the boundary layer effects along the contour of the nozzle only and neglected the effects that would be caused with the addition of side walls. To compensate for this deficiency in correcting for boundary layer displacement, the approach used by Demo [Ref. 29: p. 24] was employed. The assumption is made that the displacement thickness is the same on both contoured and side walls. The viscous displacement effects on all surfaces are then summed together and evenly distributed between the two contour surfaces only, as illustrated in Figure E4.

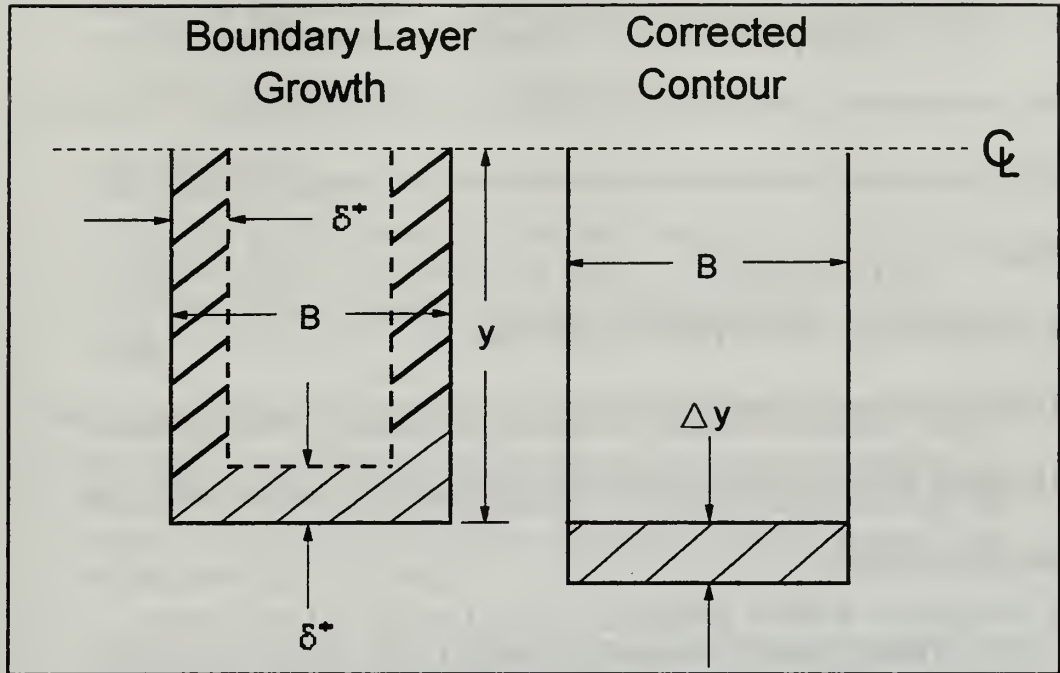


**Figure E4.** Nozzle Wall Correction for Boundary Layer

Thus, the total displacement area of the entire nozzle cross-section is compensated by modifying only the contoured walls, allowing the side walls to remain flat and parallel. The displacement required to the inviscid contour was calculated using the expression

$$\Delta y = \frac{2y\delta^* + (B - 2\delta^*)\delta^*}{B} \quad (E1)$$

where  $\delta^*$  = displacement thickness,  $B$  = nozzle width, and  $y$  = half height of the contour. This equation has been incorporated into the software. The final output, discussed later, was modified to reflect this change.

The data-output management structure, as before, is limited to storing data for one run. A successive run will overwrite the data stored from the preceding run.

Input into the program is supplied by both the output from "char6" (i.e., file outpt2) and the user using an interactive presentation similar to that discussed above for the

inviscid contour. The first category of inputs consists of a series of functional mode selections concerned with the thermal and velocity boundary layer behavior. The second category is comprised of numerical input prompts for flow conditions and nozzle dimensions.

1. CATEGORY 1: FUNCTIONAL MODES

The functional modes establish the desired profile behavior that the velocity and thermal boundary layers will undergo while traversing the length of the nozzle. The modes are outlined below.

- 1. INDICATE WHERE THE BOUNDARY LAYER CALCULATION WILL TAKE PLACE, 1. ALONG CENTERLINE ONLY, 2. ALONG THE WALL ONLY, 3. BOTH THE CENTERLINE AND THE WALL

Specifying the first option results in the message,

```
*****
*           CENTERLINE PARAMETER INPUT DATA           *
*****
```

indicating that all input into the program from this point will pertain to the effects of the boundary layer along the nozzle centerline. Selection of the second option displays

```
*****
*           WALL PARAMETER INPUT DATA                   *
*****
```

indicating further inputs will apply to the effects of the boundary layer along the nozzle contoured walls. Option three effectively causes the program to run twice, once for the effects along the centerline followed by a run associated with the boundary layer effects along the contoured walls. The final output for option three is consolidated as a single output vice individual outputs for each run.



2. INDICATE BOUNDARY LAYER MODE BEGINNING AT NOZZLE THROAT, 1. STRICTLY LAMINAR, 2. STRICTLY TURBULENT, 3. LAMINAR-TRANSITION-TURBULENT

Self-explanatory.

3. INDICATE WALL TEMPERATURE FOR NOZZLE, 1. CONSTANT TEMPERATURE, 2. ADIABATIC WALL, 3. TEMPERATURE DISTRIBUTION ALONG NOZZLE TO BE INPUT BY PROGRAM USER

Wall temperature is assumed only along the contour of the nozzle. Since the boundary layer displacement thickness for the entire cross-section of the nozzle is a function of the displacement thickness generated along the contour, it can be thought of that the temperature distribution exists both on the contour and side walls.

4. INDICATE THE CHARACTERISTIC PARAMETER ON WHICH TRANSITION WILL BE BASED, 1. REYNOLDS NUMBER, 2. "X" DISTANCE FROM THE THROAT

The transition mode only becomes active if the laminar-transition-turbulent selection of the boundary layer mode is chosen. The point of transition from laminar flow to turbulent flow may be based upon a horizontal distance "x" relative to the nozzle throat and along the centerline or a Reynolds number in which the momentum thickness of the boundary layer is used as the characteristic length

The last entry made for the mode options is followed by a listing of the selections to verify the settings:

B.L. MODE = LAMINAR (TURBULENT, LAM-TRANS-TURB)

WALL TEMP. MODE = CONSTANT (ADIABATIC, USER  
DEFINED)

\*TRANSITION PARAMETER = REYNOLDS NUMBER ("X"  
DISTANCE)

B.L. CALCULATION = CENTERLINE ONLY (WALL ONLY,  
BOTH CENTERLINE AND WALL)



"ARE INPUT VALUES CORRECT?, 1-YES, 2-NO

\*Note: Displayed only if B.L. Mode = Lam-Trans-Turb

If a mode is incorrectly set or a change is desired, "no" is subsequently chosen, resulting in a modification menu:

INPUT VALUE TO BE CHANGED (1,2,3,4):

1. B.L. MODE: A. LAMINAR, B. TURBULENT, C. LAM-TRANS-TURB
2. WALL TEMP. MODE: A. CONSTANT, B. ADIABATIC, C. USER DEFINED
3. B.L. CALCULATION: A. CENTERLINE, B. WALL, C. CENTERLINE AND WALL

\*4. TRANSITION: A. REYNOLDS NUMBER, B. "X" TRANSITION

\*Note: selection of the transition mode with the B.L. Mode set other than B.L. Mode = Lam-Trans-Turb will result in the message, "Transition parameter not required for inputs given".

The mode to be modified is selected from the menu list, which in turn causes a sub-listing of the options to which the mode may be set to be displayed. For example, if the boundary layer mode is to be changed, its selection from the modification menu would be followed by,

1. LAMINAR, 2. TURBULENT, 3. LAM-TRANS-TURB

A choice of one of the available options sets the mode and then causes a re-display of all the modes and their current status;

B.L. MODE = LAMINAR

WALL TEMP. MODE = CONSTANT

TRANSITION PARAMETER = REYNOLDS NUMBER

B.L. CALCULATION = WALL ONLY

"ANY OTHER CHANGES?, 1-YES, 2-NO"

Other modifications may be done at this point in a sequence similar to that discussed above. If no other changes are required or if the modes initially set were correct, the series of prompts for the second category of inputs will be initiated.

## **2. CATEGORY 2: FLOW CONDITIONS AND NOZZLE DIMENSIONS**

The second category of inputs includes the numerical data associated with the flow conditions, and additional dimensions of the nozzle, which will be made clear below. The onset of the second set of inputs is denoted by the message

**\* \* \* PLEASE UTILIZE DECIMAL POINTS FOR THE FOLLOWING INPUTS \* \* \***

followed by the first prompt for information. Decimal points are necessary for the numeric inputs for the reasoning previously explained.

Most of the input prompts are self-explanatory and require no elaboration. Those prompts requiring explanation or having relevant comments will be summarized following the prompt.

1. INPUT REYNOLDS NUMBER FOR TRANSITION  
(Reynolds number based on momentum thickness of boundary layer)

Displayed only if the boundary layer mode is set to B.L. Mode = Lam-Trans-Turb and the transition indication mode set to Transition Parameter = Reynolds Number.

2. INPUT TRANSITION DISTANCE FROM THE THROAT IN FEET

Displayed only if the boundary layer mode is set to B.L. Mode = Lam-Trans-Turb and the transition indication mode is set to Transition Parameter = "X" Distance From Throat.

3. INPUT MOMENTUM THICKNESS OF BOUNDARY LAYER AT THE THROAT IN FEET

A value of 1.0E-5 feet is suggested.

4. INPUT STAGNATION PRESSURE IN LBS/IN<sup>2</sup>

5. INPUT TOTAL TEMPERATURE OF SUPPLY MEDIUM IN DEGREES R

6. INPUT TEMPERATURE OF THE WALL IN DEGREES R

Displayed only if the wall temperature indication mode is set to Wall Temp. Mode = Constant.

7. INPUT THE EXTENSION LENGTH OF NOZZLE PAST THE EXIT IN INCHES AS DEFINED FOR THE ISENTROPIC CORE

The nozzle contour may be extended past the exit plane of the nozzle, as defined by "char6", if, for instance, a test section is to be added. Assumes uniform duct flow.

8. INPUT INCREMENT OF "X" IN INCHES FOR EXTENSION LENGTH TO INTERPOLATE CONTOUR OF NOZZLE

Establishes the horizontal distance between consecutive points that describe the contour of the extension length.

9. INPUT WIDTH OF NOZZLE

10. INPUT RATIO OF SPECIFIC HEATS

11. INPUT EXPONENT FOR VISCOSITY-TEMPERATURE RELATION

For air, this is ( $\omega$ ) 0.76.

12. INPUT MOLECULAR WEIGHT OF GAS SUPPLY (AIR = 28.97)

13. INPUT SPECIFIC HEAT OF GAS IN BTU/LB-DEG-R (AIR = 0.24)

14. INPUT PRANDTL NUMBER FOR GAS (AIR = 0.72)

Following the conclusion of the last prompt, a listing of all the input descriptors and the values assigned to them is displayed:

```
*REYNOLDS NUMBER = 0.50000E-02
*"X" TRANSITION = 0.60000E+01
MOMENTUM THICKNESS = 0.10000E-04
STAGNATION PRESSURE = 0.47500E+02
STAGNATION TEMPERATURE = 0.68000E+02
**WALL TEMPERATURE = 0.72000E+02
EXTENSION LENGTH PAST NOZZLE EXIT = 0.12000E+02
INCREMENT "X" FOR EXTENSION = 0.65000E+00
WIDTH OF NOZZLE = 0.40000E+01
GAMMA = 0.14000E+01
VISCOSITY-TEMP. EXPONENT = 0.76000E+00
MOLECULAR WEIGHT OF GAS = 0.28970E+02
SPECIFIC HEAT = 0.24000E+00
PRANDTL NUMBER = 0.72000E+00
```

"ARE INPUTS CORRECT?, 1-YES, 2-NO"

\*Note: Displayed only if boundary layer mode is set to B.L.  
Mode = 3 and the transition indication mode is set to  
either Transition Parameter = Reynolds Number or  
Transition Parameter = "X" Distance from Throat

\*\*Note: Displayed only if the wall temperature indication  
mode is set to Wall Temp. Mode = Constant

If the option is exercised to change any of the input values, the user will be presented with the following menu:

INPUT VALUE TO BE CHANGED (1,2,3,4,5,6,7,8,9,10,11,12,13):

1. TRANSITION PARAMETER
2. MOMENTUM THICKNESS AT THROAT
3. STAGNATION PRESSURE
4. TOTAL TEMPERATURE
5. WALL TEMPERATURE



6. EXTENSION LENGTH OF NOZZLE
7. "X" INCREMENT FOR EXTENSION LENGTH
8. WIDTH OF NOZZLE
9. RATIO OF SPECIFIC HEATS
10. VISCOSITY-TEMPERATURE EXPONENT
11. MOLECULAR WEIGHT OF GAS
12. SPECIFIC HEAT ( $C_p$ ) FOR GAS
13. PRANDTL NUMBER

Selection from the menu generates a prompt for the new information to be input for the chosen descriptor. Upon entering the new value and striking the "enter" or "return" key, the list containing the input descriptors and their assigned values will be re-displayed exhibiting the latest changes and soliciting further modifications.

If at this point no other changes are desired and if the wall temperature indication mode is set to an option other than Wall Temp. Mode = Temperature Distribution Input By User, the program will proceed to calculate the modified contour according to the inputs given. If the user has elected to enter a defined temperature distribution along the nozzle contour, the following sequence of prompts can be expected:

INDICATE THE NUMBER OF TEMPERATURE POINTS  
TO BE ENTERED. THREE OR MORE POINTS ARE  
REQUIRED OR PROGRAM WILL TERMINATE THE DATA  
OUTPUT PRIOR TO COMPLETION.

INPUT THE "X" LOCATION FOR POINT NUMBER \_\_\_\_  
RELATIVE TO THE THROAT

INPUT TEMPERATURE IN DEGREES R FOR POINT  
NUMBER \_\_\_\_

The second and third statement are repeated until the number of points designated in the first statement have been entered. When the last point is entered, the program proceeds in



its calculation of the modified contour. Completion of the routine is denoted by the message,

PROGRAM RUN COMPLETE. OUTPUT DATA  
TRANSFERRED TO FILE "outpt3"

### 3. FILE "outpt3" FORMAT DESCRIPTION

Figure E5 illustrates an example of the format used for the output file "outpt3".

Again it, as before, has been sub-divided into its major components and labeled as follows:

#### 1. Functional Modes

\*INDINP = 2

\*INDPRG = 1

INDMO = 2      (Boundary Layer Mode) where 1 = Laminar,  
2 = Turbulent, 3 = Lam-Trans-Turb

INDTW = 1      (Wall Temperature Mode) where 1 = Constant Temp.,  
2 = Adiabatic, 3 = User Defined Distribution

INDTR = 1      (Transition Indication Mode) where 1 = Transition at  
Reynolds Number, 2 = Transition at "X" Length

\*INDCF = 1

\*INDOUT = 0

\*Note: Indicates values are hardwired into the program and  
are no longer user accessible

\*\*\* INPUT DATA \*\*\*

CARD 1

INDINP = 2  
INDPRG = 1  
INDMO = 2  
INDTW = 1  
INDTR = 0  
INDWC = 3  
INDCF = 1  
INDOUT = 0

FUNCTIONAL  
MODES

CARD 2

TRCON = 0.000000E+00  
THZERO = 0.100000E-04  
PO = 0.728000E+02  
TO = 0.820000E+03  
TWALL = 0.530000E+03  
XTEND = 0.285000E+02  
DL = 0.625000E-01

FLOW CONDITIONS  
AND NOZZLE  
DIMENSIONS

CARD 3

GAMMA = 0.140000E+01  
OMEGA = 0.780000E+00  
WATE = 0.290000E+02  
CP = 0.240000E+00  
PR = 0.720000E+00  
XINC = 0.000000E+00

\* WALL DATA \*

X(IN)	Y(IN)	M
0.318238E+00	0.142340E+01	0.111979E+01
0.333082E+00	0.142386E+01	0.112352E+01
0.348089E+00	0.142434E+01	0.112726E+01

INPUT DATA

\*\*\* OUTPUT CODE \*\*\*

X(IN)	S(IN)	Y(IN)	M	REL(1/FT)	RETH	PE/PO
UE(FT/SEC)	MUE(PSEC/FT2)	RHO E(PSEC2/FT4)	TE(R)	TW(R)	TAD(R)	TE/TO
DELTA(IN)	THETA(IN)	DELSTAR(IN)	H	TW/TO	TW/TAD	TAD/TO
DPDS(P/FT2)	DMDS(1/FT)	DUOS(1/SEC)	DTHDS	TAUWAL(P/FT2)	CF	BETATH
Q(BTU/FT2/SEC)	HA(BTU/FT2SECR)	N				

OUTPUT  
CODE

POINT NO. 1

0.263755E+02	0.263987E+02	0.189800E+01	0.170000E+01	0.120507E+08	0.300775E+05	0.202583E+00
0.189944E+04	0.374381E-06	0.237520E-02	0.519645E+03	0.530000E+03	0.788847E-03	0.633714E+00
0.348474E+00	0.300135E-01	0.540986E-01	0.180251E+01	0.646341E+00	0.671866E+00	0.962009E+00
0.000000E+00	0.000000E+00	0.000000E+00	0.100080E-02	0.857629E+01	0.200085E-02	0.000000E+00
0.112397E+02	0.434220E-01	0.753040E+01				
0.307388E+02						

POINT NO. 2

0.264380E+02	0.284612E+02	0.189800E+01	0.170000E+01	0.120507E+08	0.301403E+05	0.202583E+00
0.189944E+04	0.374381E-06	0.237520E-02	0.519645E+03	0.530000E+03	0.788847E+03	0.633714E+00
0.348255E+00	0.300761E-01	0.542108E-01	0.180245E+01	0.646341E+00	0.671866E+00	0.962009E+00
0.000000E+00	0.000000E+00	0.000000E+00	0.100047E-02	0.857348E+01	0.200085E-02	0.000000E+00
0.112397E+02	0.434220E-01	0.753225E+00				
0.307953E+02						

\* WALL RESULTS \*

X(INCHES)	DELSTAR(INCHES)	YCORE+DELSTAR	MWALL	DELTA Y	YCORE+DELTA Y
0.318238E+00	0.197901E-03	0.142360E+01	0.111979E+01	0.338728E-03	0.142374E+01
0.333082E+00	0.280479E-03	0.142414E+01	0.112352E+01	0.480121E-03	0.142434E+01
0.348089E+00	0.353288E-03	0.142470E+01	0.112726E+01	0.804827E-03	0.142495E+01

FINAL  
RESULTS

Figure E5. Example Showing the Format of File "outpt3"

## 2. Flow Conditions and Nozzle Dimensions

TRCON = 0.000000E+00	(Reynolds number value or "x" length depending on the option set in the Transition Indication Mode)
THZERO = 0.100000E-04	(Momentum thickness at nozzle throat)
PO = 0.726000E+02	(Stagnation pressure)
TO = 0.820000E+03	(Stagnation temperature)
TWALL = 0.520000E+03	(Wall temperature when INDTW = 1)
XTEND = 0.265000E+02	(Extension length past nozzle exit plane)
DL = 0.625000E-01	(Increment in "x" of extension length)
GAMMA = 0.140000E+01	(Ratio of specific heats)
OMEGA = 0.760000E+00	(Viscosity-Temperature exponent)
WATE = 0.290000E+02	(Molecular weight of gas)
CP = 0.240000E+00	(Specific heat of gas)
PR = 0.720000E+00	(Prandtl number)
XINC = 0.000000E+00	(Not applicable; hardwired value)

3. Input Data from "outpt2" - Data generated from the inviscid contour software "char6".

4. Output Code - Constitutes the flow properties along the contour of the nozzle calculated by "nbl6" for each set of coordinates that define the nozzle contour.

X (IN)	x - coordinate of contour point
S (IN)	Contour length
Y (IN)	y - coordinate of contour point
M	Mach number along contour
REL (1/FT)	$REL = (\rho U_E)/\mu$
RETH	Reynolds Number; $RETH = (REL)(THETA)$

PE/PO	Static Pressure / Total Pressure
UE(FT/SEC)	Velocity
MUE (PSEC/FT2)	Absolute Viscosity ( $\mu$ )
RHOE (PSEC2/FT4)	Density ( $\rho$ )
TE (R)	Static Temperature
TW (R)	Wall Temperature
TAD (R)	Adiabatic Wall Temperature
TE/TO	Static Temperature / Total Temperature
DELTA (IN)	Boundary Layer Thickness ( $\delta$ )
THETA (IN)	Momentum Thickness ( $\theta$ )
DELSTAR (IN)	Boundary Layer Displacement ( $\delta^*$ )
H	Form Factor ( $H = \delta^*/\theta$ )
TW/TO	Wall Temperature / Total Temperature
TW/TAD	Wall Temperature / Adiabatic Wall Temperature
TAD/TO	Adiabatic Wall Temperature / Total Temperature
DPDS (P/FT2)	Change in pressure with respect to surface distance
DMDS (1/FT)	Change in Mach number with respect to surface distance
DUDS (1/SEC)	Change in velocity with respect to surface distance
DTHDS	Change in momentum thickness with respect to surface distance
TAUWAL (P/FT2)	Wall shear stress ( $\tau_w$ )
CF	Friction Coefficient
Q (BTU/FT2/SEC)	Local rate of heat transfer
HA (BTU/FT2-SEC-R)	Convection heat transfer coefficient

##### 5. Final Results - Modified contour output as calculated by "nbl6"

X (INCHES)	x - coordinate of modified contour
DELSTAR (INCHES)	Boundary layer displacement thickness
YCORE+DELSTAR	Modified contour accounting for boundary layer growth on contoured wall only
MWALL	Mach number at the wall
DELTAY	Modified displacement thickness as determined by the equation modeled by Demo [Ref. 28: p.24].

### **C. PROGRAM LISTINGS**

Listings are given as follows:

1. Program "char6"
2. Program "nbl6"





Jul 11 1996 16:04:49	char6.f	Page 3
903 WRITE(' ',35) 35 FORMAT(1X,EXIT,LENGTH,/,2-START OF TEST RHOMBUS') READ(' ',36) TYPLTH 36 FORMAT(A1) IF (TYPLTH.NE. '1'.AND. TYPLTH.NE. '2') THEN GO TO 903 END IF IF (TYPLTH.GE. 'A'.AND. TYPLTH.LE. 'Z') THEN GO TO 903 END IF 904 WRITE(' ',37) 37 FORMAT(1X,/,/,INDICATE CHARACTERISTIC HORIZONTAL LENGTH TO BE' 1',2-WALL POINTS ONLY') READ(' ',38) TYPOTH 38 FORMAT(A1) IF (TYPOTH.NE. '1'.AND. TYPOTH.NE. '2') THEN GO TO 904 END IF IF (TYPOTH.GE. 'A'.AND. TYPOTH.LE. 'Z') THEN GO TO 904 END IF C DISPLAY INPUT RESULTS C IF (TYPNO2.EQ. '1') THEN WRITE(' ',1060) 'NOZZLE = ',TYPE1 FORMAT(1X,/,A9,A5) 1060 ELSE IF (TYPNO2.EQ. '2') THEN WRITE(' ',1061) 'NOZZLE = ',TYPE2 FORMAT(1X,/,A9,A7) 1061 ELSE WRITE(' ',1062) 'NOZZLE = ',TYPE3 FORMAT(1X,/,A9,A11) 1062 END IF IF (TYPHGT.EQ. '1') THEN WRITE(' ',1063) 'HEIGHT TO BE READ = ',HGT1 FORMAT(1X,/,A20,A4) 1063 ELSE WRITE(' ',1064) 'HEIGHT TO BE READ = ',HGT2 FORMAT(1X,/,A20,A6) 1064 END IF IF (TYPLTH.EQ. '1') THEN WRITE(' ',1065) 'LENGTH TO BE READ = ',LGTH1 FORMAT(1X,/,A20,A14) 1065 ELSE WRITE(' ',1066) 'LENGTH TO BE READ = ',LGTH2 FORMAT(1X,/,A20,A17) 1066 END IF IF (TYPOTH.EQ. '1') THEN WRITE(' ',1067) 'OUTPUT FORMAT = ',OUTPT1 FORMAT(1X,/,A16,A12) 1067 ELSE WRITE(' ',1068) 'OUTPUT FORMAT = ',OUTPT2 FORMAT(1X,/,A16,A11) 1068 END IF C CHANGES TO INPUT IF NECESSARY C		

Jul 11 1996 16:04:49	char6.f	Page 4
905 WRITE(' ',39) 39 FORMAT(1X,EXIT,LENGTH,/,2-START OF TEST RHOMBUS') READ(' ',40) INSRP 40 FORMAT(A1) IF (INSRP.NE. '1'.AND. INSRP.NE. '2') THEN GO TO 905 END IF IF (INSRP.GE. 'A'.AND. INSRP.LE. 'Z') THEN GO TO 905 END IF IF (INSRP.EQ. '2') THEN WRITE(' ',43) 1030 FORMAT(1X,/,/,INPUT VALUE TO BE CHANGED (1,2,3,4):',/,3X, 1-TYPE OF NOZZLE: A-SHORT, B-REGULAR, C-EXPONENTIAL',/,3X, 2-HEIGHT TO BE READ: A-EXIT, B-THROAT',/,3X,3-LENGTH TO BE', 3-READ: A-EXIT, B-TEST RHOMBUS',/,3X,4-TYPE OF OUTPUT: 4-A-STEP-BY-STEP, B-WALL POINTS ONLY') READ(' ',44) INCON 44 FORMAT(A1) IF (INCON.EQ. '1') THEN WRITE(' ',45) 906 FORMAT(1X,/,/,1-SHORT, 2-REGULAR, 3-EXPONENTIAL') 45 READ(' ',46) TYPNO2 46 FORMAT(A1) END IF IF (TYPNO2.NE. '1'.AND. TYPNO2.NE. '2'.AND. TYPNO2.NE. '3') THEN GO TO 906 END IF IF (TYPNO2.GE. 'A'.AND. TYPNO2.LE. 'Z') THEN GO TO 906 END IF IF (INCON.EQ. '2') THEN WRITE(' ',47) 907 FORMAT(1X,/,/,1-EXIT, 2-THROAT') 47 READ(' ',48) TYPHGT 48 FORMAT(A1) END IF IF (TYPHGT.NE. '1'.AND. TYPHGT.NE. '2') THEN GO TO 907 END IF IF (TYPHGT.GE. 'A'.AND. TYPHGT.LE. 'Z') THEN GO TO 907 END IF IF (INCON.EQ. '3') THEN WRITE(' ',49) 908 FORMAT(1X,/,/,1-EXIT, 2-TEST SECTION') 49 READ(' ',112) TYPLTH 112 FORMAT(A1) END IF IF (TYPLTH.NE. '1'.AND. TYPLTH.NE. '2') THEN GO TO 908 END IF IF (TYPLTH.GE. 'A'.AND. TYPLTH.LE. 'Z') THEN GO TO 908 END IF IF (INCON.EQ. '4') THEN WRITE(' ',113) 909 FORMAT(1X,/,/,1-STEP-BY-STEP, 2-WALL POINTS ONLY') 113 READ(' ',114) TYPOTH 114 FORMAT(A1) END IF IF (TYPOTH.NE. '1'.AND. TYPOTH.NE. '2') THEN GO TO 909 END IF IF (TYPOTH.GE. 'A'.AND. TYPOTH.LE. 'Z') THEN GO TO 909 END IF IF (TYPNO2.EQ. '1') THEN WRITE(' ',1070) 'NOZZLE = ',TYPE1 FORMAT(1X,/,A9,A5) 1070		

```

      ENO IF
C
C NOZZLE FLOW CHARACTERISTICS AND SPECIFIC GEOMETRY INPUTS
C
      WRITE(*,21)
21 FORMAT(1X,////,5X,'THE NEXT SET OF INPUTS SPECIFY FLOW'
1' CHARACTERISTICS AND SPECIFIC',/,18X,' GEOMETRY DIMENSIONS'
2' FOR THE NOZZLE')
      WRITE(*,22)
22 FORMAT(1X,////,8X,'***** PLEASE UTILIZE DECIMAL POINTS FOR THESE'
1' INPUTS *****')
      ERROR=0
500 FORMAT(1X,////,10X,'INPUT RATIO OF SPECIFIC HEATS')
51 READ(*,52) TOSTAT=ERROR) GAMMA
52 FORMAT(E10.5)
      IF (ERROR .GT. 0) THEN
        GO TO 500
      ENO IF
      ERROR=0
505 WRITE(*,53)
53 FORMAT(1X,////,10X,'INPUT TEST SECTION MACH NUMBER')
      READ(*,54) TOSTAT=ERROR) SM
54 FORMAT(E10.5)
      IF (ERROR .GT. 0) THEN
        GO TO 505
      ENO IF
      IF (INOKTE .EQ. 1) THEN
        ERROR=0
510 WRITE(*,55)
55 FORMAT(1X,////,10X,'INPUT EXIT LENGTH (INCH/FS)')
      READ(*,56) TOSTAT=ERROR) XEXT
56 FORMAT(E10.5)
      IF (ERROR .GT. 0) THEN
        GO TO 510
      ENO IF
      ELSE
        ERROR=0
515 WRITE(*,57)
57 FORMAT(1X,////,10X,'INPUT BEGINNING OF TEST RHOMBUS (INCHES)')
      READ(*,58) TOSTAT=ERROR) XEXT
58 FORMAT(E10.5)
      IF (ERROR .GT. 0) THEN
        GO TO 515
      ENO IF
      ENO IF
      IF (INOUTH .EQ. 1) THEN
        ERROR=0
520 WRITE(*,59)
59 FORMAT(1X,////,10X,'INPUT HALF HEIGHT OF EXIT (INCHES)')
      READ(*,61) TOSTAT=ERROR) THEX
61 FORMAT(E10.5)
      IF (ERROR .GT. 0) THEN
        GO TO 520
      ENO IF
      ELSE
        ERROR=0
525 WRITE(*,62)
62 FORMAT(1X,////,10X,'INPUT HALF HEIGHT OF THROAT (INCHES)')
      READ(*,63) TOSTAT=ERROR) THEX
63 FORMAT(E10.5)

```

```

      ELSE IF (TYPNO2 .EQ. '2') THEN
        WRITE(*,1071) 'NOZZLE = ', TYPE2
        FORMAT(1X,/,A9,A7)
      ELSE
        WRITE(*,1072) 'NOZZLE = ', TYPE3
        FORMAT(1X,/,A9,A11)
      END IF
      IF (TYPHGT .EQ. '1') THEN
        WRITE(*,1073) 'HEIGHT TO BE READ = ', HGT1
        FORMAT(1X,/,A20,A4)
      ELSE
        WRITE(*,1074) 'HEIGHT TO BE READ = ', HGT2
        FORMAT(1X,/,A20,A6)
      ENO IF
      IF (TYPLTH .EQ. '1') THEN
        WRITE(*,1075) 'LENGTH TO BE READ = ', LGTH1
        FORMAT(1X,/,A20,A14)
      ELSE
        WRITE(*,1076) 'LENGTH TO BE READ = ', LGTH2
        FORMAT(1X,/,A20,A17)
      END IF
      IF (TYPOUT .EQ. '1') THEN
        WRITE(*,1077) 'OUTPUT FORMAT = ', OUTFT1
        FORMAT(1X,/,A16,A12)
      ELSE
        WRITE(*,1078) 'OUTPUT FORMAT = ', OUTFT2
        FORMAT(1X,/,A16,A11)
      END IF
      WRITE(*,910)
      FORMAT(1X,////,10X,'ANY OTHER CHANGES?, 1=YES, 2=NO')
      READ(*,911) INOUT
      IF (INOUT .NE. 1 .AND. INOUT .NE. 2) THEN
        GO TO 1020
      ENO IF
      IF (INOUT .EQ. 1) THEN
        GO TO 1030
      ENO IF
      END IF
C
C CONVERSION TO INTEGER FORMAT
C
      IF (TYPNO2 .EQ. '1') THEN
        INOSR=1
      ELSE IF (TYPNO2 .EQ. '2') THEN
        INOSR=2
      ELSE
        INOSR=3
      END IF
      IF (TYPHGT .EQ. '1') THEN
        INOUTH=1
      ELSE
        INOUTH=2
      ENO IF
      IF (TYPLTH .EQ. '1') THEN
        INOKTE=1
      ELSE
        INOKTE=2
      ENO IF
      IF (TYPOUT .EQ. '1') THEN
        INOOUT=1
      ELSE
        INOOUT=2

```

JUL 11 1996 16:04:49	char6.f	Page 7
530	WRITE(*,64)	
64	FORMAT(1X,/,/, 'INPUT RADIUS OF CURVATURE AT THROAT (INCHES)')	
65	READ(*,66, IOSTAT=ERROR) RCT	
66	FORMAT(E10.5)	
67	IF (ERROR .GT. 0) THEN	
68	GO TO 530	
69	END IF	
70	ERROR=0	
71	WRITE(*,67)	
72	FORMAT(1X,/,/, 'INPUT MULTIPLICATIVE FACTOR FOR X INCREMENT'	
73	1' (1.0-150 PTS, 0.5-400 PTS)')	
74	READ(*,68, IOSTAT=ERROR) OELMUL	
75	FORMAT(E10.5)	
76	IF (ERROR .GT. 0) THEN	
77	GO TO 535	
78	END IF	
79	C DISPLAY INPUT RESULTS	
80	WRITE(*,71) 'GAMMA =', GAMMA, 'SMT =', SMT, 'XEXXT =', XEXXT,	
81	1' YTHEX =', YTHEX, 'RCT =', RCT, 'OELMUL =', OELMUL	
82	7: FORMAT(1X,/,/, 1X, A9, E10.5, /, 5(1X, A9, E10.5, /))	
83	C CHANGE INPUT VALUES IF NECESSARY	
84	800 WRITE(*,72)	
85	72 FORMAT(1X,/,/, 'ARE INPUT VALUES CORRECT?, 1=YES, 2=NO')	
86	READ(*,73) INANS	
87	73 FORMAT(I1)	
88	IF (INANS .NE. 1 .AND. INANS .NE. 2) THEN	
89	GO TO 800	
90	END IF	
91	IF (INANS .EQ. 2) THEN	
92	WRITE(*,74)	
93	74 FORMAT(1X,/,/, 'INPUT VALUE TO BE CHANGED: 1-GAMMA, 2-SMT,'	
94	3-XEXXT, 4-YTHEX, 5-RCT, 6-OELMUL')	
95	READ(*,75) INCNG	
96	FORMAT(I1)	
97	IF (INCNG .EQ. 1) THEN	
98	WRITE(*,76)	
99	76 FORMAT(1X,/,/, 'INPUT NEW VALUE FOR GAMMA')	
100	READ(*,77, IOSTAT=ERROR) GAMMA	
101	FORMAT(E10.5)	
102	IF (ERROR .GT. 0) THEN	
103	GO TO 540	
104	END IF	
105	END IF	
106	IF (INCNG .EQ. 2) THEN	
107	ERROR=0	
108	WRITE(*,78)	
109	78 FORMAT(1X,/,/, 'INPUT NEW VALUE FOR SMT')	
110	READ(*,79, IOSTAT=ERROR) SMT	
111	FORMAT(E10.5)	
112	IF (ERROR .GT. 0) THEN	
113	GO TO 545	
114	END IF	
115	END IF	
116	IF (INCNG .EQ. 3) THEN	
117	END IF	

JUL 11 1996 16:04:49	char6.f	Page 8
550	ERROR=0	
551	WRITE(*,81)	
552	81 FORMAT(1X,/,/, 'INPUT NEW VALUE FOR XEXXT')	
553	READ(*,82, IOSTAT=ERROR) XEXXT	
554	FORMAT(E10.5)	
555	IF (ERROR .GT. 0) THEN	
556	GO TO 550	
557	END IF	
558	END IF	
559	IF (INCNG .EQ. 4) THEN	
560	ERROR=0	
561	WRITE(*,83)	
562	83 FORMAT(1X,/,/, 'INPUT NEW VALUE FOR YTHEX')	
563	READ(*,84, IOSTAT=ERROR) YTHEX	
564	FORMAT(E10.5)	
565	IF (ERROR .GT. 0) THEN	
566	GO TO 555	
567	END IF	
568	END IF	
569	IF (INCNG .EQ. 5) THEN	
570	ERROR=0	
571	WRITE(*,86)	
572	86 FORMAT(1X,/,/, 'INPUT NEW VALUE FOR RCT')	
573	READ(*,87, IOSTAT=ERROR) RCT	
574	FORMAT(E10.5)	
575	IF (ERROR .GT. 0) THEN	
576	GO TO 560	
577	END IF	
578	END IF	
579	IF (INCNG .EQ. 6) THEN	
580	ERROR=0	
581	WRITE(*,88)	
582	88 FORMAT(1X,/,/, 'INPUT NEW VALUE FOR DELMUL')	
583	READ(*,89, IOSTAT=ERROR) DELMUL	
584	FORMAT(E10.5)	
585	IF (ERROR .GT. 0) THEN	
586	GO TO 565	
587	END IF	
588	END IF	
589	WRITE(*,96) 'GAMMA =', GAMMA, 'SMT =', SMT, 'XEXXT =', XEXXT,	
590	1' YTHEX =', YTHEX, 'RCT =', RCT, 'OELMUL =', OELMUL	
591	7: FORMAT(1X,/,/, 1X, A9, E10.5, /, 5(1X, A9, E10.5, /))	
592	WRITE(*,91)	
593	91 FORMAT(1X,/,/, 'ANY OTHER CHANGES?, 1=YES, 2=NO')	
594	READ(*,92) INNEXT	
595	FORMAT(I1)	
596	IF ((INNEXT .NE. 1 .AND. INNEXT .NE. 2) THEN	
597	GO TO 802	
598	END IF	
599	IF (INNEXT .EQ. 1) THEN	
600	GO TO 801	
601	END IF	
602	END IF	
603	WRITE(16,40)	
604	40 FORMAT(1X,15X,'U.S. NAVAL ORDNANCE LABORATORY, WHITE OAK, MARYLAND'	
605	1,/,/, 5X,'COMPUTER PROGRAM FOR THE DESIGN OF TWO-DIMENSIONAL'	
606	2'SUPERSONIC NOZZLES',/,/, 34X,'PART 1',/,/, 20X,'THE ISENTROPIC'	
607	3'CORE OF THE NOZZLE',/,/, /)	
608	WRITE(16,406) (SMT(I), I=1,10)	
609	406 FORMAT(20X,10A8,/, /)	
610	WRITE(16,41) INSR, INDYTH, INOCTE, INOOUT, INOCAL, INOTAP, INOCRD,	
611	1GAMMA, SMT, XEXXT, YTHEX, RCT, OELMUL	
612	41 FORMAT(	
613	20X,' INPUT DATA',/,/, 20X,'CARO NO. 1',	







JUL 11 1996 16:04:49 char6.f Page 11

```

      SML(J) = SML(NJ)
      SHW(J) = SHW(NJ)
      XL(J) = XL(NJ)*YEXIT
      YW(J) = YW(NJ)*YEXIT
      THEN(J) = THEN(NJ)*.57.3
      990 CONTINUE
      XEXIT=XEXIT*YEXIT
      XT=XT*YEXIT
      J11=J0-1
      DO 991 J4=2,J11
        DS=SQRT((XW(J4+1)-XW(J4-1))**2+(YW(J4+1)-YW(J4-1))**2)
        DTRE=THEM(J4+1)-THEM(J4-1)
        F1=DTRE/DS*0.001
        DTNE=1.E-6
        991 CONTINUE/DTNE*.57.3
        R(J1)=0.0
        R(J2)=0.0
        WRITE(16,493)
        493 FORMAT(1X,///,30X,'FINAL OUTPUT TO PART 1, ISENTROPIC CORE CONTOUR
        1,///,5X,'1',4X,'X(INCHES)',6X,'Y(INCHES)',5X,'CL MACH NO.',4X,
        2,'WALL MACH NO.',3X,'WALL ANGLE, 2X,'RAD OF CURV (IN) ',//)
        494 FORMAT(16,495)
        495 FORMAT(1X,15,EL15.6)
        CONT=0.0
        WRITE(17,142) (FMT(J),J=1,10)
        142 FORMAT(10A8)
        WRITE(17,140)J0,YTH,YEXIT,XT,XEXIT
        140 FORMAT(15,4E20.7)
        141 FORMAT(15,4X)
        141 CONTINUE
        ENO FILE 17
        REMINO 17
      CLOSE(17)
      1100 FMT(1X,///)
      1100 FMT(1X,///) 'OUTPUT ISENTROPIC DATA FOR NOZZLE CONTOUR'
      1, 'STORED IN FILENAME OUTP1.'
      2, '///, 'DATA FROM THIS FILE TO BE USED IN THE VISCIOUS'
      3, 'PROGRAM NB16.F IS STORED',//, 'IN FILENAME OUTP2.F'
      STOP
      ENO
      SUBROUTINE REC(XL,SML,XCOR,SMT,YTH,YEXIT,XT,RC,T,B,LASTN,NEND,GAMMA
      1,XEXIT,ETAW,DELMUL)
      IMPLICIT DOUBLE PRECISION (A-H,O-Z)
      DIMENSION XL(600),SML(600),XCOR(600)
      SKIFC(XL-SMT*(1.0-X/XT)*(1.0-X/XT)*((1.0-X/XT)*(1.0-X/XT)
      WRITE(16,101) SMT,YTH,YEXIT,XEXIT,XT
      101 FORMAT(1X,///,19X,'NOZZLE PARAMETERS (LENGTHS IN INCHES)'
      1,///,5X,'MACH NO.',5X,'YTH',10X,'YEXIT',7X,'XEXIT',8X,'XT'
      2,1X,SE13.5,1X,RC,T,B
      201 FMT(1X,27X,'RCT',10X,'B',/,22X,2E13.5,///,10X,
      1,CENTERLINE MACH NUMBER DISTRIBUTION USING CUBIC EQUATION',
      2,///,20X,'N',7X,'X',15X,'MACH NO.',/)
      XT=XT*YEXIT
      XEXIT=XEXIT*YEXIT
      XB=0.0
      DO 50 I5=1,600
        SML(I5)=SML
        XCOR(I5)=XCOR*YEXIT
        XEXIT=XEXIT*YEXIT
        IF(SMB.GE.1.0001) GO TO 60
      50 CONTINUE
      60 XL(I1)=XB
      SML(I1)=SMB
      XCOR(I1)=XB*YEXIT
      XEXIT=3.0
      DELX=0.0001
      DO 88 I=2,600
        IF(I.LE.20) GO TO 80
        OELX=LOG(100.*(XL(I-1)/XEXIT)*.1)/460.*XEXIT
        DELX=OELX*DELMUL
      80 XL(I)=XL(I-1)+DELX
        GO TO NU,(81,83)
      81 XCC=XL(I)/ETAW
        IF(XCC.LE.1.40174) GO TO 82
        C1=1.4554
        C2=0.17251
        C3=0.17251
        C4=-0.031244
        C5=0.62572E-2
        C6=-0.34138E-3
        ASSIGN 83 TO NU
      GO TO 83

```

JUL 11 1996 16:04:49 char6.f Page 12

```

      DO 88 I=2,600
        IT=1
        IF(I.LE.20) GO TO 80
        IF(XC-LOG(100.*(XL(I-1)/XEXIT)*.1)/460.*XEXIT
        OELX=OELX*DELMUL
      80 XL(I)=XL(I-1)+DELX
        XCOR(I)=XL(I)*YEXIT
        SML(I)=SKIFC(XL(I))
        IF(XL(I).GE.XT) GO TO 85
      88 CONTINUE
      85 LASTN=IT
      SML(I1)=SMT
      XL(I1)=XT
      XCOR(I1)=XL(I1)*YEXIT
      XT=XT*YEXIT
      DO 90 J=1,600
        JTN=J
        OELX=LOG(100.*(XL(J-1)/XEXIT)*.1)/460.*XEXIT
        DELX=DELX*DELMUL
        XL(J)=XL(J-1)+DELX
        XCOR(J)=XL(J)*YEXIT
        SML(J)=SMT
        IF(XL(J).GE.XEXIT) GO TO 95
      90 CONTINUE
      95 NEND=JTN
      XL(NEND)=XEXIT
      XCOR(NEND)=XL(NEND)*YEXIT
      SML(NEND)=SMT
      WRITE(16,100) (K,XCOR(K),SML(K),K=1,NEND)
      100 FDMAT(16X,15,EL15.6,X,EL15.6)
      RETURN
      SUBROUTINE SHD(XL,SML,XCOR,SMT,YTH,YEXIT,XT,RC,T,B,LASTN,NEND,GAMMA
      1,XEXIT,ETAW,DELMUL)
      IMPLICIT DOUBLE PRECISION (A-H,O-Z)
      DIMENSION XL(600),SML(600),XCOR(600)
      SKIFC(XL-SMT*(1.0-X/XT)*(1.0-X/XT)*((1.0-X/XT)*(1.0-X/XT)
      C1=1.0
      C2=0.023652
      C3=0.04309
      C4=-0.04309
      C5=0.09893
      C6=-0.78644E-2
      ASSIGN 81 TO NU
      XB=0.0
      DO 50 I5=1,600
        SML(I5)=SML
        XCOR(I5)=XCOR*YEXIT
        XEXIT=XEXIT*YEXIT
        IF(SMB.GE.1.0001) GO TO 60
      50 CONTINUE
      60 XL(I1)=XB
      SML(I1)=SMB
      XCOR(I1)=XB*YEXIT
      XEXIT=3.0
      DELX=0.0001
      DO 88 I=2,600
        IF(I.LE.20) GO TO 80
        OELX=LOG(100.*(XL(I-1)/XEXIT)*.1)/460.*XEXIT
        DELX=OELX*DELMUL
      80 XL(I)=XL(I-1)+DELX
        GO TO NU,(81,83)
      81 XCC=XL(I)/ETAW
        IF(XCC.LE.1.40174) GO TO 82
        C1=1.4554
        C2=0.17251
        C3=0.17251
        C4=-0.031244
        C5=0.62572E-2
        C6=-0.34138E-3
        ASSIGN 83 TO NU
      GO TO 83

```

```

B2 XCOR(1)=XL(I)*YEXIT
   XC=XL(I)/ETAW
   SMT=1.0
   GO TO 85 SKIFG(XC)
B3 XCOR(1)=XL(I)*YEXIT
   XC=LOG(XL(I)/ETAW)
   SML(I)=SKIFG(XC)
86 IF(SML(1).GE.SMT) GO TO 85
88 CONTINUE
85 LASTN=IT
   SML(I)=SMT
   XCOR(1)=XT*YEXIT
   XCOR(1)=XT*YEXIT
   XEXIT=XT*SORT(SMT**2-1.)
   NI=LASTN+1
   DO 90 J=N1, 600
      JTM=J
      DELX=LOG(100.*(XL(J-1)/XEXIT)+1.)/460.*XEXIT
      DELX=DELX*DELMUL
      XL(J)=XL(J-1)*DELX
      XCOR(J)=XL(J)*YEXIT
      SML(J)=SKIFG(XC)
      IF(XL(J).GE.XEXIT) GO TO 95
90 CONTINUE
95 NEND=JTM
   XL(NEND)=XEXIT
   XCOR(NEND)=XL(NEND)*YEXIT
   SML(NEND)=SMT
   WRITE(16,96) SMT,YTH,YEXIT,XCOR(NEND),XCOR(LASTN)
1 96 '1.//,5.//,MACH NO.,5X,YTH,10X,YEXIT,7X,XEXIT,8X,
2 //,1X,5E13.5,
3 //,10X,CENTERLINE MACH NUMBER DISTRIBUTION FOR A SHORT NOZZLE',
4 //,20X,N,7X,X,10X,MACH NO.,/'
   WRITE(16,100) (K,XCOR(K),SML(K),K=1,NEND)
100 FORMAT(16X,15,ZE15.6)
      RETURN
      SUBROUTINE XPO(XL,SML,XCOR,SMT,YTH,YEXIT,XT,RCT,B,LASTN,NEND,GAMMA)
1  XEXIT,ETAW,DELMUL
      IMPLICIT DOUBLE PRECISION (A-H,O-Z)
      DIMENSION XL(600),SML(600),XCOR(600)
      SKIFG(X)=TM2*(1.-(EXP(C2*(1.-X/XT))-1.-X/XT))/(TM1)+1.
      DMXD=0.5*SORT((GAMMA+1.)/RCT/YTH)
      T=DMXD*XT/(SMT-1.)
      ITER=0
      DO 30
         T1=T
         T2=2.*G2*EP/(EP-1.)
         IF(ABS(E2).LE.0.0001) GO TO 45
         B1=(G2-G1)/(E2-E1)
         G1=G2
         G2=EXP(T)
         G1-G2
         ITER=ITER+1
         GO TO 35
      E1=E2
      G2=G1-B1*E1
      IF(G2.EQ.0.00) G2=0.0001
      GO TO 30
35 WRITE(16,40) ITER
      IF(ITER.EQ.20X,ITERATION IN SUB XPO EQUALS',15)
      STOP
45 G2=G2
      WRITE(16,47) SMT,YTH,YEXIT,XCOR,XT
47 FORMAT(1X,/'1.//,5.//,MACH NO.,5X,YTH,10X,YEXIT,7X,XEXIT,8X,XT',
2.//,1X,5E13.5,/'
2.//,10X,CENTERLINE MACH NUMBER DISTRIBUTION FOR A SHORT NOZZLE',
48 FORMAT(1X,23X,RCT,DMXD,C2
1'CENTERLINE MACH NUMBER DISTRIBUTION USING EXPONENTIAL'

```

```

2'EQUATION' //,23X,N',7X,X',10X,MACH NO.,/'
   TM1=EXP(C2)-1.0
   TM2=SMT-1.0
   XT=XT/YEXIT
   XEXIT=XEXIT/YEXIT
   XB=0.0
   DO 50 I=1,600
      XB=XB+0.00001
      SMT=SKIFG(XB)
      IF(SMT.GE.1.0001) GO TO 60
50 CONTINUE
60 CONTINUE
   SML(1)=SMT
   XCOR(1)=XB*YEXIT
   OELX=0.0001
   DO 80 I=2,600
      IT=I
      IF(I.LE.20) GO TO 80
      DELX=LOG(100.*(XL(I-1)/XEXIT)+1.)/460.*XEXIT
      OELX=DELX*DELMUL
      XL(I)=XL(I-1)*DELX
      XCOR(I)=XL(I)*YEXIT
      SML(I)=SKIFG(XL(I))
      IF(XL(I).GE.XT) GO TO 85
88 CONTINUE
85 LASTN=IT
   SML(1)=SMT
   XL(1)=XT
   XCOR(1)=XL(1)*YEXIT
   XT=LASTN
   DO 90 J=N1, 600
      JTM=J
      OELX=LOG(100.*(XL(J-1)/XEXIT)+1.)/460.*XEXIT
      OELX=DELX*DELMUL
      XL(J)=XL(J-1)*DELX
      XCOR(J)=XL(J)*YEXIT
      SML(J)=SMT
      IF(XL(J).GE.XEXIT) GO TO 95
90 CONTINUE
95 NEND=JTM
   XL(NEND)=XEXIT
   XCOR(NEND)=XL(NEND)*YEXIT
   SML(NEND)=SMT
   WRITE(16,100) (K,XCOR(K),SML(K),K=1,NEND)
100 FORMAT(16X,15,ZE15.6)
      RETURN
      SUBROUTINE ACOM(P,Q,H,S,R,EPSC,LOLITA,AC)
      IMPLICIT DOUBLE PRECISION (A-H,O-Z)
1005 DIMENSION ANOT(100),AP(100)
1030 ANOT(1)=(P-Q)/2.
1040 AP(1)=W*ATAN(1./W*ANOT(1))-ATAN(1./ANOT(1))*(S-R)/2.
1050 ANOT(2)=ANOT(1)+1
1060 AP(2)=W*ATAN(1./W*ANOT(2))-ATAN(1./ANOT(2))*(S-R)/2.
1070 DO 1110 KOUNT=3,LOLITA
1080 ANOT(KOUNT)=ANOT(KOUNT-1)-AP(KOUNT-1)*ANOT(KOUNT-2)
1110 AP(KOUNT)=AP(KOUNT-1)-AP(KOUNT-2)
1090 AP(KOUNT)=W*ATAN(1./W*ANOT(KOUNT))-ATAN(1./ANOT(KOUNT))*(S-R)/2.
1095 JULES=KOUNT
1100 IF(ABS(ANOT(KOUNT)-ANOT(KOUNT-1))/ANOT(KOUNT))-EPSC)1145,1111
1110 CONTINUE
1145 AC=ANOT(JULES)
      IF(ABS(1-LOLITA).GT.1E-16) GO TO 1150
      WRITE(16,1146)
1146 FORMAT(20X,'KOUNT')
1150 RETURN
      ENO
      SUBROUTINE WINTER (EXH,R,S,T,X1,XJ,XX,TERP,K)

```

Jul 11 1996 16:04:49 char6.f Page 15

```

      IMPLICIT DOUBLE PRECISION (A-H,O-Z)
      DIFF(X1,XJ)=X1-XJ
      DIVAYF(R,S,X1,XJ)=DIFF(R,S)/DIFF(X1,XJ)
      DIVBYF(R,S,T,X1,XJ,XI)=DIVAYF(DIVAYF(R,S,X1,XJ),DIVAYF(S,T,XJ,XI),
      11, XJ)
      DO 20 J=1,NPTS
      11, XJ)
      TERP=R-DIFF(EXM,X1)*(DIVAYF(R,S,X1,XJ)+DIFF(EXM,XJ)*DIVBYF(R,S,T,X
      11, XJ,XJ))
      GO TO 15
10 TERP=(EXM-XJ)*R/(X1-XJ)*(EXM-XI)*S/(XJ-XI)
15 RETURN
END
SUBROUTINE ATC(CA,GO,SHAB,CB,THETA,ETA1,X2,X1,Y2,Y1,SM1,SM2,ETA2)
      IMPLICIT DOUBLE PRECISION (A-H,O-Z)
      POFF(SM1)=PM*(GM/(2.*GM*PM*.2))**GO
      X2X1=X2-X1
      Y2Y1=Y2-Y1
      SNA=.5*(1./SM1+1./SM2)
      ETA2=ETA1+.5*(POFF(SM1)+POFF(SM2))*SNA*SQRT(X2X1*X2X1+Y2Y1*Y2Y1))
      RETURN
END
SUBROUTINE SETYED(XM,NO,XL,SM1,NEND)
      IMPLICIT DOUBLE PRECISION (A-H,O-Z)
      DIMENSION XM(600),XL(600),SM1(600),SUM(600)
      DO 70 J=1,600
      70 J=1,600
      JT=J
      IF (XL(J).GE.XM(ND)) GO TO 71
      71 K=JT
      KEND=NEND-3
      IF (XM(K).LE.XL(K)) GO TO 10
      K=K+1
      GO TO 5
10 IF (K.LE.KEND) GO TO 20
      20 CALL LAGINT(XL(K-2),SM1(K-2),5,XM(1),SUM(1),DYO)
      GO TO 40
30 DO 40 INT(XL(K-4),SM1(K-4),5,XM(1),SUM(1),DYO)
      40 CONTINUE
      DO 60 J=NO,NEND
      XL(J)=XM(JT)
      SM1(J)=SM1(JT)
      60 CONTINUE
      RETURN
END
SUBROUTINE LAGINT(X,Y,NPTS,XX,YY,DYY)
      IMPLICIT DOUBLE PRECISION (A-H,O-Z)
      DIMENSION X(1),Y(1)
      YY=0.
      DO 40 I=1,NPTS
      DYY=0.
      C1=1.
      C2=1.
      DO 10 J=1,NPTS
      IF (J.EQ.1) GO TO 10
      C1=C1*(X(X(J))-X(J))
      C2=C2*(X(X(1))-X(J))
      10 CONTINUE
      SUM=D.
      DO 30 J=1,NPTS
      IF (J.EQ.1) GO TO 30
      C3=1.
      DO 20 K=1,NPTS
      IF (K.EQ.1.OR.K.EQ.J) GO TO 20
      C3=C3*(X(X(K))-X(J))
      20 CONTINUE
      SUM=SUM+C3
      C=Y(1)/C2
      DYY=DYY+C*C1
      30 CONTINUE
      40 CONTINUE

```

Jul 11 1996 16:04:49 char6.f Page 16

RETURN  
END

Jul 11 1996 16:03:07

nbl6.f

Page 1

```

.....
PROGRAM NBL6
Modified by: Lt Douglas L. Selwright
March 1994

PROGRAM INPUTS:

INDHO-BOUNDARY LAYER MODEL: 1. STRICTLY LAMINAR, 2. STRICTLY
INDHO-TURBULENCE, 3. LAMINAR-TRANS-CONSTANT=THALL, 2. AOIA WALL TEMP,
INDHO-WALLTEMP, INDHO-TURBULENCE, INDHO-CONSTANT=THALL, 2. AOIA WALL TEMP,
3. TEMPERATURE DISTRIBUTION INPUT BY USER
INDTR-TRANSITION INLOCATION( IF INDOHO=3): 1. TRANS AT RETHETA VALUE
GIVEN IN TRCON, 2. TRANS AT X GIVEN IN TRCON
INDHOC- INDICATE BOUNDARY LAYER CALCULATION:
1. CALCULATE CENTERLINE ONLY, 2. CALCULATE WALL ONLY,
3. CALCULATE BOTH

TRCON-TRANSITION CONSTANT EQUAL TO RETHETA (BEYONDLOS NUMBER BASED
ON THE MOMENTUM THICKNESS OF THE BOUNDARY LAYER) OR XTRANS
(HORIZONTAL DISTANCE RELATIVE TO THE THROAT) DEPENDING
ON INOTR
THZERO-TNETHA (MOMENTUM THICKNESS) AT THROAT IN FEET
(USUALLY= 1.0E-5)
PO-STAGNATION PRESSURE IN LBS/IN2
ID-SUPPLY TEMP IN DEGREES R (INOTR=1)
THALL-TRANSITION LOCATION IN INCHES NOZZLE WALL
XTENO-EXTENSION LENGTH IN INCHES NOZZLE WALL
BY THE ISENTROPIC CORE( INCHES) (ASSUMES UNIFORM DUCT FLOW)
OL-INCREMENT IN X FROM ISENTROPIC EXIT TO EXTENSION LENGTH
IN (INCHES)
B-WIDTH OF NOZZLE

GAMMA-RATIO OF SPECIFIC HEATS
DUC-EXTENSION DUCT LENGTH IN INCHES
WATE-MOLECULAR WT OF GAS (AIR=29)
CP-SPECIFIC HEAT OF GAS IN BTU/LB-DEG R (AIR=0.24) OR LEAVE
BLANK AND LET PROGRAM PICK VALUES
PR-PRANDTL NUMBER (AIR=0.72)

** IFINOTR=3:
NUM-NUMBER OF WALL TEMP INPUT CARDS (THREE OR MORE POINTS
TO COMPLETING RUN)
XXX-DISTANCE FROM THROAT IN INCHES
TNH-WALL TEMPS. (DEGREES R) CORRESPONDING TO X=XXX

.....
IMPLICIT DOUBLE PRECISION (A-N, D=2)
DIMENSION X(1000), Y(1000), P(1000), CHMS(1000), H(16), XILN(16),
2DELTA(1000), S(1000), POVP(1000), OHMS(1000), PHT(10), YSAV(1000),
2DELTA(1000), YS(1000), DELY(1000), YTY(1000), YCZOLY(1000),
CHARACTER*8, FMT
REAL B
COMMON CFOV2, CFV0V2, DELRAT, DELTA, DELTTH, DELTTH, DNEAT, OTHDS
1, OUES, EN, ENBAR, ENTURB, N, HINC, OLDOTH, REL, RETN, RETHR, RHOT, THETA,
2TAUMAL, TNBAR, THETA2, THOVDL, TLT, ULUE, TRCON, TNZERO, PO, TO, THALL,
3GAMMA, OHEGA, WATE, CP, CHMS, SW, AI, B1, A2, B2, CP, A3, B3, GNEU, TLT, TAO,
4SENE(1000), PHT(10), YSAV(1000), YCZOLY(1000), YTY(1000), POVP(1000),
5OHMS(1000), PHT(10), IT, L, N, LINES, KOUNT, LAP, NK, INDCF, INDMO, INDHU,
6MDMS(1000), PHT(10), IT, L, N, LINES, KOUNT, LAP, NK, INDCF, INDMO, INDHU,
7INOTR, INOTR, INDMO, MAX, MIN, INDIRP, INDDUT, ITRES, INDIRG, B
OPEN(UNIT=17, FILE='outp17', STATUS='UNKNOWN')
OPEN(UNIT=26, FILE='outp26', STATUS='UNKNOWN')
NHALF A(1) = .01357623

```

Jul 11 1996 16:03:07

nbl6.f

Page 2

```

11 NHALF A(2) = .03112672
12 NHALF A(3) = .01157925
13 NHALF A(4) = .062314485
14 NHALF A(5) = .074797995
15 NHALF A(6) = .084578260
16 NHALF A(7) = .091301710
17 NHALF A(8) = .094725305
18 NHALF A(9) = HALFA(8)
19 NHALF A(10) = HALFA(7)
20 NHALF A(11) = HALFA(6)
21 NHALF A(12) = HALFA(5)
22 NHALF A(13) = HALFA(4)
23 NHALF A(14) = HALFA(3)
24 NHALF A(15) = HALFA(2)
25 NHALF A(16) = HALFA(1)
26 XI(1) = .005299535
27 XI(2) = .02771249
28 XI(3) = .0671844
29 XI(4) = .1229978
30 XI(5) = .19106188
31 XI(6) = .2700017
32 XI(7) = .35919822
33 XI(8) = .45249374
34 XI(9) = .54750626
35 XI(10) = .64080178
36 XI(11) = .72900839
37 XI(12) = .80893812
38 XI(13) = .8777022
39 XI(14) = .9328156
40 XI(15) = .9770046
41 XI(16) = .52401361
42 XILN(1) = -.52401361
43 XILN(2) = -.3.5858719
44 XILN(3) = -.2.7003143
45 XILN(4) = -.2.1012962
46 XILN(5) = -.1.6551579
47 XILN(6) = -.1.3056674
48 XILN(7) = -.1.0238809
49 XILN(8) = -.0.7201217
50 XILN(9) = -.0.60238131
51 XILN(10) = -.44501503
52 XILN(11) = -.31606998
53 XILN(12) = -.21203278
54 XILN(13) = -.13044784
55 XILN(14) = -.069547711
56 XILN(15) = -.028103680
57 XILN(16) = -.0053135801

C INTRODUCTION TO PROGRAM
C
WRITE(*,120)
120 FORMAT(1X,///////1X,15X,'U.S. NAVAL ORDNANCE LABORATORY, WHITE'
1' OK, HARVLANO',//5X,'COMPUTER PROGRAM FOR THE DESIGN OF'
2' A TWO-DIMENSIONAL SUPERSONIC NOZZLE',//34X,'PART II',//15X,
3' ISENTROPIC CORE CONTOUR MODIFIED FOR VISCOUS EFFECTS')
125 FORMAT(1X,125)
1' isentropic', 'Introduction',//1X,'This program modifies the '
2' effects of the boundary layer. The program has been modified to',
3' take',//, 'into account both the boundary layer for the side',
4' plate as well',//, 'as the contour of the nozzle.')

PRINT*
PRINT*
PRINT*
PRINT*
PAUSE
XINC=0.0
INDCF=1
INDPRG=2

```







```

WRITE(26, 631) (FMT(II), I=1, 10)
631 FORMAT(1X, 10AB, // 30X, 'CONTOUR FOR TAPERED PLATE', //, T25, 'N',
      1T42, 'X', T62, 'Y', //)
DO 615 I=2, MNC
  YS(1)=YS(1)+0.021-3.5777E-03-S(1)
615 CONTINUE
  WRITE(26, 610) (I, S(1), YS(1), I=2, MNC)
  GO TO 9
END

END MAIN PROGRAM

SUBROUTINE RESTOR
IMPLICIT DOUBLE PRECISION (A-H, O-Z)
CHARACTER*9, FMT
1TH(1000), XY(1000), YX(1000), HALF4(16), XI(16), XILN(16),
2DEL(1000), YY(1000)
COMMON CF0V2, CF0V2L, DELRAT, DELTA, DELTRE, DELTTH, OMEAT, DTDS
1, DUEDS, EN, ENBAR, ENTURB, H, HINC, GLDTH, REC, RETH, RETHR, RHOE, THETA,
2XUALM, THBAR, THETA2, THOVLD, TITE, ULUE, FCON, THZERO, FO, TO, THALL,
3XANNA, OMEGA, WATE, CP, PR, GRUO, SH, A1, BL, AZ, B2, CZ, AJ, B3, GRU1, TE, TAD,
4SEME(1000), HALF4(16), XI(16), XILN(16), TW(1000), S(1000), P0VPO(1000),
6NDS(1000), FMT(10), IT, L, N, LINES, KOUNT, LAP, NN, INDCP, INDMO, INDMU,
7INDTH, INDR, INDMC, MAX, MIN, INDIRP, INDOUT, ITMES, INDRPG
1910 CF0V2L=0
1911 CF0V2L=0

```

[illegible]

```

SUBROUTINE IN
SUBROUTINE IN READS INPUT FROM char6 AND KEYBOARD INPUT
IMPLICIT DOUBLE PRECISION (A-H, O-Z)
INTEGER COUNT,COUNTI,ERROR,INVALD
CHARACTER*8, FMT
REAL B

```

[illegible]









# Program "nbl6" (cont.)

Jul 11 1986 16:03:07

nbl6.1

Page 13

```

GO TO 460
ELSE IF (INDIR .GE. 'A' .AND. INDIR .LE. '2') THEN
GO TO 460
END IF
END IF
)F (INANS .EQ. '2' .AND. INDIR .EQ. '1') THEN
WRITE(*,465)
FORMAT(1X,/, 'INPUT VALUE TO BE CHANGED (1,2,3,4,5,6,7,8,9',
1 '10,11,12,13):',/, '3X', '1. TRANSITION PARAMETER',/, '3X',
2 '2. THROAT THICKNESS',/, '3X', '3. TOTAL TEMPERATURE',
3 '4. PRESSURE',/, '3X', '5. EXTENSION LENGTH OF NOZZLE',/, '3X',
4 '6. TEMPERATURE',/, '3X', '7. EXTENSION LENGTH OF NOZZLE',/, '3X',
5 '8. INCREMENT FOR EXTENSION LENGTHS',/, '3X', '9. WIDTH',
6 '10. RATIO OF SPECIFIC HEATS',/, '2X', '11. MOLECULAR WEIGHT',
7 '12. VISCOSITY TEMPERATURE EXPONENT',/, '2X', '13. MOLECULAR WEIGHT',
8 '14. SPECIFIC HEAT (CP) FOR GAS',/, '2X', '15. MOLECULAR WEIGHT',
9 '16. PRANDTL NUMBER')
READ(*,470) INCHG
FORMAT(AZ)
IF (INCHG .EQ. '1') THEN
IF (INCHG .EQ. '3') THEN
ERROR=0
IF (INOTR .EQ. '1') THEN
WRITE(*,475)
FORMAT(1X,/, 'INPUT NEW REYNOLDS NUMBER')
READ(*,480, IOSTAT=ERROR) TRCON
FORMAT(E10.3)
IF (ERROR .GT. 0) THEN
GO TO 471
END IF
ELSE
WRITE(*,485)
FORMAT(1X,/, 'INPUT NEW "X" TRANSITION',
'DISTANCE (INCHES)')
READ(*,490, IOSTAT=ERROR) TRCON
FORMAT(E10.3)
IF (ERROR .GT. 0) THEN
GO TO 481
END IF
END IF
ELSE INVAL=1
END IF
ELSE IF (INCHG .EQ. '2') THEN
WRITE(*,500)
FORMAT(1X,/, 'INPUT NEW VALUE OF MOMENTUM THICKNESS',
' AT THROAT (FEET)')
READ(*,505, IOSTAT=ERROR) THZERO
FORMAT(E10.3)
IF (ERROR .GT. 0) THEN
GO TO 499
END IF
END IF
ELSE IF (INCHG .EQ. '3') THEN
ERROR=0
WRITE(*,510)
FORMAT(1X,/, 'INPUT NEW STAGNATION PRESSURE (1b3/1n2)')
READ(*,515, IOSTAT=ERROR) PO
FORMAT(E10.3)
IF (ERROR .GT. 0) THEN
GO TO 509
END IF
END IF
ELSE IF (INCHG .EQ. '4') THEN
ERROR=0
WRITE(*,520)
FORMAT(1X,/, 'INPUT NEW TOTAL TEMPERATURE (DEGREES R)')
READ(*,525, IOSTAT=ERROR) TO
FORMAT(E10.3)
IF (ERROR .GT. 0) THEN
GO TO 519
END IF
END IF
ELSE IF (INCHG .EQ. '5') THEN

```

Jul 11 1986 16:03:07

nbl6.1

Page 14

```

IF (INOTR .EQ. '1') THEN
ERROR=0
WRITE(*,530)
FORMAT(1X,/, 'INPUT NEW WALL TEMPERATURE',
' (DEGREES R)')
READ(*,535, IOSTAT=ERROR) TWALL
FORMAT(E10.3)
IF (ERROR .GT. 0) THEN
GO TO 529
END IF
END IF
ELSE
WRITE(*,540)
FORMAT(1X,/, 'INPUT NOT NECESSARY FOR DATA',
' PREVIOUSLY GIVEN')
END IF
ELSE IF (INCHG .EQ. '6') THEN
ERROR=0
WRITE(*,545)
FORMAT(1X,/, 'INPUT NEW EXTENSION LENGTH (INCHES)')
READ(*,550, IOSTAT=ERROR) XTENO
FORMAT(E10.3)
IF (ERROR .GT. 0) THEN
GO TO 541
END IF
ELSE IF (INCHG .EQ. '7') THEN
ERROR=0
WRITE(*,555)
FORMAT(1X,/, 'INPUT NEW "X" INCREMENT (INCHES)')
READ(*,560, IOSTAT=ERROR) OL
FORMAT(E10.3)
IF (ERROR .GT. 0) THEN
GO TO 551
END IF
END IF
ELSE IF (INCHG .EQ. '8') THEN
ERROR=0
WRITE(*,565)
FORMAT(1X,/, 'INPUT NEW WIDTH OF NOZZLE (INCHES)')
READ(*,570, IOSTAT=ERROR) B
FORMAT(E10.3)
IF (ERROR .GT. 0) THEN
GO TO 561
END IF
END IF
ELSE IF (INCHG .EQ. '9') THEN
ERROR=0
WRITE(*,575)
FORMAT(1X,/, 'INPUT NEW RATIO OF SPECIFIC HEATS')
READ(*,580, IOSTAT=ERROR) GAMMA
FORMAT(E10.3)
IF (ERROR .GT. 0) THEN
GO TO 571
END IF
END IF
ELSE IF (INCHG .EQ. '10') THEN
ERROR=0
WRITE(*,585)
FORMAT(1X,/, 'INPUT VISCOSITY-TEMP. EXPONENT')
READ(*,590, IOSTAT=ERROR) OMEGA
FORMAT(E10.3)
IF (ERROR .GT. 0) THEN
GO TO 581
END IF
END IF
ELSE IF (INCHG .EQ. '11') THEN
ERROR=0
WRITE(*,595)
FORMAT(1X,/, 'INPUT NEW MOLECULAR WEIGHT')
READ(*,600, IOSTAT=ERROR) WATE
FORMAT(E10.3)
IF (ERROR .GT. 0) THEN
GO TO 591
END IF
END IF
ELSE IF (INCHG .EQ. '12') THEN
ERROR=0
WRITE(*,605)
FORMAT(1X,/, 'INPUT NEW SPECIFIC HEAT (CP- BTU/LB-',

```



CH 17 1998 16:03:07

[illegible]

mb16.f

JUL 11 1996 16:03:07

```

1      'DEG-R')
610    READ(6, 610, IOSTAT=ERROR) CP
        FORMAT(E10.3)
        IF (ERROR .GT. 0) THEN
            GO TO 601
        ELSE
            IF ((INCHG .EQ. '13') THEN
                IF ((INCHG .EQ. '13') THEN
                    WRITE(*, 615)
                    FORMAT(1X, '//, INPUT NEW PRANOTL NUMBER')
                READ(6, 620, IOSTAT=ERROR) PR
                IF (ERROR .GT. 0) THEN
                    GO TO 611
                END IF
            END IF
            COUNT1=COUNT1+1
            GO TO 635
        END IF
CONVERSION TO INTEGRAL FORMAT
        IF (INDMO .EQ. '1') THEN
            INDMO=1
        ELSE IF (INDMO .EQ. '2') THEN
            INDMO=2
        ELSE IF (INDMO .EQ. '3') THEN
            INDMO=3
        END IF
        IF (INDTW .EQ. '1') THEN
            INTW=1
        ELSE IF (INDTW .EQ. '2') THEN
            INTW=2
        ELSE IF (INDTW .EQ. '3') THEN
            INTW=3
        END IF
        IF (INDMC .EQ. '1') THEN
            INMC=1
        ELSE IF (INDMC .EQ. '2') THEN
            INMC=2
        ELSE IF (INDMC .EQ. '3') THEN
            INMC=3
        END IF
        IF (INTNR .EQ. '1') THEN
            INTNR=1
        ELSE IF (INTNR .EQ. '2') THEN
            INTNR=2
        END IF
END OF KEY BOARD INPUTS

IF (VTEND-LE.X(MAXI)) GO TO 640
D 645 Y=1, 800
NT=1 MAX
IF (NT.EQ. 600) GO TO 650
X(INT)=X(INT-1)+DL
YS(NT)=YS(MAX)
EMS(NT)=EMS(MAX)
YIS(NT)=YIS(MAX)
EMES(NT)=EMES(MAX)
YEMES(NT)=YEMES(MAX)
GO TO 650
CONTINUE
645 MAX=NT
650 GO TO (710, 710, 655), INTDW

```

```

WRITE (26,770)NUMB,XXX(J1),TWH(J1)
770 FORMAT(1X,/,15X,'CARD',13,1X,XXX =,E15.6,/,35X,'TWH =',E15.6)
765 IF(LAP.EQ.2) GO TO 775
760 WRITE(26,780)
780 FORMAT(1X,20X,////,52X,'** WALL DATA **',//,
16X,'X(IN)',16X,'Y(IN)',16X,'M',//)
GO TO 785
775 WRITE(26,790)
790 FORMAT(1X,20X,////,50X,'** CENTERLINE DATA **',//,
16X,'X(IN)',16X,'Y(IN)',16X,'M',//)
785 WRITE(26,795)(X(L),Y(L),EHE(L),L=1,MAX)
795 DO 800 L=1,360.6
X(L1)=X(L1)/12.0
Y(L1)=Y(L1)/12.0
800 CONTINUE
RETURN
END

C SUBROUTINE OATA COMPUTES OH/OS
SUBROUTINE OATA
IMPLICIT DOUBLE PRECISION (A-H, O-Z)
CHARACTER*8, FMT
DIMENSION X(1000), Y(1000), EME(1000), HALF(16), XI(16), XLIN(16),
2DEL(1000), S(1000), P(1000), CVOV2(1000), DELTAT, DELTAR, DELTET, DELTETM, OHEAT, OTHOS
1, OUEOS, EN, ENBAR, ENTURB, H, HINC, OLODTH, REL, RETH, RETHR, RHOE, THETA,
2TAUHAL, THBAR, THETA2, THOVL, ULTE, ULUE, TRCON, THZERO, PO, TO, THALL,
3GAMMA, OMEGA, WATE, CP, PR, GHUO, SH, A1, B1, A2, B2, C2, A3, B3, GHUE, TE, TAO,
4TAOTE, TWTE, QUAY, TETO, UE, GHUE, HA, OPOS, OL, XINC, X(1000), Y(1000),
5EME(1000), HALF(16), XI(16), XLIN(16), TM(1000), P(1000), P(1000),
6DMS(1000), FMT(10), IT, L, N, LINES, KOUNT, LAP, NN, INDOCF, INOH, INOHU,
7INDTM, INDTR, INOH, MAX, MIN, INDINP, INDOUT, ITMES, INDRPG
IF(LAP.EQ.2) GO TO 15
DO 10 I=1,2 MAX
S(I)=S(I-1)*SORT((X(I)-X(I-1))**2+(Y(I)-Y(I-1))**2)
10 CONTINUE
GO TO 21
15 DO 20 I=1, MAX
S(I)=X(I)
20 CONTINUE
1 DO 101 J=1, MAX
101 DO 102 J=1, MAX
IF (J.GE. MAX) GO TO 92
IF (J.GE. 1) GO TO 91
90 OHOS(J)=(EME(J-1)-EME(J-1))/(S(J-1)-S(J-1))
GO TO 100
91 OHOS(J)=(EME(J-1)-EME(J-1))/(S(J-1)-S(J-1))
GO TO 100
92 OHOS(J)=(EME(J)-EME(J-1))/(S(J)-S(J-1))
10 IF OHOS(J).LT.0.01 OHOS(J)=0.0
101 RETURN
END

SUBROUTINE CHLOE
IMPLICIT DOUBLE PRECISION (A-H, O-Z)
CHARACTER*8, FMT
DIMENSION X(1000), Y(1000), EME(1000), HALF(16), XI(16), XLIN(16),
17M(1000), S(1000), P(1000), P(1000), OHOS(1000), FMT(10),
2DEL(1000), Y(1000)
COMMON CVOV2, CVOV2L, CVOV2T, DELRAT, DELTAR, DELTET, DELTETM, OHEAT, OTHOS
1, OUEOS, EN, ENBAR, ENTURB, H, HINC, OLODTH, REL, RETH, RETHR, RHOE, THETA,
2TAUHAL, THBAR, THETA2, THOVL, ULTE, ULUE, TRCON, THZERO, PO, TO, THALL,
3GAMMA, OMEGA, WATE, CP, PR, GHUO, SH, A1, B1, A2, B2, C2, A3, B3, GHUE, TE, TAO,
4TAOTE, TWTE, QUAY, TETO, UE, GHUE, HA, OPOS, OL, XINC, X(1000), Y(1000),
5EME(1000), HALF(16), XI(16), XLIN(16), TM(1000), P(1000), P(1000),
6DMS(1000), FMT(10), IT, L, N, LINES, KOUNT, LAP, NN, INDOCF, INOH, INOHU,
7INDTM, INDTR, INOH, MAX, MIN, INDINP, INDOUT, ITMES, INDRPG
END

```

```

1110 SW=PI(N)/70.1 (SW)**0.1821-51.8
1112 B1=1-51-0.125*(SBS (SW)**0.425)
1113 A2=((7.776*SW+16.125)*SW+7.151)*SW-2.363
1114 B2=((0.328*SW+0.034)*SW-0.174)*SW+0.73
1115 C2=2.6*(SW+1.0)
1116 A3=1.28-1.106*(ABS (SW)**0.964)
1117 B3=0.903-0.088*(ABS (SW)**4.533)
1118 GHUE=GHUE/RHOE
1119 RETURN
END

SUBROUTINE LAM IT E
IMPLICIT DOUBLE PRECISION (A-H, O-Z)
CHARACTER*8, FMT
DIMENSION X(1000), Y(1000), EME(1000), HALF(16), XI(16), XLIN(16),
17M(1000), S(1000), P(1000), P(1000), OHOS(1000), FMT(10),
2DEL(1000), Y(1000)
COMMON CVOV2, CVOV2L, CVOV2T, DELRAT, DELTAR, DELTET, DELTETM, OHEAT, OTHOS
1, OUEOS, EN, ENBAR, ENTURB, H, HINC, OLODTH, REL, RETH, RETHR, RHOE, THETA,
2TAUHAL, THBAR, THETA2, THOVL, ULTE, ULUE, TRCON, THZERO, PO, TO, THALL,
3GAMMA, OMEGA, WATE, CP, PR, GHUO, SH, A1, B1, A2, B2, C2, A3, B3, GHUE, TE, TAO,
4TAOTE, TWTE, QUAY, TETO, UE, GHUE, HA, OPOS, OL, XINC, X(1000), Y(1000),
5EME(1000), HALF(16), XI(16), XLIN(16), TM(1000), P(1000), P(1000),
6DMS(1000), FMT(10), IT, L, N, LINES, KOUNT, LAP, NN, INDOCF, INOH, INOHU,
7INDTM, INDTR, INOH, MAX, MIN, INDINP, INDOUT, ITMES, INDRPG
1210 ENBAR=(THETA**2)*OUEOS/(GHUE*TE)
1211 HINC=A2*(ENBAR**B2)*C2
1212 H=HINC/TE*(TO-TE)/TE
1213 EN=ENBAR
1214 RETH=REL/THETA
1215 CVOV2L=CVOV2
DOOT=0.
IF (ENBAR+.3) 10,15,15
10 DS=-.3
DOOTND=-28.613546-(14.046635*SW-62.021031)*SW
S*75.901060)*SW
DOOT=DOOTND*(ENBAR+.3)
15 DS=ENBAR
16 DOOT=7.9160948*((30.38170*DS-59.418345*SW-82.319725)*OS+
152.310133*SW+112.21677)*SW-65.130652)*DS-((-14.046635*SW
2-30.634951)*SW-24.61395)*SW-8.2910568)*DS-(((
3-3.4832207*SW-0.99506674)*SW-94367191)*SW+2.254166)*SW
DOOT=DOOT+DOOT
THOVL=1./((DOOT*(TO/TE-1.)*(MNC+1.))
RETH=H*THOVL
1216 RETURN
END

SUBROUTINE TRATUR
IMPLICIT DOUBLE PRECISION (A-H, O-Z)
CHARACTER*8, FMT
DIMENSION X(1000), Y(1000), EME(1000), HALF(16), XI(16), XLIN(16),
17M(1000), S(1000), P(1000), P(1000), OHOS(1000), FMT(10),
2DEL(1000), Y(1000)
COMMON CVOV2, CVOV2L, CVOV2T, DELRAT, DELTAR, DELTET, DELTETM, OHEAT, OTHOS
1, OUEOS, EN, ENBAR, ENTURB, H, HINC, OLODTH, REL, RETH, RETHR, RHOE, THETA,
2TAUHAL, THBAR, THETA2, THOVL, ULTE, ULUE, TRCON, THZERO, PO, TO, THALL,
3GAMMA, OMEGA, WATE, CP, PR, GHUO, SH, A1, B1, A2, B2, C2, A3, B3, GHUE, TE, TAO,
4TAOTE, TWTE, QUAY, TETO, UE, GHUE, HA, OPOS, OL, XINC, X(1000), Y(1000),
5EME(1000), HALF(16), XI(16), XLIN(16), TM(1000), P(1000), P(1000),
6DMS(1000), FMT(10), IT, L, N, LINES, KOUNT, LAP, NN, INDOCF, INOH, INOHU,
7INDTM, INDTR, INOH, MAX, MIN, INDINP, INDOUT, ITMES, INDRPG
1310 RETH=REL*THETA
GO TO (1311,1311), INDOCF
311 ENTURB=LOG(ENTURB)-1.29
GO TO 312
1311 ENTURB=89030368*LOG(ENTURB)-1.65
1312 IF(L=4) 1315,1315,1313
1313 EN=ENTURB
1314 GO TO 1317
1315 DELTRE=RETH-RETHTR

```

```

1316 EN=(5,256-3)-(1,96-6)*DELTR1*DELTR1-1,25
1317 A=1,-TADTE
1318 B=TAGE-TWTE
1319 POWR=EN
1320 GD 1331 J=1,2
1321 SUM=0
1322 DO 1324 I=1,16
1323 GZMD=HALFA(I)*(EXP(XILN(I)*POWR))/(A*(X(I)*B)+X(I)*(TWTE)
1324 SUM=SUM+GZMD
1325 IF(J=1) 1326,132B,1331
1326 POWR=EN
1327 DELTR1=EN-CAOGET
1328 POWR=EN-1-CAOGET
1329 POWR=EN-1
1330 POWR=EN-1
1331 CONTINUE
1332 THOVL=CAOGET-EN*SUM
1333 H=DELTR1/THOVL
1334 OO 1336 I=1,2
1335 TLE=1.-.448*(GANMA-1.)*(EME(N)*2)-(1.-*(ULUE**2))*(TWTE-TADTE)*
1336 I*(1.-ULUE*DELTR1/THOVL)*(TLE***(1.-OMEGA)/RETH)**(1./EN+1.))
1337 CPOV2=DD2265*TEID*0.5*(TWTE/TAOTE)**0.345/RETH*0.1
1338 GD TD 1338
1339 CPOV2=(128.-ENTURB)**((1.-ENTURB)/(1.-ENTURB))*(1-THOVL/RETH)
1340 **((1.-ENTURB)/(1.-ENTURB+1.))*(TLE**((1.-2.*DMEGA-ENTURB)/(ENTURB+1.)))
1341 IF(L=4) 1339,1342,1343
1342 CPOV2=CPOV2-CPOV2*(RETH**2)
1343 GD TD 1343
1344 CPOV2=CPOV2-QUAY*(RETH**2)
1345 REAN=REAN+CPOV2
1346 ENDO
1347 SUBROUTINE DUT
1348 IMPLICIT DOUBLE PRECISION (A-H, O-Z)
1349 CHARACTER*8, FMT
1350 DIMENSION X(1000), YY(1000), HALFA(16), XI(16), XILN(16),
1351 ZMLY(1000), S(1000), POWP(1000), OMOS(1000), FMT(10),
1352 COMON CPOV2, CPOVZL, CPOVZL, DELTR1, DELTA, DELTRE, DELTH, DHEAT, OPHDS
1353 CPOV2=EN, ENBAN, ENTURB, H, HINC, DLOOT, REL, RETR, RHEAT, RHOE, THETA,
1354 TAGE, THEMA, WATE, CF, PR, GMD, SK, A1, B1, Z, B2, C2, A3, B3, GMD, TE, TAD,
1355 GAMMA, DHEAT, QUAY, TETO, UE, CHUE, HA, DPDS, OL, XINC, X(1000), YY(1000),
1356 EMOE(1000), HALFA(16), XI(16), XILN(16), TW(1000), POWP(1000),
1357 OMOS(1000), FMT(10), IT, L, N, LINES, MOUNT, LAP, NN, INDCF, INOMO, INDOU,
1358 7INOT, INDIR, INDCN, MAX, MIN, INOIN, INODUT, LTIMES, INDPAG
1359 XCDR=X(N)*12.
1360 SCOR=S(N)*12.
1361 YCOR=YY(N)*12.
1362 TCLAUS=THEAT*12.
1363 DELSIN=DELTA*12.
1364 OELN=THEIN/THDVL
1365 TMTAD=TW(N)/TAD
1366 TMTD=TW(N)/TD
1367 TMTD=TAD/TD
1368 IF(N.GT.MIN) GD TD 12
1369 CF=CPOV2*2.
1370 WRITE(26,4)
1371 FORMAT(1X,9X,////,56X,**** DUTPUT CODE ****,////)
1372 4 FDMAT(202,X(1N),10X,S(1N),10X,X(1N),12X,H',M',10X,
1373 1,REL(1/FT2),8X,'RETH',11X,'PE/PD',////)
1374 WRITE(26,6)
1375 6 FDMAT(17,X,'UE(FT/SEC)',4X,'MUE(PSEC/FT2)',1X,'RHOE(PSEC2/FT4)',
1376 15X,'TE(R)',10X,'TW(TAD)',10X,'TAD/TD',////)
1377 WRITE(26,7)
1378 7 FDMAT(18X,'DELTA(1N)',6X,'THETA(1N)',6X,'DELSTAR(1N)',9X,H',H',11X,
1379 1,'TMTD',10X,'TW/TAD',10X,'TAD/TD',////)
1380 WRITE(26,8)
1381 8 WRITE(26,9)
1382 9 FDMAT(17X,'DPOS(P/FT2)',4X,'DMDOS(1/FT)',7X,'DUDS(1/SEC)',6X,
1383 1,'DTHOS',6X,'TAUHAL(P/FT2)',7X,'CF',11X,'BETAH',////)
1384 WRITE(26,9)
1385 9 FDMAT(16X,'Q(FT/FT2/SEC)',1X,'HA(BTU/FT2/SEC)',8X,'N',N',////)

```

```

12 IF (L=4113,1B,22
13 WRITE(26,15)N,IT
15 FORMAT(1X,/,15X, 'POINT ND.',14,4X,'LAMINAR',5X,13,1X,
16 1'ITERATIONS')
GD TD 30
18 WRITE(26,20)N,IT
20 FORMAT(1X,/,15X, 'POINT ND.',14,4X,'TRANSITIDN',5X,13,1X,
21 1'ITERATIONS')
GD TD 30
22 GO TD 30
23 GO TD 30
24 GO TD 30
25 FORMAT(1X,/,15X, 'POINT ND.',14,4X,'TURBULENCE',5X,13,1X,
26 1'ITERATIONS')
30 WRITE(26,35)XCOR,SCDR,VCOR,EHE(N),REL,RETH,PDPD(N),UE,GHUE,RUDE,
1DMS(N),TQO,TAETO,DELIN,THEIN,DELSIN,H,TMTD,THTAO,TADTD,DPDS,
1DMS(N),AUGOS,DPHOS,TAUMAL,CF,BAUGOS,OEHEAT,HA,EN
35 FORMAT(15X,'7E15.6)
IT=0
RETURN
END
SUBROUTINE IPSD
IMPLICIT DOUBLE PRECISION (A-H, D-Z)
CHARACTER*8,FMT
DIMENSION S(1000),YY(1000),EHE(1000),HALFA(16),XI(16),XILN(16),
17M(1000),S(1000),PDPD(1000),OMDS(1000),FMT(10),
2DELY(1000),YYI(1000)
COMMON CFV2L,CFDV2L,CFDV2T,OEBA7A,DELTRA,DELTRH,DELTRH,OEHEAT,PHOS
1,OEUES,EN,ENBAR,ENTURB,H,HINC,DLOOTH,REL,RETH,RETRH,RHOE,THETA,
2TAUMAL,THBAR,THETA,PHOVOL,TLITE,ULUE,TRCIN,THZERO,PD,TQ,THALL,
3JAMPA,MDEGA,WKTE,CF,FR,GHOD,SH,AL,B1,A2,C2,A3,B3,GHUE,TE,TAO,
4TAUO,TAUO,TAUO,TAUO,TAUO,TAUO,TAUO,TAUO,TAUO,TAUO,TAUO,TAUO,
5EHE(1000),AUGOS(16),FMT(16),FMT(16),FMT(16),FMT(16),FMT(16),FMT(16),
6PHOS(1000),FMT(10),IT,L,N,LINES,KOUNT,LAP,NM,INDCT,INOMO,INOMU,
7INOMT,INOMD,INDMC,MAX,MIN,INOPIN,INOOT,ITMES,INOPRG
1610 IT=0
GD TD 1614,1614,1624,1624,1647,1647,1
1614 L=2
1615 IF (INDTR.EQ.2) GD TD 1616
1616 IF (TRCIN-RETH) 1619,1618,1642
1617 IF (TRCIN-XI(N)) 1619,1618,1642
1618 RETRH=RETH
1619 RETRH=RETH
1620 ULUP=1,OE-4
1621 ULUP=1,OE-4
1622 CFV2L=CFDV2
1623 GD TD 1642
1624 L=4
1642 L=4
1647 L=5
1648 L=5
1649 L=5
END
SUBROUTINE SETEQ(SW,ND,XL,SML,NEND)
IMPLICIT DOUBLE PRECISION (A-H, D-Z)
DIMENSION SW(1600),XL(1600),SML(400),SWH(600)
DD TO J=1,600
JT=J
IF (XL(JT).GE.XH(ND)) GD TD 71
70 CONTINUE
71 K=JT
KEND=NEND-3
DD 40 I=ND,NEND
5 K=K+1
5 K=K+1
5 K=K+1
10 IF (K.LE.KEND) GD TD 20
GD TD 30
20 CALL LAGINT (XL(K-2),SML(K-2),5,XH(1),SWH(1),DYO)
GD TD 40
30 CALL LAGINT (XL(K-4),SML(K-4),5,XH(1),SWH(1),DYO)
40 CONTINUE
50 GO J=ND,NEND
50 J=J+1
60 CONTINUE
60 RETURN
END

```

```

SUBROUTINE LAGINT(X, Y, NPTS, XX, YY, OYY)
  IMPLICIT DOUBLE PRECISION (A-H, O-Z)
  DIMENSION X(1), Y(1)
  C1=1.
  DO 40 I=1, NPTS
    OYY=0.
    YY=0.
    DO 10 J=1, NPTS
      C2=1.
      C3=1.
      C1=C1*(XX-X(J))
      IF (J.EQ.1) GO TO 10
      C2=C2*(X(I)-X(J))
      C3=C3*(XX-X(K))
    10 CONTINUE
    SUM=0.
    DO 30 J=1, NPTS
      IF (J.EQ.1) GO TO 30
      C3=1.
      K=1, NPTS
      IF (K.EQ.1 OR K.EQ. J) GO TO 20
      C3=C3*(XX-X(K))
    20 CONTINUE
    SUM=SUM+C3
    30 CONTINUE
    C=Y(1)/C2
    YY=YY+C*C1
    OYY=OYY+C*SUM
  40 CONTINUE
  RETURN
  ENDO

```



## LIST OF REFERENCES

1. Kavandi, J.L., Callis, J.B., Gouterman, M., Green, G., Khalil, G., Burns, D. and McLachlan, B.G., "Surface Pressure Field Mapping using Luminescent Coatings", *Experiments in Fluids*, v.14, pp. 33-41, 1993.
2. Kavandi, J.L., Callis, J.B., Gouterman, M., Khalil, G., Wright, D., Green, E., Burns, D. and McLachlan, B.G., "Luminescent Barometry in Wind Tunnels", *Rev. Sci. Instruments*, Vol. 61, No. 5, pp. 3340-3347, November 1990.
3. Peterson, J.I. and Fitzgerald, R.V., "New Technique of Surface Flow Visualization Based on Oxygen Quenching of Fluorescence", *Rev. Sci. Instruments*, Vol. 51, pp.670-671, May 1980.
4. Vollan, A. and Alati, L., "A New Optical Pressure Measurement System", 14th International Congress on Instrumentation in Aerospace Simulation Facilities (ICIASF), Paper No. 10, Rockville, Md., October 1991.
5. Morris, M.J., Donovan, J.F., Kegelman, J.T., Schwab, S.D., Levy, R.L. and Crites, R.C., "Aerodynamic Applications of Pressure-Sensitive Paint", AIAA Paper No. 92-0264, 30th AIAA Aerospace Sciences Meeting, Reno, Nevada, January 1992.
6. Morris, M.J., Benne, M.E., Crites, R.C. and Donovan, J.F., "Aerodynamic Measurements Based on Photoluminescence", AIAA Paper No. 93-0175, 31th AIAA Aerospace Sciences Meeting, Reno, Nevada, January 1993.
7. McLachlan, B.G., Bell, J.H., Kennelly, R.A., Schreiner, J.A., Smith, S.C., and Strong, J.M., "Pressure-Sensitive Paint Use in the Supersonic High-Speed Oblique Wing (SHOW) Test", AIAA Paper No. 92-2686, 10th AIAA Applied Aerodynamics Conference, Palo Alto, Ca., June 1992.
8. McLachlan, B.G., Bell, J.H., Espina, J., Gallery, J., Gouterman, M., Demandante, C.G.N. and Bjarke, L., "Flight Testing of a Luminescent Surface-Pressure Sensor", NASA Technical Memorandum 103970, October 1992.
9. Kavandi, J.L., *Luminescence Imaging for Aerodynamic Pressure Measurements*, Doctoral Thesis, Chemistry Department, University of Washington, 1990.
10. Moore, W.J., *Physical Chemistry*, Prentice Hall, Inc., 1962.



11. Pringsheim, P., *Fluorescence and Phosphorescence*, Interscience Publishers, 1949.
12. Calvert, J.G. and Pitts, J.P. Jr., *Photochemistry*, John Wiley and Sons, Inc., 1966.
13. Wayne, R.P., *Photochemistry*, American Elsevier Publishing Company, Inc., 1970.
14. Rice, O.C., *Electronic Structure and Chemical Binding*, Dover Publications, Inc., 1969.
15. Parker, C.A., *Photoluminescence of Solutions*, Elsevier Publishing Company, 1968.
16. Cundall, R.B. and Gilbert, A., *Photochemistry*, Appleton-Century-Crofts, 1970.
17. Wendland, R.A., *Upgrade and Extension of the Data Acquisition System for Propulsion and Gas Dynamics Laboratories*, M.S.A.E. Thesis, Naval Postgraduate School, Monterey, California, June 1992.
18. Adamson, T.C. Jr. and Nicholls, J.A., "On the Structure of Jets From Highly Underexpanded Nozzles Into Still Air", *J. Aero/Space Sciences*, Vol. 26 No. 1, 1959.
19. James H. Bell, (Private Communication) NASA Ames, Moffet Field, CA., January 1994.
20. Instruction and Operating Manuals, *Quartz Tungsten Halogen Lamp Housing Model 66186 and Lamp Controller Model 6405*, Oriel Corporation, 1992.
21. Hord, M.R., *Digital Image Processing of Remotely Sensed Data*, Academic Press, 1982.
22. McLachlan, B.G., and Bell J.H., "Image Registration for Luminescent Paint Sensors", AIAA Paper No. 93-0178, 31<sup>st</sup> Aerospace Sciences Meeting and Exhibit, Reno, Nevada, January 1993.
23. User's Manual, *EPIX 4MIP - 4MIPTOOL Interactive Image Analysis Software*, EPIX Incorporated, 1993.
24. Perretta, D.A., *Laser Doppler Velocimetry Measurements Across A Normal Shock In Transonic Flow*, M.S.A.E. Thesis, Naval Postgraduate School, Monterey, California, March 1993.
25. Kooi, J.W., "Experiment on Transonic Shock-Wave Boundary Layer Interaction", *Advisory Group for Aerospace Research and Development (AGARD)*, AGARD-CP-168, pp. 30-1, 30-10, November 1975.

26. Sebra, D.K., *Electronic Structure and Chemical Bonding*, Blaisdell Publishing Company, 1964.
27. Rice, O.K., *Electronic Structure and Chemical Binding*, Dover Publications, Inc., 1969.
28. Beynon, J.D.E. and Lamb, D.R., *Charge-Coupled Devices and Their Applications*, McGraw-Hill, 1980.
29. Demo, Jr., W.J., *Cascade Wind Tunnel for Transonic Compressor Studies*, M.S.A.E. Thesis, Naval Postgraduate School, Monterey, California, June 1978.



## INITIAL DISTRIBUTION LIST

1. Defense Technical Information Center 2  
8725 John J. Kingman Rd., STE 0944  
Ft. Belvoir, VA 22060-6218
2. Dudley Knox Library 2  
Naval Postgraduate School  
Monterey, California 93943-5002
3. Chairman, Department of Aeronautics and Astronautics 1  
Code AA  
Naval Postgraduate School  
699 Dyer Road - Room 137  
Monterey, California 93943-5106
4. Professor R.P. Shreeve 10  
Department of Aeronautics and Astronautics  
Code AA/SF  
Naval Postgraduate School  
699 Dyer Road - Room 137  
Monterey, California 93943-5106
5. Professor G.V. Hobson 1  
Department of Aeronautics and Astronautics  
Code AA/HG  
Naval Postgraduate School  
699 Dyer Road - Room 137  
Monterey, California 93943-5106
6. Commander, Naval Air Systems Command 1  
Code Air 4.4 T  
1421 Jefferson Davis Hwy  
Arlington, Virginia 22243
7. Naval Air Warfare Center-Aircraft Division 1  
Code Air 4.4.3.1 [S. McAdams]  
Propulsion and Power Engineering Bldg. 100  
Patuxent River, Maryland 20670-5304

- |   |   |
|---|---|
| 8. Curricular Officer,<br>Department of Aeronautics and Astronautics<br>Code 31<br>Naval Postgraduate School<br>699 Dyer Road - Room 135<br>Monterey, California 93943-5106 | 1 |
| 9. Lieutenant D.L. Seivwright<br>149 Edde Court<br>Marina, California 93933   | 3 |





17 51NPS 1302  
TH  
1/99 22527-200 NILEB









DUDLEY KNOX LIBRARY



3 2768 00361186 4